# THE IMPACT OF THE PLASMA PROTEIN CORONA ON THE ADHESION EFFICIENCY OF DRUG CARRIERS TO THE BLOOD VESSEL WALL

by

Daniel J. Sobczynski

A dissertation submitted in partial fulfillment
of the requirements for the degree of
Doctor of Philosophy
(Chemical Engineering)
in the University of Michigan
2016

Doctoral Committee:

Associate Professor Lola Eniola-Adefeso, Chair
Professor Jennifer J. Linderman
Assistant Professor Greg M. Thurber
Associate Professor Angela Violi

## DEDICATION

To my family and friends, thank you for all your love and support throughout this experience; I am forever grateful.

## ACKNOWLEDGEMENTS

First, I would graciously like to thank my advisor, Dr. Eniola-Adefeso, for mentoring me throughout my graduate career and having me in her lab. My graduate experience in Lola's lab has not only taught me a great deal about scientific research but also how to grow as a professional. I have always felt that Lola has a sincere investment in her students and recognizes the unique talents of each individual student, and I am glad to have been a part of that experience. I am excited to see new research publications from the lab in the future.

Second, I would also like to extend a special thank you to my committee: Dr. Eniola, Dr. Linderman, Dr. Thurber, and Dr. Violi. I am honored to have you serve on my committee. In addition, I am thankful for the helpful discussions and feedback upon completion of my PhD.

Third, thanks to all the members of the lab for help and assistance on various research projects: Ploy Charoenphol, Alex Thompson, Peter Onyskiw, Michael Heslinga, Katawut Namdee, Ted Zaroff III, Mariana Carrasco-Teja, Hanieh Safari, Margaret Fish, Genesis Lopez, William Kelly, Cathy Fromen and several others with whom I've worked. I would also like to thank Liang Zhang, Cornelius Cilliers, Dr. Fei Wen, Mason Smith, and Brett Hill for their helpful discussions about proteins and experimental techniques. Also, I am especially grateful for all participants who donated blood for my research experiments.

Lastly, I would like to thank my family and friends for their tremendous support throughout this challenging experience. Your love has meant so much to me, and I hope you know that.

## TABLE OF CONTENTS

## LIST OF TABLES

## LIST OF FIGURES

## LIST OF ABBREVIATIONS

| | |
|---|---|
| **VTC** | Vascular targeted carrier |
| **HUVEC** | Human umbilical vein endothelial cells |
| **PLGA** | Poly(lactic-co-glycolic acid) |
| **PLA** | Poly(lactic acid) |
| **PCL** | Polycaprolactone |
| **WBC** | White blood cells |
| **sLe$^a$** | Sialyl-Lewis A |
| **RBC** | Red blood cells |
| **ACD** | Acid-citrate-dextrose |
| **PEG** | Poly(ethylene glycol) |
| **PVA** | Polyvinyl alcohol |
| **VB** | Viscous buffer |
| **PPFC** | Parallel plate flow chamber |
| **PS** | Polystyrene |
| **NP** | Nanoparticle |
| **HSA** | Human serum albumin |
| **Si** | Silica |
| **Igs** | Immunoglobulins |
| **WB** | Whole blood |

**ABSTRACT**

THE IMPACT OF THE PLASMA PROTEIN CORONA ON THE ADHESION EFFICIENCY OF DRUG CARRIERS TO THE BLOOD VESSEL WALL

by

Daniel J. Sobczynski

Chair: Omolola Eniola-Adefeso

Upon injection of vascular-targeted drug carriers into the bloodstream, plasma proteins rapidly coat the carrier surface, forming a plasma protein corona. This corona is dependent on a host of parameters, including physicochemical particle properties and the plasma composition. Although several studies have identified key roles of the protein corona regarding circulation time, clearance, and biodistribution, the role of the plasma protein corona on the adhesion efficiency of vascular-targeted carriers (VTCs) to inflamed human umbilical vein endothelial cells (HUVECs) in human blood flow remains relatively unknown. In this dissertation, it is observed that the plasma protein corona exerts a negative effect on the adhesion of drug carriers in blood flow; however, the extent of these observations depend on a host of parameters including drug carrier material type, targeting ligand density, flow profile, plasma exposure time, and plasma anticoagulant. Furthermore, the magnitude of the corona-induced negative adhesion effects is shown to be heavily linked to the adsorption of immunoglobulin antibodies in plasma. This work has a variety of important implications for the intelligent design of VTCs. First, the fact that

immunoglobulins heavily dictate adhesion reduction of drug carriers offers insight into specific directions to limit the effects of the protein corona. Specifically, tuning the corona to avoid adsorption of these proteins or coating with non-fouling dysopsonin proteins offers a method to maintain targeting efficiency in the presence of corona formation. Second, this work may explain why current targeted drug delivery systems often exhibit poor accumulation to the target site based on the large reduction of particles upon exposure to human plasma. Third, this work could be used to develop strategies to predict or "diagnose" a specific drug carrier based on its protein corona profile, hopefully leading to more successful translations of drug delivery systems to the market. Overall, this work shows that protein corona is a critical parameter when designing high-efficient targeted drug carriers and may be exploited or eliminated to achieve maximum adhesion specificity *in vivo*.

# CHAPTER 1: INTRODUCTION

## 1.1 Dissertation Outline

The focus of this dissertation is on the impact of plasma protein adsorption on the adhesion efficiency of biodegradable polyester VTCs to HUVECs in human blood flow. In particular, this thesis probes a variety of parameters which are known to affect the composition of the protein corona, and thus, could play a role in modulating the adhesion efficiency of VTCs in blood flow. In addition, this work seeks to identify specific protein which may be causing the observed effects on VTC adhesion efficiency.

Chapter 1 provides the motivation to consider vascular targeting as a therapeutic strategy, highlights important VTC design criteria (particularly interaction with blood flow), reviews recent studies on VTC localization and adhesion in blood flow, and establishes the basis for considering plasma as an important parameter that prescribes VTC adhesion via experiments with PS and PLGA particles. In addition, the current understanding of plasma protein in drug delivery is reviewed as well as important parameters which affect the corona formation. Lastly, the focus and outline of this dissertation is discussed.

Chapter 2 describes the materials and methods used to complete the experimental studies in this work.

Chapter 3 seeks to elucidate the role of plasma protein adsorption on the adhesion efficiency of PLGA VTCs. In particular, various particle (size, ligand density) and blood

flow properties (shear rate, human donor) are explored to understand which parameters are critical in determining the extent of the negative plasma adhesion effect on PLGA particles.

Chapter 4 seeks to further develop understanding the source of the initially observed plasma effect with PLGA, particularly its association with immunoglobulin (Ig) proteins. Adhesion assays are performed involving presoaking of particles in plasma depleted of specific proteins, particularly immunoglobulin G (IgG), with the intent to pinpoint which proteins could be causing the negative adhesion effect. In addition, IgA, IgM, and IgG solutions are re-constituted to plasma depleted of all immunoglobulins and it is observed that IgA plays a dominant role in re-establishing corona-induced negative adhesion.

Chapter 5 explores the blood flow adhesion of other biodegradable polyesters besides PLGA, including PLA and PCL for different targeting ligands and densities.

Chapter 6 focuses on the role of plasma anticoagulant—an important parameter which can significantly affect plasma composition and thus the VTC protein corona. In addition, understanding how anticoagulant may prescribe VTC adhesion is critical in helping to bridge *in vitro* assays with VTC expectations *in vivo*, where anticoagulant is absent.

Chapter 7 provides ideas for future studies aimed at exploiting the plasma protein corona as well as a general outlook on new directions for the role of the protein corona in vascular targeting.

## 1.2 Background

### 1.2.1 Vascular targeting

Targeting drugs to the site of disease (e.g., vascular endothelium, tumor mass) is of great interest to several types of diseases, including atherosclerosis and cancer. It has enormous potential to maximize therapeutic efficacy, reduce required therapeutic dosages, and greatly mitigate side effects over systemic drug delivery. This "targeted" delivery approach has been rigorously applied to cancer and cardiovascular diseases, given the concern over deleterious side effects of current treatments such as statins and chemotherapeutics[1–5]. Vascular targeting refers to specifically targeting the diseased endothelium and represents an incredible opportunity for disease intervention given the ubiquitous involvement of vascular dysregulation (e.g. inflammation, angiogenesis) in several diseases[6–8]. Furthermore, the employment of targeted therapies designed to achieve localized delivery, facilitated via particulate drug vehicles, has shown growing promise in both preclinical and clinical models. However, there still remains a need to improve on these approaches, as at most only ~3% of "targeted" therapies actually reach the diseased region of interest[9].

### 1.2.2 Key parameters for designing VTCs

A variety of parameters must be considered when designing a VTC. First, the VTC chosen needs a high drug loading capacity and provides sustained, controlled release. Second, the VTC needs to be equipped with an appropriate targeting ligand based on the biomarkers overexpressed in the diseased cell. Third, and vitally important, the VTC must navigate the complex blood flow environment, evade immune clearance, bind to the diseased vascular endothelium, and locally release therapeutic cargo or be internalized first.

#### *1.2.2.1 Drug carrier type*

A variety of drug carrier types have been proposed for use in drug delivery and imaging applications. Some common types include soluble carriers, lipid-based carriers, and inorganic and polymer matrix nanoparticles[6]. Soluble carriers such as antibodies and modified plasma proteins maintain the advantage of easily reaching the tissue space, but are limited in their loading capacity and may jeopardize the activity of the drug since covalent linkages are commonly required[10]. Lipid-based carriers include liposomes and micelles. Liposomes are composed of a phospholipid bilayer structure and have shown improved bioavailability over conventional capsule formulations due to increased targeting/loading capability compared to soluble carriers. However, one concern of liposomes is their stability and lifetime in blood flow, where high shear forces are consistently at play, particularly in larger blood vessels. Liposomes have shown success in the market for cancer therapy and Doxil® is an example of chemotherapeutic liposomal formulation[11]. Micelles are nano-sized colloids composed of a hydrophobic core and hydrophilic shell and have proven useful in loading poorly aqueous soluble bioactive agents. Simultaneous plaque imaging and drug delivery has been achieved using dual function capabilities of micelles[12]. One disadvantage is the storage stability and limited polymer materials which are considered non-toxic to fabricate micelles. Nanoparticles represent a major class of drug carriers which are of special interest, evidenced by the vast array of literature characterizing their properties and testing their applications in preclinical models of various diseases[11,13]. Inorganic nanoparticles, such as gold, maintain robust blood stability and have been shown to cause minimal cell toxicity[14]. One limitation of these types of nanoparticles is the feasibility in achieving sustained release, since this

requires tuning of pore sizes[10]. Polymer-based nanoparticles are also of great importance to the field of drug delivery, and these include dendrimers, polymersomes, and solid-matrix nanoparticles. Dendrimers have shown success in extending the circulation time of antithrombotic agents; however, toxicity concerns have been raised regarding dendimer use. Polymersomes have a similar structure as liposomes and maintain the benefit of membrane flexibility and integrity. Solid-matrix nanoparticles, such as biodegradable poly (lactic-co-glycolic) acid (PLGA) nanoparticles are highly attractive for their robust stability, high level of control of loading/release properties, and overall versatility in tuning physical properties such as size, shape, and surface functionalization[15]. One disadvantage of biodegradable polyester nanoparticles, such as PLGA, includes the acidic environment produced as the particle degrades, which could affect the drug activity, but use of agents such as trehalose can offer solutions to this problem[16]. This thesis will focus primarily on the use of biodegradable polymer nanoparticles as potential VTCs.

#### *1.2.2.2 Targeting system*

Vascular targeting employs an active targeting approach. This involves a specific receptor-ligand interaction, as opposed to passive targeting, which is based on filtering nanoparticles to various tissues due to the size of endothelial fenestrations[17]. The receptor-ligand system of interest depends on the disease. Identification of suitable molecular targets has been greatly advanced via *in vivo* phage display, allowing for a better understanding of diseases and optimal targets in treating vascular diseases[18]. For example, a primary feature of cardiovascular diseases is a chronic inflammatory response of the arteries[6]. Inflammation of the arterial wall causes the upregulation of proteins, including cell adhesion molecules and selectins. These inflammatory proteins overexpressed on the

diseased vascular wall offer great opportunities to exploit for vascular-targeted therapies[19]. In particular, this work will focus on targeting E-selectin, which has been shown to exhibit high upregulation during inflammation and low background levels on quiescent endothelial cells[20].

#### *1.2.2.3 Hemodynamic effects*

VTCs will immediately come into contact with blood flow upon intravenous injection. Blood is a complex fluid consisting of red blood cells (RBCs), leukocytes or white blood cells (WBCs), platelets, and protein-rich plasma fluid. Furthermore, blood is dynamic and exerts hemodynamic (flow) forces on VTCs.

In order to localize and bind to the vascular wall in blood flow, a VTC must navigate this complex fluid, evade immune clearance, and dock via receptor-ligand interactions at the wall, where it can act as an imaging/drug delivery agent. As mentioned earlier, vascular diseases are often associated with a chronic inflammatory response. When inflammation occurs, WBCs via the leukocyte adhesion cascade[21] localize and bind to the vascular wall, in order to fight the infection. However, in the disease state, this process is chronic, which results in accumulation of cellular debris in the endothelium and progression of the disease. This process of leukocyte recruitment to the vascular wall during inflammation offers a model for designing VTCs to target the endothelium. Thus, a leukocyte-mimetic approach is applied here in designing VTCs, namely, by decorating VTCs with similar ligands as found on WBCs, or leukocytes. In particular, VTCs will mainly be targeted with sialyl-Lewis$^a$ (sLe$^a$), a tetrasaccharide carbohydrate which has high affinity for E-selectin. A similar version of this ligand (with lower affinity for E-selectin), sialyl-Lewis$^x$ is expressed on leukocytes, which facilitates their rolling on upregulated

selectins during inflammation[22]. It is known from the literature that RBCs impact the WBC recruitment process to the vascular wall, and thus it is expected that VTC adhesion would also be impacted by the complex nature of the blood environment[23]. Surprisingly, early work characterizing the adhesion of drug carriers in flow was often done in the absence of RBCs or at a sub-physiological level of RBCs, which thus limits how these results would translate to the whole blood environment *in vivo*[24–27]. In addition, limited studies probed the role of particle size on adhesion, and often the results were performed in non-physiological environments or assumed particles were already close to the wall, neglecting the impact of navigating the complex flow environment[28,29]. Recent studies from our lab and others has focused on probing the role of RBCs, WBCs, flow profile, shear rate, as well as physiochemical properties of the VTCs on prescribing the adhesion efficiency of VTCs in human blood flow at physiologically relevant conditions[30–35]. Several key results have been observed but a paramount conclusion is that particle size plays an important role in the adhesion efficiency of VTCs in blood flow. Specfiically, microparticles vastly outperform the localization and adhesion of nanoparticles at a fixed concentration and ligand density[30–32]. Microparticles ~3 μm in diameter exhibit optimal adhesion at high shear rates (~1500 $s^{-1}$) associated with cardiovascular diseases. Similar to WBCs, microparticles enjoy near wall excess effects from RBCs, resulting in better localization and adhesion than smaller nano-sized particles[30,34]. The poor adhesion of nanoparticles in comparison is largely attributed to their ineffective transport to the vascular wall, and thus, the nanoparticles remain co-localized in the RBC core, limiting near wall excess effects and thus probability to reach and bind to the vascular wall in blood flow. Larger microparticles of 5 μm in diameter show better adhesion in some instances, but also more

sensitivity to negative WBC effects, shear forces, and overall too large a size for any intravenous application. Despite the perceived benefits of efficient microparticle adhesion, nanoparticles remain critical to the drug delivery field for their ease in navigating the microcirculation, evasion of systemic clearance, and overall better internalization efficiency. Thus, work in our lab has and continues to pursue options for improvement of nanoparticle adhesion for vascular targeting applications. Some avenues currently being explored include particle shape, density, and rigidity[36–38].

### 1.2.3 Translation of *in vitro* blood flow assays to biodegradable systems

Undoubtedly, important knowledge regarding how hemodynamic properties of blood affect VTC adhesion was gained in the experimental studies from our lab and computational work by others. However, one limitation of the experimental studies from our lab was the use of polystyrene (PS) micro/nanoparticles, which are not viable for drug delivery applications and known to be toxic. Thus, the transition to biodegradable systems is a relevant next step in better understanding VTC design for vascular targeting applications. Initially, an experiment is performed which compares PS and PLGA 2 μm particles in whole blood and buffer flow (Fig. 1.1). As seen in the case of blood flow, PLGA adhesion is substantially reduced relative to PS. As mentioned earlier, blood is complex, composed of RBCs, WBCs, platelets, and protein-rich plasma, all of which may be responsible for the observed low adhesion of PLGA particles. Studies performed by

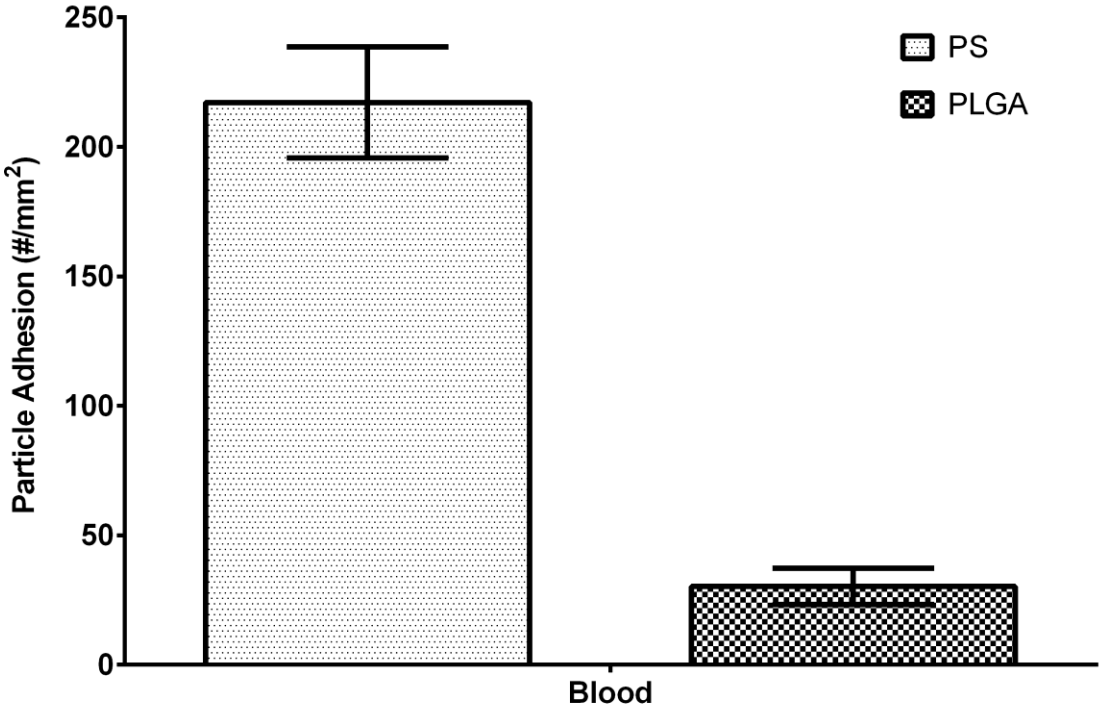


**Figure 1.1** HUVEC adhesion of sLea-targeted (~800 sites/μm$^2$) PS and PLGA 2 μm particles in human whole blood flow in a parallel plate flow chamber (PPFC) at 200 s-1 for 5 mins at a concentration of $5 \times 10^5$ particles/mL.

Charoenphol et al. showed that the presence of RBCs increases adhesion density of micro/nanoparticles by providing a normal force on the particle in flow; thus, it would be expected that the effect exerted by RBCs on PS particles would be the same on PLGA VTCs, since RBCs are relatively inert and are not involved in any phagocytic mechanisms. Activated WBCs, on the other hand, have a higher propensity to interact with particles as studies from our lab have shown potential negative-adhesion events on VTCs due to WBCs. However, these negative-adhesion effects of WBCs were seen only in pulsatile flow environments and occurred at the point of adhesion due to physical effects, not molecular[32]. WBCs could potentially engulf particles in the bloodstream, but this is likely not the case since PS binding doesn't show any such impact. Furthermore, the anticoagulant being employed is acid-citrate-dextrose (ACD) which chelates $Ca^{2+}$ ions, thus limiting the probability of phagocytosis in general. Platelets are not expected to be involved in prescribing VTC adhesion based on previous work with PS spheres[32]. Thus, since plasma is the remaining major component in blood, it is the hypothesis and instinct that plasma is a player in this observed differential adhesion between PS and PLGA.

However, this seems counterintuitive, since cellular adhesion is classically understood as a force-driven process governed by the strength of the receptor/ligand system, which is largely influenced by parameters such as particle size, local shear forces, and receptor/ligand densities[25]. Interestingly, these parameters are expected to be essentially constant between PS and PLGA in this experiment. Based on these initial results, the overarching aim of this thesis is to elucidate the potential role of plasma protein adsorption on the adhesion efficiency of VTCs in human blood flow, which remains relatively unknown. A vast array of literature, however, does discuss the relevance of

plasma protein adsorption in drug delivery processes such as cell signaling and clearance mechanisms.

### 1.2.4 The plasma protein corona

When a particle is exposed to blood plasma (e.g., intravenous injection), protein adsorption onto the particle surface occurs in seconds, forming what is typically referred to as the "plasma protein corona"[39]. The plasma protein corona is known to influence several key drug delivery processes and the literature has shown growing interest in understanding the corona's significance to the field of targeted drug delivery[40]. Plasma is a highly complex protein solution, consisting of over 3,700 proteins, and thus the resulting plasma protein corona formed on nanoparticles comprises various types of proteins each with unique association/dissociation kinetics. The corona is classically understood via the Vroman effect, where highly abundant (low affinity) proteins such as albumin are replaced over time by scarce (high affinity) proteins; however, recent works have suggested this may not entirely explain the dynamics of corona formation[40–42]. The plasma protein corona varies significantly based on physicochemical properties of the nanoparticle, the physiological environment (e.g. plasma composition or type), and exposure time to the nanoparticle. The plasma protein corona alters the nanoparticle interface, resulting in a new biological identity of the nanoparticle. This new identity is often referred to as what the cell actually "sees" rather than the pristine nanoparticle surface. This nanoparticle biological identity determines various aspects of the physiological response, including toxicity, cell uptake, circulation time, biodistribution, and recently, implications in targeting. This section will provide details of factors governing plasma protein corona

formation followed by a discussion of the current understanding of the role of the plasma protein adsorption in drug delivery processes.

#### *1.2.4.1 Key parameters governing plasma protein corona formation*

Gessner et al. probed the impact of surface charge on plasma protein adsorption with hydrophobicity kept relatively constant across the differentially charged particles[43]. Overall, increasing the surface charge changed only the amount of protein in the corona, but did not change the specific types of proteins. Generally, increases in surface charge density were met with an increase in the amount of protein adsorption. The increase in protein adsorption amount over surface charge density is attributed mainly to Coulombic forces and less to van der Waal's forces since the particles are of similar hydrophobicity. The results of this study contribute to understanding plasma protein adsorption at a fundamental level. The expectations, based on this investigation, are that a moderate surface charge gradient should leave the protein adsorption profile unaffected. In another study, cationic vesicles showed heavy binding of plasma proteins, another example of electrostatic interactions driving the extent of plasma protein adsorption[36]. Surface charge may also affect the conformation of the protein being adsorbed, as seen in the case of gold nanoparticles where charged ligands resulted in denaturing of the adsorbed protein[44].

Hydrophobicity can affect both the type and amount of proteins formed in the corona. In another study by Gessner et al., it was found that decreasing the surface hydrophobicity and keeping all other parameters constant, led to decreased protein adsorption as well as changes in the composition of the protein corona[45]. Surface hydrophobicity was observed to affect both the amount and composition of the protein corona; however, these results could also be influenced by the fact that different functional

groups were employed to achieve different hydrophobicity. In other reports, it has been observed that hydrophobic particles tend to adsorb more protein and also increase the extent of protein denaturation relative to hydrophilic or neutral particles[39]. The enhanced protein binding of hydrophobic particles is thought to be linked to the clustering of hydrophobic chains, which result in protein binding patches on the surface. In general, hydrophobic particles tend to have a greater affinity for albumin compared to hydrophilic ones[39]. Overall, similar to surface charge, increasing the particle hydrophobicity leads to greater protein adsorption, but hydrophobicity has also been observed to affect the type and, therefore, composition of the protein corona.

Nanoparticle material type is another parameter which greatly affects the type of proteins adsorbed in the corona. A study by Deng et al. showed that different metal oxide nanoparticles of similar size and nearly equal zeta potential, adsorbed widely different plasma protein profiles[46]. In addition, differences in protein corona composition has been observed between single-walled carbon nanotubes and silica nanospheres[47]. A different study showed that the extent and type of adsorbed proteins on PLA, PCL, and polyanhydride poly(ethylene glycol) (PEG) particles varied significantly, potentially linked to differences in hydrophobicity[48].

It is known that the binding affinity of proteins depends on surface curvature, which varies with particle size. For instance, α-Synuclein binding affinity to lipid vesicles increased >15 fold on smaller particles relative to larger ones[49]. In the case of gold nanoparticles, increased protein adsorption has been observed on 30 nm versus 50 nm particles[47]. Over larger size ranges of nanoparticles from 70 – 700 nm, the amount of protein binding was shown to scale with available surface area[50]. Larger sized particles

have been observed to more likely cause protein denaturation upon adsorption. This was observed in the case of silica nanoparticles (20 versus 100 nm) where the larger 100 nm particles caused significant loss in α-helicity of adsorbed lysozyme protein[51]. In addition, thicker protein coronas have been observed with larger particles[39]. Overall, size can significantly affect the composition of the protein corona, particularly when the particle diameter is on the size scale of individual proteins[50].

One parameter unchanged in all the previous blood flow adhesion work with PS particles from our lab was the choice of anticoagulant. Experiments from our lab over the last decade have always employed acid-citrate-dextrose (ACD) as the working anticoagulant. The literature has shown that the type of anticoagulant affects properties of blood cells (particularly leukocyte uptake of particles)[52], as well as the plasma protein composition[53,54]. Thus, the plasma composition in ACD versus heparinized (another common anticoagulant) blood is different. In addition, serum (contains no anticoagulant) also shows a unique protein composition compared to plasma. A major difference in protein composition between serum and plasma is the absence of fibrinogen and other clotting-related proteins[54]. A recent study has shown that the differences in plasma versus serum protein composition results in unique protein coronas formed on silica nanoparticles[52]. Thus, in addition to physicochemical properties of the nanoparticles, the plasma environment (i.e. type of/presence of anticoagulant) is an important parameter which could influence plasma-associated adhesion effects on drug carrier adhesion in blood flow. In addition, it is of great importance to probe the role of anticoagulant to provide a better platform for translation of *in vitro* assays involving drug carriers interaction with blood to *in vivo*/clinical studies where plasma is not artificially anticoagulated.

### *1.2.4.2 Role of plasma protein corona in uptake, circulation time, and biodistribution*

Plasma protein adsorption onto nanoparticles causes opsonization, a process by which any foreign material (e.g. nanoparticles) in the bloodstream are coated with primarily complement and immunoglobulin proteins which mark the foreign substance for engulfment by the mononuclear phagocytic system (MPS) via Fc receptor interaction leading to clearance from the blood circulation[55]. In the case of developing targeted drug delivery systems, rapid clearance of particles from the bloodstream is a highly unwanted phenomenon as this potentially jeopardizes the impact of the particle for an application. Correlations between protein adsorption and clearance time have been studied by Chonn et al., where increased adsorption of beta 2-glycoprotein 1 resulted in shorter clearance times of negatively charged liposomes[56]. In another study, Schreier suggested the role of fibronectin protein in the clearance of liposomes[57]. In general, it has been observed that highly charged, hydrophobic particles lead to greater protein adsorption, which tends to result in higher and faster opsonization/uptake rates in plasma/serum than observed with neutral particles, which would be expected result in shorter clearance times[58]. In addition, particles with increasing hydrophobicity tend to adsorb more proteins which results in faster uptake rates[58]. Another study has probed the role of PEGylated nanoparticle size on macrophage uptake in the presence of serum and shown that larger particles (90 nm) were more efficient at being taken up than the smaller 15 nm particles[59]. Overall, the effect of serum/plasma protein adsorption on cellular uptake of nanoparticles significantly depend on the nanoparticle material type studied as well as physicochemical properties such as hydrophobicity, surface charge, material type, and particle size.

Given the tendency of particulate delivery systems to be cleared rapidly from circulation by phagocytosis due to plasma protein adsorption, widespread use of "stealth" mechanisms on particles designed to limit protein adsorption, increase *in vivo* circulation time and prevent interactions with the immune system have been explored. Potential avenues for limiting plasma protein adsorption often include the use of PEGylation[48,55,60]. PEGylation has long been known to limit protein adsorption by creating a hydrophilic layer and steric repulsion of proteins[61,62]. Thus, it is of interest to explore the possibility that PEG may eliminate, or at least, greatly reduce the negative plasma protein effects on VTCs. However, this may be a challenging because stealth effects are reduced when adding targeting ligands to PEGylated drug carriers. Properties of the targeting ligand and PEG density, molecular weight, and conformation can dramatically impact ligand affinity and VTC specificity, as well as corona presence and circulation time[60,63–66]. A debate remains whether PEGylated VTCs are truly free of the plasma effects *in vivo*[48,60,67,68], and PEGylation may never completely limit protein adsorption on VTCs. In addition, prolonged circulation time via PEGylation, liver and spleen accumulation will still comprise a majority of the injected dose. Other hydrophilic coatings such as poloxamers have been applied to increase circulation lifetime and decrease macrophage recognition similar to PEG.

Longer circulation times due to PEGylation of nanoparticles potentially offers better drug distribution throughout the body. In the case of quickly opsonized particles, rapid accumulation of nanoparticles in the liver and spleen may limit the potential for a nanoparticle to accumulate in the organ of interest. Like PEGylation, the adsorption of dysopsonin proteins like albumin and apolipoproteins may have stealth-like qualities as

adsorption of these proteins has been observed to decrease liver uptake and increase circulation time. Preferential adsorption of specific plasma proteins such as apolipoproteins has been observed to cause preferential uptake to brain endothelial cells, resulting in higher distribution to this organ[69]. In this instance, the protein corona may be highly beneficial if targeting the brain is of interest to the application. In another example, the preferential adsorption/covalent attachment of dysopsonin proteins such as albumin behave like PEGylated particles, evidenced by albumin helping nanoparticles to evade opsonization and uptake the immune system[70]. There also have been instances where receptor-mediated cell uptake is hindered due to protein adsorption, as observed by Salvati et al., where transferrin-targeted nanoparticles showed reduced uptake in serum via obstruction between the transferrin ligand/receptor system, suggesting that serum proteins crowd the surface and prevent the particle from interacting with its ligand[68].

Overall, the plasma protein corona impacts various processes such as particle circulation time, biodistribution, and cellular uptake. Furthermore, this is compounded by the fact that the formation of the plasma protein corona is heavily dependent on a host of physicochemical properties of nanoparticles, particularly surface charge, material (hydrophobicity), and size/curvature as well as the nature of the plasma (i.e. anticoagulant type or its absence). Although important knowledge has been gained by these studies characterizing the formation of the corona and its role in drug delivery relevant processes, the role of the protein corona on the adhesion efficiency of VTCs in human blood flow remains relatively unknown. Thus, the focus of this thesis is to elucidate the role that the plasma protein corona plays in the context of VTC adhesion in human blood flow via an *in vitro* parallel plate flow chamber. Specifically, this work will first probe PLGA-

associated plasma adhesion effects for a variety of parameters classically known to impact VTC adhesion (e.g. shear rate, flow profile, ligand density) as well as physicochemical properties of the particle (size, ligand density, ligand type). Furthermore, this corona-induced effect is found to be linked to the adsorption of large molecular weight proteins (i.e. immunoglobulins) and the impact of this protein class in causing these effects is explored in the following chapter. Another aspect of this thesis will evaluate the blood flow adhesion of other biodegradable materials besides PLGA, including PLA and PCL. In addition, a chapter will be dedicated to exploring the role of plasma anticoagulant (and its absence) on VTC adhesion efficiency since plasma is not a universal medium and recent work has shown that the choice of anticoagulant can have profound effects on the corona composition and thus may prescribe the corona-induced VTC adhesion effects. Understanding the role of anticoagulant is also important for translating/predicting VTC adhesion for eventual use in humans where anticoagulant is absent.

## References


1. Gotto, A. M. Risks and Benefits of Continued Aggressive Statin Therapy. *Clin. Cardiol.* **26,** 3–12 (2003).

2. O'Brien, M. E. R. *et al.* Mortality within 30 days of chemotherapy: a clinical governance benchmarking issue for oncology patients. *Br. J. Cancer* **95,** 1632–6 (2006).

3. Steichen, S. D., Caldorera-Moore, M. & Peppas, N. A. A review of current nanoparticle and targeting moieties for the delivery of cancer therapeutics. *Eur. J. Pharm. Sci.* **48,** 416–427 (2013).

4. Brannon-Peppas, L. & Blanchette, J. O. Nanoparticle and targeted systems for cancer therapy. *Adv. Drug Deliv. Rev.* **64,** 206–212 (2012).

5. Ray, K. *et al.* Statins and All-Cause Mortality in High-Risk Primary Prevention: A Meta-analysis of 11 Randomized Controlled Trials Involving 65,229 Participants. *Arch. Intern. Med.* **170,** 1024–1031 (2010).

6. Libby, P., Ridker, P. M. & Maseri, A. Inflammation and atherosclerosis. *Circulation* **105,** 1135–1143 (2002).

7. Coussens, L. M. & Werb, Z. Inflammation and cancer. *Nature* **420,** 860–867 (2002).

8. Bikfalvi, A. & Bicknell, R. Recent advances in angiogenesis, anti-angiogenesis and vascular targeting. *Trends Pharmacol. Sci.* **23,** 576–582 (2002).

9. Bae, Y. H. & Park, K. Targeted drug delivery to tumors: Myths, reality and possibility. *J Control Release* **153,** 198–205 (2011).

10. Eniola-Adefeso, O., Heslinga, M. J. & Porter, T. M. Design of nanovectors for therapy and imaging of cardiovascular diseases. *Methodist Debakey Cardiovasc. J.* **8,** 13–17 (2012).

11. Malam, Y., Loizidou, M. & Seifalian, A. M. Liposomes and nanoparticles: nanosized vehicles for drug delivery in cancer. *Trends Pharmacol. Sci.* **30,** 592–9 (2009).

12. Torchilin, V. P. Micellar nanocarriers: Pharmaceutical perspectives. *Pharm. Res.* **24,** 1–16 (2007).

13. Kamaly, N., Xiao, Z., Valencia, P. M., Radovic-Moreno, A. F. & Farokhzad, O. C. Targeted polymeric therapeutic nanoparticles: design, development and clinical translation. *Chem. Soc. Rev.* **41,** 2971–3010 (2012).

14. Ghosh, P., Han, G., De, M., Kim, C. K. & Rotello, V. M. Gold nanoparticles in delivery applications. *Adv. Drug Deliv. Rev.* **60,** 1307–1315 (2008).

15. Danhier, F. *et al.* PLGA-based nanoparticles : An overview of biomedical applications. *J. Control. Release* **161,** 505–522 (2012).

16. Gupta, P. N. *et al.* Lectin anchored stabilized biodegradable nanoparticles for oral immunization 1. Development and in vitro evaluation. *Int. J. Pharm.* **318,** 163–73 (2006).

17. Wang, M. & Thanou, M. Targeting nanoparticles to cancer. *Pharmacol. Res.* **62,** 90–9 (2010).

18. Hajitou, A., Pasqualini, R. & Arap, W. Vascular targeting: recent advances and therapeutic perspectives. *Trends Cardiovasc. Med.* **16,** 80–88 (2006).

19. Ulbrich, H., Eriksson, E. E. & Lindbom, L. Leukocyte and endothelial cell adhesion molecules as targets for therapeutic interventions in inflammatory disease. *Trends Pharmacol. Sci.* **24,** 640–647 (2003).

20. Barthel, S. R., Gavino, J. D., Descheny, L. & Dimitroff, C. J. Targeting selectins and selectin ligands in inflammation and cancer. *Expert Opin. Ther. Targets* **11,** 1473–1491 (2007).

21. Springer, T. A. Traffic signals for lymphocyte recirculation and leukocyte emigration: The multistep paradigm. *Cell* **76,** 301–314 (1994).

22. Eniola, A. O., Willcox, P. J. & Hammer, D. A. Interplay between rolling and firm adhesion elucidated with a cell-free system engineered with two distinct receptor-ligand pairs. *Biophys. J.* **85,** 2720–31 (2003).

23. Munn, L. L., Melder, R. J. & Jain, R. K. Role of erythrocytes in leukocyte-endothelial interactions: mathematical model and experimental validation. *Biophys. J.* **71,** 466–478 (1996).

24. Patil, V. R. S., Campbell, C. J., Yun, Y. H., Slack, S. M. & Goetz, D. J. Particle Diameter Influences Adhesion under Flow. *Biophys. J.* **80,** 1733–1743 (2001).

25. Decuzzi, P., Lee, S., Bhushan, B. & Ferrari, M. A Theoretical Model for the Margination of Particles within Blood Vessels. *Ann. Biomed. Eng.* **33,** 179–190 (2005).

26. Gentile, F., Curcio, A., Indolfi, C., Ferrari, M. & Decuzzi, P. The margination propensity of spherical particles for vascular targeting in the microcirculation. *J. Nanobiotechnology* **6,** 9 (2008).

27. Eckstein, E. C., Tilles, A. W. & Millero, F. J. Conditions for the occurrence of large near-wall excesses of small particles during blood flow. *Microvasc. Res.* **36,** 31–39 (1988).

28. Deosarkar, S. P. *et al.* Polymeric particles conjugated with a ligand to VCAM-1 exhibit selective, avid, and focal adhesion to sites of atherosclerosis. *Biotechnol. Bioeng.* **101,** 400–407 (2008).

29. Nahrendorf, M. *et al.* Noninvasive vascular cell adhesion molecule-1 imaging identifies inflammatory activation of cells in atherosclerosis. *Circulation* **114,** 1504–1511 (2006).

30. Namdee, K., Thompson, A. J., Charoenphol, P. & Eniola-adefeso, O. Margination Propensity of Vascular-Targeted Spheres from Blood Flow in a Micro fluidic Model of Human Microvessels. *Langmuir* **29,** 2530–2535 (2013).

31. Charoenphol, P., Huang, R. B. & Eniola-Adefeso, O. Potential role of size and hemodynamics in the efficacy of vascular-targeted spherical drug carriers. *Biomaterials* **31,** 1392–1402 (2010).

32. Charoenphol, P., Onyskiw, P. J., Carrasco-Teja, M. & Eniola-Adefeso, O. Particle-cell dynamics in human blood flow: implications for vascular-targeted drug delivery. *J. Biomech.* **45,** 2822–2828 (2012).

33. Charoenphol, P. *et al.* Targeting therapeutics to the vascular wall in atherosclerosis--carrier size matters. *Atherosclerosis* **217,** 364–370 (2011).

34. Lee, T.-R. *et al.* On the near-wall accumulation of injectable particles in the microcirculation: smaller is not better. *Sci. Rep.* **3,** 2079 (2013).

35. Müller, K., Fedosov, D. a & Gompper, G. Margination of micro- and nano-particles in blood flow and its effect on drug delivery. *Sci. Rep.* **4,** (2014).

36. Thompson, A. J., Mastria, E. M. & Eniola-Adefeso, O. The margination propensity of ellipsoidal micro/nanoparticles to the endothelium in human blood flow. *Biomaterials* **34,** 5863–5871 (2013).

37. Thompson, A. J. & Eniola-Adefeso, O. Dense nanoparticles exhibit enhanced vascular wall targeting over neutrally buoyant nanoparticles in human blood flow. *Acta Biomater.* **21,** 99–108 (2015).

38. Doshi, N., Zahr, A. S., Bhaskar, S., Lahann, J. & Mitragotri, S. Red blood cell-mimicking synthetic biomaterial particles. *Proc. Natl. Acad. Sci. U. S. A.* **106,** 21495–9 (2009).

39. Rahman, M., Laurent, S., Tawil, N., Yahia, L. H. & Mahmoudi, M. *Protein-Nanoparticle Interactions*. (Springer, 2013).

40. Monopoli, M. P. *et al.* Physical-Chemical aspects of protein corona: Relevance to in vitro and in vivo biological impacts of nanoparticles. *J. Am. Chem. Soc.* **133,** 2525–2534 (2011).

41. Dell'Orco, D., Lundqvist, M., Oslakovic, C., Cedervall, T. & Linse, S. Modeling the time evolution of the nanoparticle-protein corona in a body fluid. *PLoS One* **5,** e10949 (2010).

42. Tenzer, S. *et al.* Rapid formation of plasma protein corona critically affects nanoparticle pathophysiology. *Nat. Nanotechnol.* **8,** 772–781 (2013).

43. Gessner, A., Lieske, A., Paulke, B. R. & Mu, R. H. Influence of surface charge density on protein adsorption on polymeric nanoparticles : analysis by two-dimensional electrophoresis. *Eur. J. Pharm. Biopharm.* **54,** 165–170 (2002).

44. Walkey, C. D. & Chan, W. C. W. Understanding and controlling the interaction of nanomaterials with proteins in a physiological environment. *Chem. Soc. Rev.* **41,** 2780–2799 (2012).

45. Gessner, A., Waicz, R., Lieske, A., Paulke, B. & Ma, K. Nanoparticles with decreasing surface hydrophobicities : influence on plasma protein adsorption. *Int. J. Pharm.* **196,** 245–249 (2000).

46. Deng, Z. J. *et al.* Differential plasma protein binding to metal oxide nanoparticles. *Nanotechnology* **20,** 455101 (2009).

47. Dobrovolskaia, M. A. *et al.* Interaction of colloidal gold nanoparticles with human blood : effects on particle size and analysis of plasma protein binding profiles. *Nanomedicine Nanotechnology, Biol. Med.* **5,** 106–117 (2009).

48. Gref, R., Lück, M. & Quellec, P. 'Stealth'corona-core nanoparticles surface modified by polyethylene glycol (PEG): influences of the corona (PEG chain length and surface density) and of the core. *Colloids Surfaces B Biointerfaces* **18,** 301–313 (2000).

49. Middleton, E. R. & Rhoades, E. Effects of curvature and composition on α-synuclein binding to lipid vesicles. *Biophys. J.* **99,** 2279–2288 (2010).

50. Lynch, I. & Dawson, K. a. Protein-nanoparticle interactions. *Nano Today* **3,** 40–47 (2008).

51. Vertegel, A. A., Siegel, R. W. & Dordick, J. S. Silica nanoparticle size influences the structure and enzymatic activity of adsorbed lysozyme. *Langmuir* **20,** 6800–6807 (2004).

52. Baumann, D. *et al.* Complex encounters: nanoparticles in whole blood and their uptake into different types of white blood cells. *Nanomedicine* **8,** 699–713 (2012).

53. Mirshafiee, V., Kim, R., Mahmoudi, M. & Kraft, M. L. The importance of selecting a proper biological milieu for protein corona analysis in vitro : human plasma vs . human serum. *Int. J. Biochem. Cell Biol.* (2015).

54. Ayache, S. *et al.* Comparison of proteomic profiles of serum, plasma, and modified media supplements used for cell culture and expansion. *J. Transl. Med.* **4,** 40 (2006).

55. Owens, D. E. & Peppas, N. A. Opsonization, biodistribution, and pharmacokinetics of polymeric nanoparticles. *Int. J. Pharm.* **307,** 93–102 (2006).

56. Chonn, A., Semple, S. C. & Cullis, P. R. Beta 2 glycoprotein I is a major protein associated with very rapidly cleared liposomes in vivo, suggesting a significant role in the immune clearance of 'non-self' particles. *J. Biol. Chem.* **270,** 25845–25849 (1995).

57. Schreier, H., Abra, M. I., Kaplan, J. E. & Anthony, C. Murine plasma fibronectin depletion after intravenous injection of liposomes. *Int. J. Pharm.* **37,** 233–238 (1987).

58. Aggarwal, P., Hall, J. B., McLeland, C. B., Dobrovolskaia, M. a & McNeil, S. E. Nanoparticle interaction with plasma proteins as it relates to particle biodistribution, biocompatibility and therapeutic efficacy. *Adv. Drug Deliv. Rev.* **61,** 428–437 (2009).

59. Walkey, C. D., Olsen, J. B., Guo, H., Emili, A. & Chan, W. C. W. Nanoparticle size and surface chemistry determine serum protein adsorption and macrophage uptake. *J. Am. Chem. Soc.* **134,** 2139–2147 (2012).

60. Dai, Q., Walkey, C. & Chan, W. C. W. Polyethylene glycol backfilling mitigates the negative impact of the protein corona on nanoparticle cell targeting. *Angew. Chem. Int. Ed. Engl.* **53,** 5093–5096 (2014).

61. Wattendorf, U. & Merkle, H. P. PEGylation as a tool for the biomedical engineering of surface modified microparticles. *J. Pharm. Sci.* **97,** 4655–4669 (2008).

62. Ham, A. S., Klibanov, A. L. & Lawrence, M. B. Action at a distance: Lengthening adhesion bonds with Poly(ethylene glycol) spacers enhances mechanically stressed affinity for improved vascular targeting of microparticles. *Langmuir* **25,** 10038–10044 (2009).

63. Onyskiw, P. J. & Eniola-Adefeso, O. Effect of PEGylation on Ligand-Based Targeting of Drug Carriers to the Vascular Wall in Blood Flow. *Langmuir* **29,** 11127–11134 (2013).

64. Liu, T. & Thierry, B. A solution to the PEG dilemma: Efficient bioconjugation of large gold nanoparticles for biodiagnostic applications using mixed layers. *Langmuir* **28,** 15634–15642 (2012).

65. Hatakeyama, H., Akita, H. & Harashima, H. A multifunctional envelope type nano device (MEND) for gene delivery to tumours based on the EPR effect: A strategy for overcoming the PEG dilemma. *Adv. Drug Deliv. Rev.* **63,** 152–160 (2011).

66. Hennig, R., Pollinger, K., Veser, A., Breunig, M. & Goepferich, A. Nanoparticle multivalency counterbalances the ligand affinity loss upon PEGylation. *J. Control. Release* **194,** 20–27 (2014).

67. Kang, B. *et al.* Carbohydrate-Based Nanocarriers Exhibiting Specific Cell Targeting with Minimum Influence from the Protein Corona. *Angew. Chemie - Int. Ed.* **54,** 7436–7440 (2015).

68. Salvati, A. *et al.* Transferrin-functionalized nanoparticles lose their targeting capabilities when a biomolecule corona adsorbs on the surface. *Nat. Nanotechnol.* **8,** 137–143 (2013).

69. Wagner, S. *et al.* Uptake mechanism of ApoE-modified nanoparticles on brain capillary endothelial cells as a blood-brain barrier model. *PLoS One* **7,** e32568 (2012).

70. Yasuhik, T. & Ikada, Y. Phagocytosis of Polymer Microspheres by Macrophages. *New Polym. Mater.* 107–141 (1990).

# CHAPTER 2: MATERIALS AND METHODS

This chapter describes the procedures and materials used to complete the experimental *in vitro* flow assays described throughout this work. Detailed descriptions are provided to allow for reproduction of the results.

## 2.1 Particles used for *in vitro* flow assays

### 2.1.1 Biodegradable particles

#### *2.1.1.1 PLGA microparticle fabrication*

PLGA 5 μm particles were fabricated using a commonly employed oil-in-water solvent evaporation technique[1,2]. Briefly, 50:50 PLGA polymer with carboxylated end groups purchased from Evonik Industries (Parsippany, NJ) was dissolved in 20 mL of dichloromethane at ~2 mg/mL (oil phase) and injected into 90 mL polyvinyl alcohol (PVA) containing poly(ethylene-*alt*-maleic anhydride) (PEMA) for two hrs at 1800 rpm using a Lightnin' mixer, allowing for evaporation of the dicholormethane and formation of solid particles. Differential centrifugation was employed to narrow the particle size polydispersity and reduce the amount of residual PVA. Particle solutions were then lyophilized overnight and the dry powder stored at -20°C until use.

#### *2.1.1.2 Purchased nanoparticles*

Fluorescent and blank carboxylated 500 nm and 2 μm PLGA particles as well as 500 nm polylactic acid (PLA) and polycaprolactone (PCL) carboxylated particles were purchased from Phosphorex, Inc. (Hopkinton, MA).

### 2.1.2 Non-biodegradable particles

Green fluorescent carboxylated Si (Cat# 140574-10) and PS 500 nm particles were purchased from Corpuscular (Cold Spring, NY) and Polysciences, Inc. (Warrington, PA) as a comparison with the biodegradable materials. PS carboxylated 2 μm particles were purchased from Bangs Laboratories, Inc.

## 2.2 Particle characterization

### 2.2.1 Concentration

Particle concentration was measured using a hemacytometer (Hausser-Scientific). Blank PLGA, PLA, and PCL 500 nm particles were diluted and stained with biotin-PE to allow visualization of particles prior to manual counting.

### 2.2.2 DLS sizing

VTC size was measured by dynamic light scattering (DLS) using a Malvern Zetasizer instrument. Carboxylated stocks were dispersed in PBS++, with 1% bovine serum albumin (BSA) and then washed with 50 mM PBS prior to making the DLS measurement. Carboxylated biodegradable PLGA, PLA, and PCL particles were soaked in 50 mM MES at pH 7 (for PCL, pH ~5) for $\geq$ 20 hr prior to DLS measurement which corresponds to the time required for NeutrAvidin conjugation to these particles. Particle concentrations tested for DLS measurements ranged from $10^8$-$10^9$ #particles/mL as this concentration range was observed to yield the most reliable results.

### 2.2.3 Zeta potential

Zeta potential measurements were obtained using the Malvern Zetasizer instrument. Concentration of particles in deionized water varied from 0.65 to $2.5 \times 10^7$ #particles/mL which is similar to the concentrations used in the flow assays. Zeta potential

was measured for particles soaked in buffer, plasma, and serum with subsequent washing in deionized water prior to the measurement.

### 2.2.4 Surface ligand conjugation

#### *2.2.4.1 NeutrAvidin, albumin conjugation*

Particle stocks were first conjugated with NeutrAvidin via covalent carbodiimide chemistry followed by linkage to biotinylated sialyl-Lewis$^a$ (sLe$^a$) (Glycotech Corporation) or anti-ICAM-1 (R&D Systems). The coupling of NeutrAvidin has been described elsewhere[3]. Briefly, an approximate particle surface area of $9.1 \times 10^9$ μm$^2$/mL of conjugation volume was used. The conjugation volume consisted of equal parts NeutrAvidin (5 mg/mL) and *N*-Ethyl-*N*′-(3-dimethylaminopropyl) carbodiimide hydrochloride (EDAC) (Sigma) (75 mg/mL) dissolved in 50 mM 2-(*N*-morpholino)ethanesulfonic acid (MES) buffer. VTCs were first incubated with 5 mg/mL NeutrAvidin for 15 min, followed by addition of an equal volume of EDAC at 75 mg/mL. 1 M sodium hydroxide (NaOH) was added (~47 μL/mL conjugation volume) to pH the solution to ~7.4 and allowed to rotate on an end-to-end rotator for ~20 hr. For PCL VTCs, no NaOH was added as this caused precipitation during the overnight conjugation process, and thus the reaction was carried out at pH ~5. Following the 20-hr incubation step, ~7.5 mg glycine/mL was added to the conjugation solution stop the crosslinking reaction and allowed to incubate for 30 min. Conjugated VTCs were washed and re-suspended in 1 mL of 50 mM phosphate buffered saline (PBS).

For some assays, human serum albumin (HSA) was covalently linked to the surface of PLGA particles by adding in a 4:1 ratio with NeutrAvidin with a final concentration of 10 mg/mL HSA and 2.5 mg/mL NeutrAvidin.

#### *2.2.4.2 sLe$^a$, anti-ICAM-1, and polyethylene glycol (PEG) conjugation*

Attachment of targeting ligands was performed by suspending NeutrAvidin coated particles in 100 μL of biotinylated sLe$^a$ or anti-ICAM-1 (dissolved in PBS with calcium and magnesium (PBS++) with 1% BSA) at concentrations ranging from 0.4 to 10 μg/mL. Surface area to volume ratio of the various VTCs was varied to achieve the desired ligand site density. NeutrAvidin-coated particles were allowed to rotate in the targeting ligand solutions for 45 mins, and then washed 3 times with PBS++ 1% BSA buffer and suspended in a final volume of 1 mL.

For PEGylated PLGA particle assays, PLGA particles were grafted with PEG chains prior to targeting ligand conjugation, as previously described[4]. Briefly, amine-PEG (5 kDa)-biotin was covalently linked to the PLGA surface in the same manner as described with NeutrAvidin. For ligand conjugation onto the PEG, biotinylated sLe$^a$ was premixed with 20 μg/mL of NeutrAvidin at an equal volume ratio for 20 mins. This premixed solution was then allowed to incubate for 45 mins with the PEGylated PLGA particles.

### 2.2.5 sLe$^a$, anti-ICAM-1, PEG and albumin density quantification

sLe$^a$ ligand density was quantified via flow cytometry using an Attune flow cytometer (Applied Biosystems) as described elsewhere[3]. For quantifying sLe$^a$ density, 0.5-1 × $10^6$ particles were incubated for 20 mins in a 1:10 solution (100 μL volume) of anti-CLA-PE (Miltenyi Biotec). Following the incubation step, VTCs were washed 3 times with PBS++ with 1% BSA buffer and suspended in a final volume of 1 mL. Rat-IgM-PE (Fisher Scientific) was used as the isotype control. Quantification of the number of ligand sites on the particle surface was achieved via use of Quantum R-PE MESF calibration beads (Bangs Laboratories).

Biotinylated anti-ICAM-1 was quantified in a similar manner. The dye used was goat-anti-mouse-IgG-FITC (Jackson ImmunoResearch), and the isotype control, goat IgG FITC (Jackson ImmunoResearch). Anti-CLA-PE and goat anti-mouse IgG FITC were used to quantify $sLe^a$ and anti-ICAM-1 density on VTCs, respectively. To assist in gating and visualization of non-fluorescent 500 nm particles during flow cytometry, $sLe^a$ and anti-ICAM-1 coated particles were stained with biotin-FITC or biotin-PE prior to sample testing.

The PEG density on PLGA particles was quantified via staining surface PEG-biotin molecules with avidin-FITC purchased from Thermo Scientific (Waltham, MA). This protocol is described elsewhere[4], and similar to anti-ICAM-1 quantification, the Quantum™ FITC-5 MESF (Premix) beads were used.

Lastly, HSA was quantified on the particle surface using a human albumin FITC-conjugated antibody purchased from antibodies-online Inc. (Atlanta, GA).

## 2.3 HUVEC cell culture

HUVECs were obtained via a commonly used collagenase perfusion method[5]. Umbilical cords were generously donated by the U of M hospital under a Medical School Internal Review Board (IRB-MED) approved human tissue transfer protocol (HUM00026898). The protocol is exempt from informed consent per federal exemption category #4 of the 45 CFR 46.101.(b). HUVECs isolated from the umbilical cords were pooled and grown in tissue culture using T-75 flasks pre-coated with 0.2 wt%/v gelatin. Preparation of HUVEC coated coverslips for flow chamber assays is described elsewhere[5,6]. HUVEC monolayers were activated with 1 ng $mL^{-1}$ interleukin 1-beta (IL1-β) for 4 hrs prior to performing the flow experiment.

## 2.4 Blood preparation

### 2.4.1 Whole blood

ACD or heparinized whole blood was prepared by drawing blood from healthy human donors into a syringe containing acid-citrate dextrose (ACD) or heparin. Anticoagulant solutions were added at a ratio of 0.14 mL/mL blood.

### 2.4.2 Plasma

For preparation of plasma, whole blood with anticoagulant (ACD or heparin) was centrifuged at 2250g for 20 min, typically at 4°C and the supernatant collected. An additional spin at 6797g for 5 min was used to ensure any residual cells were removed.

### 2.4.3 Serum

For preparing serum, blood without any additive was allowed to sit upright in a 50 mL conical tube for ~2 hr, and then centrifuged at 2000g for 10 min at 4°C. An additional 5-min spin at 6797g was performed to ensure any residual cells were removed.

### 2.4.4 Immunoglobulin/albumin depleted plasma and serum

Plasma depletion of immunoglobulins and albumin using the PureProteome™ Human Albumin/Immunoglobulin Depletion Kit (EMD Millipore). Specifically, 25 μL of human plasma or serum was diluted with 1X PBS (1:4) to a total volume of 100 μL. This 25% plasma solution was then incubated with 900 μL of the depletion beads and incubated for 1 hr at room temperature on an end-to-end rotator. Solution was centrifuged and the supernatant contained the immunoglobulin/albumin depleted plasma. Commerically obtained human serum albumin was added for depleted Igs assays.

### 2.4.5 IgG depletion and isolation

To prepare IgG-depleted plasma, a Protein A antibody purification kit from Sigma-Aldrich (St. Louis, MO) was used. A detailed protocol regarding use of this product provided in the technical bulletin was followed with slight modifications. Briefly, ~2 mL of plasma was mixed with 4 mL of PBS and filtered with a 0.45 μm filter. The desalting cartridge is equilibrated with HEPES buffer and the Protein A cartridge washed with regeneration buffer. Then, the Protein A cartridge is equilibrated with the binding buffer used to dilute the plasma. The plasma/binding buffer mixture is passed through the Protein A cartridge which binds IgG. The outlet contains IgG depleted plasma. Bound IgG was isolated using the provided elution buffer and concentration via Amicon® Ultra-4 centrifugal filters. Protein concentration was measured via NanoDrop 2000c.

### 2.4.6 IgA depletion and isolation

To prepare IgA-depleted plasma, an IgA depletion column was purchased from GenWay Biotech, Inc (San Diego, CA). 40 μL of plasma was diluted with tris buffered saline (TBS) to a total volume of 400 μL and incubated with anti-IgA beads in a spin column for 15 mins and the resulting filtrate (IgA-depleted plasma) collected. Isolation of bound IgA was performed by incubation for 2-3 mins with 0.1 M glycine (pH=2.5). IgA protein was then concentrated using the Amicon® Ultra-4 centrifugal filters. Protein concentration was measured via NanoDrop 2000c.

### 2.4.7 RBCs-in-Buffer

RBCs-in-Buffer was prepared by adding 0.14 mL of 6 wt%/v dextran/ mL whole blood and allowing to sit upright for ~2 hr. After this process, RBCs were collected and washed via centrifugation.

### 2.4.8 Reconstituted blood: RBCs-in-VB, RBCs-in-Serum

Suspension of washed RBCs in viscous buffer (RBCs-in-VB) was used as the control assay for adhesion in plasma-containing whole blood/RBCs-in-Serum flow. VB refers to a buffer solution with viscosity matching that of human plasma and consisted of PBS++ with 1 wt% BSA and 1.4 wt% dextran. To prepare reconstituted blood assays (e.g. RBCs-in-VB, RBCs-in-Serum), RBCs from ACD WB were washed 3 times with PBS(--) via centrifugation at 1000g for 30 mins. A final wash was performed at 2250g for 20 min, and VB or serum was added to the RBC pellet to achieve a matching hematocrit to that obtained with ACD whole blood.

### 2.4.9 Hematocrit

To determine the hematocrit, whole blood was centrifuged at 2250g for 20 min, and the volume of the RBC pellet/total volume added was taken as the hematocrit value.

## 2.5 Parallel plate flow chamber assays

### 2.5.1 Laminar flow assays

Flow adhesion assays were performed using a Nikon TE 2000-S inverted microscope fitted with a digital camera. The microscope incubator was heated to ~37°C prior to the experiment. Circular parallel plate flow chambers (Glycotech Corporation) containing a straight rectangular channel and rubber gasket were used in these assays, as described elsewhere[3,5–7]. Briefly, for each trial, an activated coverslip containing a monolayer of HUVEC was vacuum-sealed to the bottom of the flow chamber deck. The outlet of the flow chamber is connected to a syringe pump, which controls the flow rate. VTCs were first mixed with blood, RBCs-in-Serum, or RBCs-in-VB at a concentration of $1 \times 10^6$ particles $mL^{-1}$. Next, the VTC-blood mixture was added to a syringe connected to

the flow chamber inlet. The duration of each flow assay was 5 min at a shear rate of 200 or 500 $s^{-1}$. After the flow experiment, images of bound VTCs on the HUVEC monolayer were collected along the channel width at a fixed position from the channel entrance. The amount of bound VTCs were counted and the adhesion density obtained.

For the biodegradable VTCs (PLGA, PLA, PCL), non-fluorescent particles were used to limit any effect of a fluorescent dye on VTC-protein interaction. These particles were exposed to plasma, serum, or VB (300 μL) for 5 min to set the corona based on PLGA, PLA, or PCL material interaction. After the plasma/serum/VB incubation, particles were labeled with biotin-PE antibody (added 3 μL of 1 mg $mL^{-1}$ biotin-PE solution) and the flow assay immediately performed. For anticoagulant-free (ACF) WB assays, biotin-PE stained biodegradable VTCs were stored in flow buffer or soaked in VB prior to the assay.

### 2.5.2 Pulsatile flow assays

In addition, some assays were performed using an oscillating pulsatile flow profile, which maintained an average shear of 0 $s^{-1}$, pulsing back and forth with a peak shear rate of 1000 $s^{-1}$ for a total of 15 min.

### 2.5.3 Plasma depleted soaking assays

In the case of depleted plasma assays, 5 μm particles were soaked for 1 hr in PBS 1X, plasma, or depleted plasma prior to performing the flow assay in buffer. For the 500 nm particles, RBCs-in-VB (38% hematocrit) was used as the flow medium.

## 2.6 SDS-PAGE

SDS-PAGE was performed using 4-20% precast gels from Bio-Rad laboratories. $sLe^a$ VTCs were exposed to plasma (ACD or heparinized), serum or VB similar to preparation for flow assay. The total exposure time of VTCs to the different media—

anticoagulated plasma, serum, or VB was ~10 min, including a 5-min soaking step and 5-min centrifugation spin (6797g) to collect the soaked particles and remove the media supernatant. VTCs were then washed 3 times with 50 mM PBS, and suspended in a final volume of 50 µL of detergent solution (0.06 M Tris-HCl, 1% SDS, 10% glycerol, lane marker tracking dye, pH 6.8) obtained from a SDS-PAGE Sample Prep Kit (Pierce). The VTC solution was then heated to 95°C for 5 mins using a thermocycler to remove the corona proteins and then centrifuged for 5 min to collect the protein supernatant. For each condition, 15 µL of the protein supernatant was loaded into an individual lane on the gel and ran for ~25 min at 200 V. The molecular weight standard was obtained from Bio-Rad Laboratories, Precision Plus Dual Color Protein Standards.

## 2.7 ELISA

Sandwich ELISA was employed for measurement of human plasma IgG, IgA1, and IgM concentrations. Clear, high-binding 96-well plates were coated with the appropriate antibody at 1 µg/mL overnight (50 µL/well). To capture IgG, IgA1, and IgM, goat anti-human IgG-unlabeled, Goat anti-human IgA-unlabeled, and goat anti-human IgM-unlabeled were used as the coating antibodies and purchased from Southern Biotech (Birmingham, AL). Plates were washed with PBS 1X + 0.05% Tween-20 and blocked for ~1 hr with 10% FBS (200 µL/well). Plasma was diluted 1:1e5 – 1:1e8 as this provided a linear working range for the different immunoglobulin proteins. Quantification was achieved by comparison with a standard curve consisting of commercially obtained IgG, IgA, and IgM solutions. For assay detection, horseradish peroxidase (HRP) conjugated antibodies were incubated with samples at ~0.1-0.8 µg/mL for 1 hr, depending on the specific antibody type. The following detection antibodies (Southern Biotech) at 100

µL/well were used in this assays: mouse anti-human IgG Fc-HRP (Clone: H2), mouse anti-human IgA1-HRP (Clone: B3506B4), and mouse anti-human IgM-HRP (Clone: SA-DA4). After washing, 50 µL/well of TMB substrate was added, and after ~5 min, 1N $H_2SO_4$ was added to stop the reaction. Absorbance measurements were taken at 450 nm with 570 nm as the background.

## 2.8 Mass spectrometry

Selected gel bands were digested using trypsin and analyzed using LC/MS/MS on a ThermoFisher Velos Orbitrap mass spectrometer. The NCBI protein database allowed for identification of product ion data using the Mascot and X-Tandem Search engines. Output files from Mascot were parsed into Scaffold software to confirm the correct identification of proteins.

## 2.9 Data analysis

Data was analyzed using Prism. Data in figures was plotted with standard error and comparisons between adhesion assays were performed using 1 way ANOVA with Tukey post-test and confidence interval of 99% ($\alpha$=0.01).

## References


1. Heslinga, M. J., Mastria, E. M. & Eniola-Adefeso, O. Fabrication of biodegradable spheroidal microparticles for drug delivery applications. *J. Control. Release* **138,** 235–242 (2009).

2. Watts, P. J., Davies, M. C. & Melia, C. D. Microencapsulation using emulsification/solvent evaporation: an overview of techniques and applications. *Crit. Rev. Ther. Drug Carrier Syst.* **7,** 235–259 (1989).

3. Charoenphol, P., Huang, R. B. & Eniola-Adefeso, O. Potential role of size and hemodynamics in the efficacy of vascular-targeted spherical drug carriers. *Biomaterials* **31,** 1392–1402 (2010).

4. Onyskiw, P. J. & Eniola-Adefeso, O. Effect of PEGylation on Ligand-Based Targeting of Drug Carriers to the Vascular Wall in Blood Flow. *Langmuir* **29,** 11127–11134 (2013).

5. Huang, R. B. & Eniola-Adefeso, O. Shear stress modulation of IL-1β-induced E-selectin expression in human endothelial cells. *PLoS One* **7,** 1–9 (2012).

6. Huang, R. B., Gonzalez, A. L. & Eniola-Adefeso, O. Laminar shear stress elicit distinct endothelial cell e-selectin expression pattern via TNFα and IL-1β activation. *Biotechnol. Bioeng.* **110,** 999–1003 (2013).

7. Sobczynski, D. J. *et al.* Plasma protein corona modulates the vascular wall interaction of drug carriers in a material and donor specific manner. *PLoS One* **9,** e107408 (2014).

# CHAPTER 3: PLASMA PROTEIN CORONA MODULATES THE VASCULAR WALL INTERACTION OF DRUG CARRIERS IN A MATERIAL- AND DONOR-SPECIFIC MANNER

A bulk of the work in this chapter is published as Sobczynski, D. J. *et al.* Plasma protein corona modulates the vascular wall interaction of drug carriers in a material and donor specific manner. *PLoS One* **9,** e107408 (2014).

## ABSTRACT

The nanoscale plasma protein interaction with intravenously injected particulate carrier systems is known to modulate their organ distribution and clearance from the bloodstream. However, the role of this plasma protein interaction in prescribing the adhesion of carriers to the vascular wall remains relatively unknown. Here, we show that the adhesion of vascular-targeted poly(lactide-co-glycolic-acid) (PLGA) spheres to endothelial cells is significantly inhibited in human blood flow, with up to 90% reduction in adhesion observed relative to adhesion in simple buffer flow, and the extent of this reduction depends on blood flow magnitude and pattern. In addition, this reduced PLGA adhesion in blood flow is linked to the adsorption of certain high molecular weight plasma proteins on PLGA and is donor-specific, where large reductions in particle adhesion in blood flow (80% relative to buffer) is seen with 60% of unique donor bloods while others exhibit moderate to no reductions. Furthermore, the extent of the reduced adhesion of PLGA is a function of ligand density and plasma exposure time. The observed plasma protein effect on PLGA is likely due to material characteristics since the effect is not replicated with polystyrene or silica spheres, which effectively adhere to the endothelium at a higher level in blood over buffer flow. Overall, understanding how distinct plasma

proteins modulate the vascular wall interaction of vascular-targeted carriers of different material characteristics would allow for the design of highly functional delivery vehicles for the treatment of many serious human diseases.

## 3.1 Introduction

Injectable vascular-targeted carrier (VTC) systems hold great promise for the effective diagnosis and treatment of many human diseases by non-invasively providing localized delivery of imaging agents or potent therapeutics. However, to date, only a few VTCs have been effectively translated into the clinic[1]. A potential source for the limited utility of VTCs could be linked to the assumption that drug carriers will efficiently localize and bind to the vascular endothelium in blood flow irrespective of size, shape, and material characteristics. Recent studies from our lab and others have shown that particle size, shape, and interaction with blood cells prescribe successful adhesion of VTCs in blood flow[2–4]. However, the experimental studies probing the impact of red blood cells (RBCs) and forces on VTC adhesion have been largely been limited to non-degradable, toxic polystyrene (PS) particles. Thus, it is a natural step to consider the adhesion of biodegradable VTCs, such as poly(lactic-co-glycolic-acid) (PLGA), as they are more representative of drug carriers for clinical application.

A preliminary experiment testing the adhesion of PLGA and PS particles (Chapter 1, Figure 1.1) revealed that the adhesion of PLGA particles is substantially reduced in human blood flow. It is the hypothesis that plasma is involved in the reduced adhesion effect of PLGA, since the main component of blood, RBCs, are mainly inert and would likely interact in a similar way with both PLGA and PS particles and are known to have a positive effect on adhesion in the experimental setting in Figure 1.1. In addition, previous work with PS VTCs revealed insignificant effects on adhesion due to white blood cells (WBCs) and platelets. Furthermore, WBC processes such as phagocytosis which, may reduce availability of particles, are largely limited in these assays due to the anticoagulant

employed here (acid-citrate-dextrose (ACD)) and the duration of the experiments (5-15 min).

Interestingly, the majority of published literature on plasma protein interaction with targeted drug carriers has focused on opsonization[5,6], which leads to particle recognition and clearance from the bloodstream by macrophages. Only recently have a few studies reported that the plasma protein corona (the layer(s) of surface bound protein) formed on nanoparticles (NPs) can interfere with the ligand-receptor interaction, suggesting such impacts highly depend on the targeted cell or protein[7–9]. However, it is known that the plasma protein corona which rapidly forms on drug carrier surfaces after exposure to blood depends on a variety of physicochemical properties, including the particle material type[10], which can result in distinct cellular interactions. While these studies undoubtedly provide useful insight into the range of possible impacts of the corona on carrier targeting, the impact of plasma protein adsorption with regard to particle material composition has largely been overlooked. Moreover, these analyses of corona effects on targeting have been conducted with simple animal sera or culture media in static assays that may not encompass the complexity of the realistic human blood flow environment in which VTCs must function, i.e., presence of hydrodynamic forces and blood cell interactions.

The preliminary experiment in Figure 1.1 suggests that plasma protein adsorption could play a critical role in the adhesion of PLGA carriers in human blood flow. In this work, the potential role of plasma protein adsorption on the adhesion efficiency of PLGA VTCs in human blood flow is explored. Specifically, PLGA particle adhesion to HUVEC in human blood flow is measured via an *in vitro* parallel plate flow chamber (PPFC) for a variety of carrier (e.g., size, ligand density), flow (e.g., shear rate, profile), and blood (i.e.,

donor) properties, as these variables may regulate any potential plasma-associated effect since protein corona formation is dependent on many types of parameters.

## 3.2 Results

### 3.2.1 Evaluation of PLGA adhesion in a variety of blood flow media

The objective of this study is to elucidate the potential role of the plasma protein corona on the adhesion of PLGA VTCs to HUVEC in blood flow for a variety of particle, flow, and blood properties. First, the adhesion of 5 μm, 2 μm, and 500 nm PLGA spheres is tested under laminar flow in a PPFC at a shear rate of 200 $s^{-1}$ for a variety of blood flow media (Figure 3.1A) to tease out the effect of individual components of blood on PLGA adhesion and determine if plasma is the source for the low adhesion in blood. Based on dynamic light scattering (DLS) measurements, the actual average sizes for the 500 nm, 2 μm and 5 μm particles used here were 330 nm, 1.4 μm and 4.6 μm respectively (Table 3.1).

**Table 3.1** Particle size measurements via dynamic light scattering (DLS)

| ***Particle diameter (μm)*** | ***Material*** | ***Dispersant*** | ***Z-average (μm)*** | ***PDI*** $\left(\frac{\sigma^2}{\bar{X}^2}\right)$ |
|---|---|---|---|---|
| 0.490 | PLGA (YG) | PBS++ | 0.334 | 0.232 |
| 0.534 | PS (G) | PBS++ | 0.567 | 0.032 |
| 2.35 | PLGA | PBS++ | 1.407 | 0.496 |
| 2.1 | PS | PBS++ | 2.219 | 0.150 |
| 5 | PLGA | PBS++ | 4.586 | 0.243 |
| 5 | PS | PBS++ | 4.946 | 0.047 |

On average, the adhesion of the 4.6 μm PLGA microspheres to activated HUVEC is 93% lower in low shear human whole blood flow relative to the adhesion of the same particles in a simple buffer flow system (Figure 3.1B). This discrepancy in particle adhesion between simple buffer versus blood flow is not solely explained by the viscosity difference between the two different mediums since the adhesion level observed for the

spheres in blood is still 89% lower than their adhesion in the viscous buffer flow. On average, the HUVEC adhesion of 1.4 μm $sLe^a$-PLGA spheres in blood flow is 83% lower relative to the adhesion of the same particles in simple buffer flow (Figure 3.1C). Again, the adhesion level of the 1.4 μm spheres in blood is still 73% lower than their adhesion level in the viscous buffer. For the 330 nm $sLe^a$-PLGA spheres, particle adhesion in low shear laminar blood flow is 83% less than the observed adhesion in simple buffer, while this same blood adhesion is 85% less than the adhesion of nanospheres in high viscosity buffer (Figure 3.1D). To determine whether the reduced PLGA adhesion in human blood flow is due to particle-blood cell interactions or particle-plasma protein interactions, the HUVEC adhesion of sLea-PLGA spheres was evaluated in plasma (cell-free) flows. Overall, PLGA spheres also exhibit significantly lower adhesion to activated HUVECs in plasma flows relative to adhesion in viscous buffer flows, with 92%, 80%, and 63% reduction in adhesion in plasma flow for the 330 nm, 1.4 μm, and 5 μm spheres, respectively. To further confirm the role of plasma proteins, experiments were conducted with particles in laminar flow of human RBCs washed and then suspended in buffer (RBC-in-Buffer). The adhesion levels of the 330 nm and 1.4 μm spheres in RBC-in-Buffer flow are 176% and 55% higher than the values observed in simple buffer flow, respectively. As such, the levels of reduction in the adhesion of these particles in whole blood (essentially RBCs-in-Plasma) are 94% and 89% lower compared to the observed adhesion in their respective RBC-in-buffer assays. Visualization of particle stability (spheres in solution placed on a glass coverslip) via phase or fluorescent imaging shows all particles to exhibit uniform dispersity in buffer and plasma (Figure 3.2), suggesting that particle aggregation

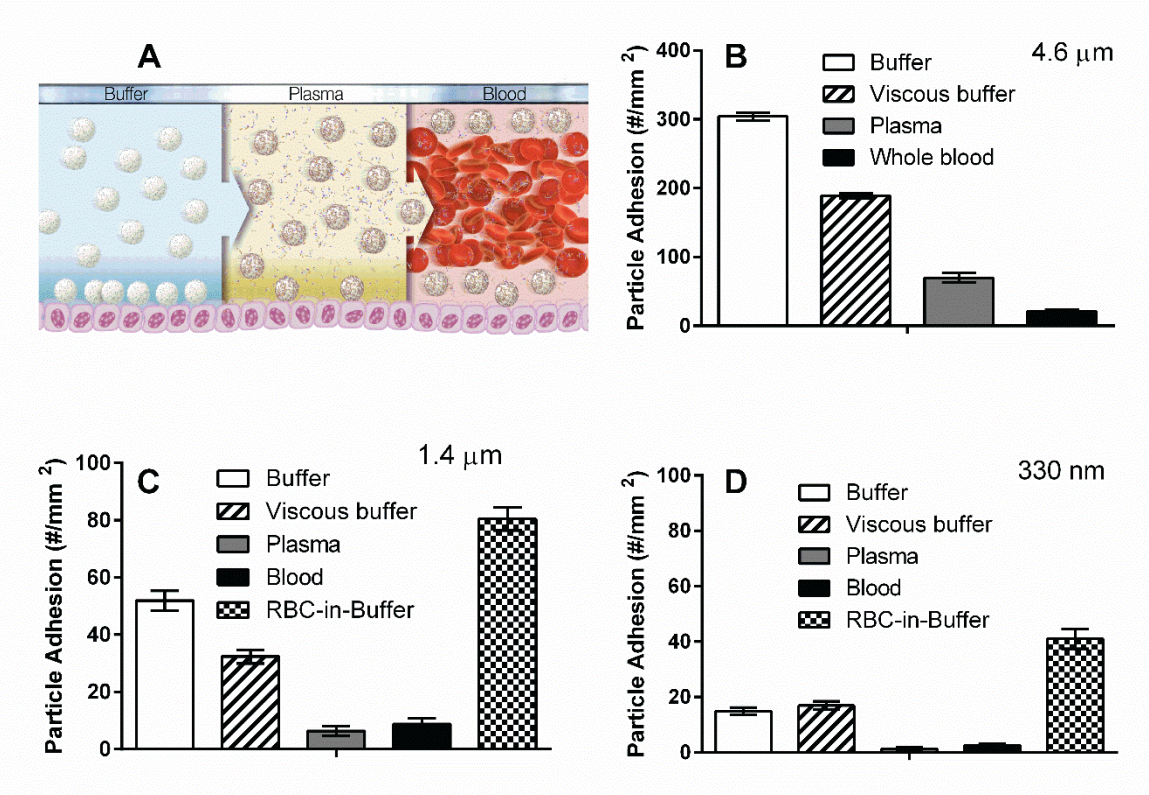


**Figure 3.1** Summary of the adhesion of PLGA spheres from flow of buffer, plasma, and blood to an activated endothelial cell monolayer. (A) A depiction of particle margination in buffer, plasma, and blood flow. Binding density after 5 min of flow for (B) 4.6 μm, (C) 1.4 μm and (D) 330 nm $sLe^a$-coated PLGA particles to activated HUVEC monolayer from laminar buffer, plasma, or whole blood at 200 $s^{-1}$. Particle concentration = 5 × $10^5$ particles/mL for 4.6 and 1.4 μm data and 1 × $10^6$ particles/mL for the 330 nm particles. $sLe^a$ density = 1,700 +/- 100 sites/$\mu m^2$ (SEM) surface for 4.6 μm, 1500 +/- 100 sites/$\mu m^2$ (SEM) for 1.4 μm and 9,000 +/- 400 sites/$\mu m^2$ (SEM) for 330 nm particles. N = 3 distinct donors (donors A, B, and C).

which has been previously reported for particles (e.g., iron oxide nanoparticles) upon exposure to cell culture media or plasma[11–13] is likely not responsible for the observed reduced adhesion of PLGA spheres to HUVECs in the whole blood/plasma flow environment. In addition, sample images of the HUVEC monolayer in the PPFC after perfusion of PLGA spheres in RBCs-in-buffer, whole blood, and plasma flow are shown in Figure 3.3. Several bound PLGA particles are easily visualized on the monolayer for the assays with the particles in RBC-in-buffer (Figure 3.3A) whereas minimal particles are found on the monolayers perfused with particles in blood (Figure 3.3B) or plasma (Figure 3.3C). The HUVEC monolayers exposed to RBC-in-buffer and whole blood flows were visually similar and the monolayer integrity is shown to be intact with binding of WBCs visible in both images. The image of the monolayer exposed to particles in cell-free plasma also shows essentially no particle binding and a robust cell monolayer remains even after exposure to human plasma.

### 3.2.2 Evaluation of human blood donor on PLGA adhesion

The adhesion of 4.6 μm $sLe^a$-PLGA spheres in low shear laminar flows of plasma was analyzed for several individual donors to determine any variation in particle adhesion that may be linked to differences in the plasma protein composition of each donor. The 4.6 μm PLGA sphere size is highlighted in the individual donor assays since the magnitude of the reduction in particle adhesion in plasma flow relative to buffer flow is smaller for this particle size. As shown in Figure 3.4A, the 4.6 μm PLGA spheres in flow of plasma from ~42% of the donors evaluated show an average of 72 ±15 % (SEM) reduction in adhesion relative to the adhesion in the viscous buffer control (donors A, C, H, J, and N are referred to as "low-HUVEC binding donors" hereafter), whereas there was no evidence of reduced

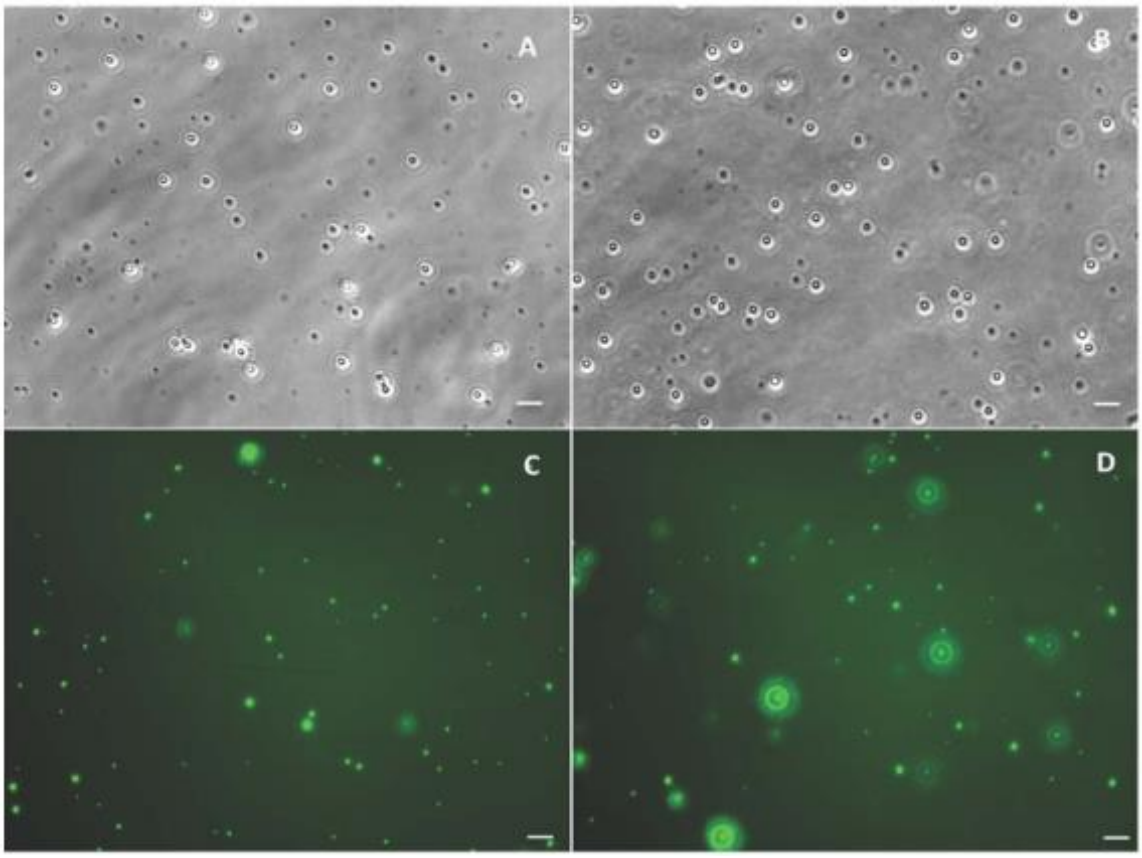


**Figure 3.2** Phase and fluorescence images of small PLGA spheres. Phase image of 1.4 μm PLGA particles in PBS+/+ (A) and plasma (B), and fluorescence image of 330 nm PLGA in PBS+/+ (C) and plasma (D). Particles were added to the desired medium for 5 min in static after which a small amount of the particle solution is placed on a coverslip for imaging. All images shown were taken at a 40X magnification. Scale bar = 10 μm.

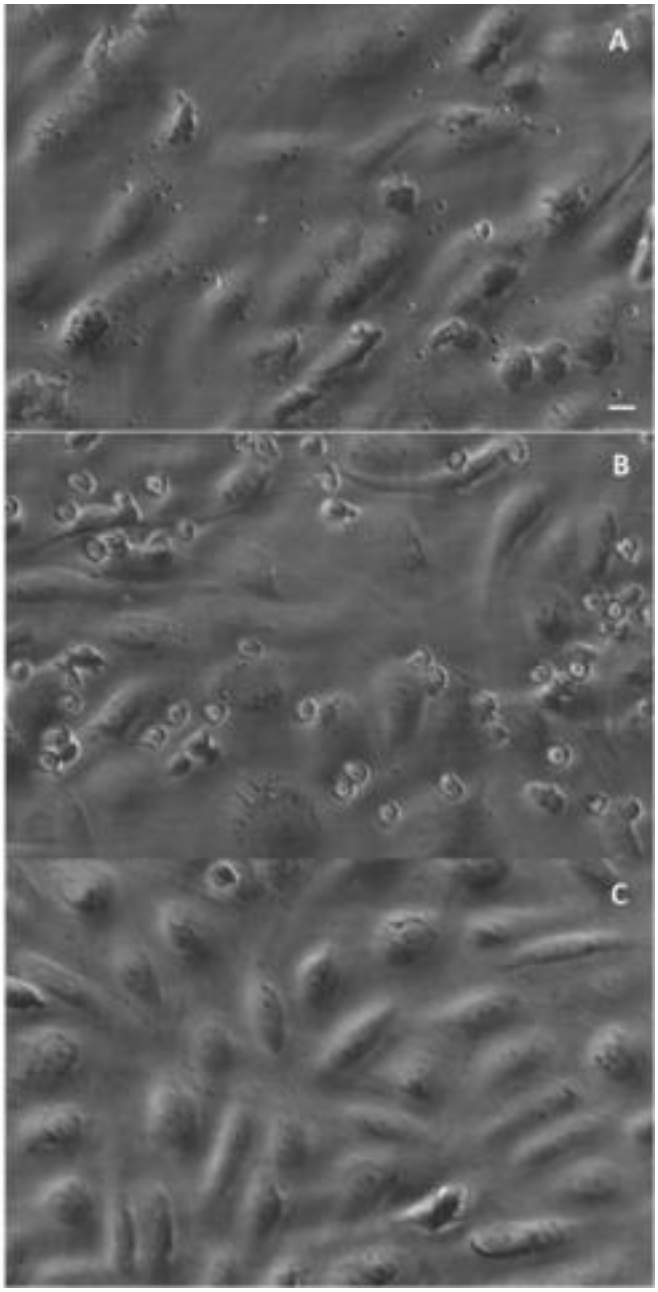


**Figure 3.3** Sample images of activated HUVEC monolayers exposed to PLGA under different flow types. Phase image of 1.4 μm $sLe^a$-coated PLGA spheres bound to IL1-β-activated HUVEC monolayer after 5 min of flow of particles in (A) RBC-in-Buffer, (B) whole blood, and (C) plasma at 200 $s^{-1}$. Image taken at 20X magnification. $sLe^a$ density = 1500 +/- 100 sites/$\mu m^2$ (SEM). Particle concentration = 5e5 particles/mL. Scale bar = 20 μm.

adhesion for the 4.6 μm PLGA spheres in plasma flow assays with another 50% of donors (donors D, E, I, K, L, and R are referred to as "high-HUVEC binding donors" hereafter).

Specifically, PLGA adhesion in plasma flow of this subset of high HUVEC binding donors occurred at a similar level to the adhesion in viscous buffer flow. PLGA adhesion in the plasma flow of one donor B displays an intermediate level of reduction (~45%) relative to adhesion in viscous buffer. Interestingly, the PLGA adhesion levels between plasma and whole blood assays for the low binding donor bloods are not statistically significant, whereas the opposite is the case for the adhesion of the spheres in the whole blood versus plasma flow assays for most of the high-binding donor bloods. To determine whether the donor effect observed for the 4.6 μm PLGA particles also exists for the smaller sized particles, the flow adhesion of 330 nm spheres was evaluated in a subset of the same donors used for the 4.6 μm particle adhesion assays.

Interestingly, while there is minimal impact of plasma proteins seen in the adhesion of the 4.6 μm PLGA particles in the plasma flow assays with high HUVEC binding donors compared to viscous buffer, the plasma adhesion of the PLGA nanospheres is statistically lower in both the low and high HUVEC binding donors than their adhesion in viscous buffer flow (Figure 3.4B). However, nanospheres do exhibit a smaller reduction in their adhesion levels in assays with high HUVEC binding donor plasmas relative to buffer versus the reduction levels observed in assays with low HUVEC binding donor plasmas (donors D, L versus A, C). The adhesion of the nanospheres in whole blood flow of the high donors is not statistically different from adhesion in viscous buffer. We also evaluated the individual donor plasma flow adhesion of 4.6 μm PLGA spheres that were prepared

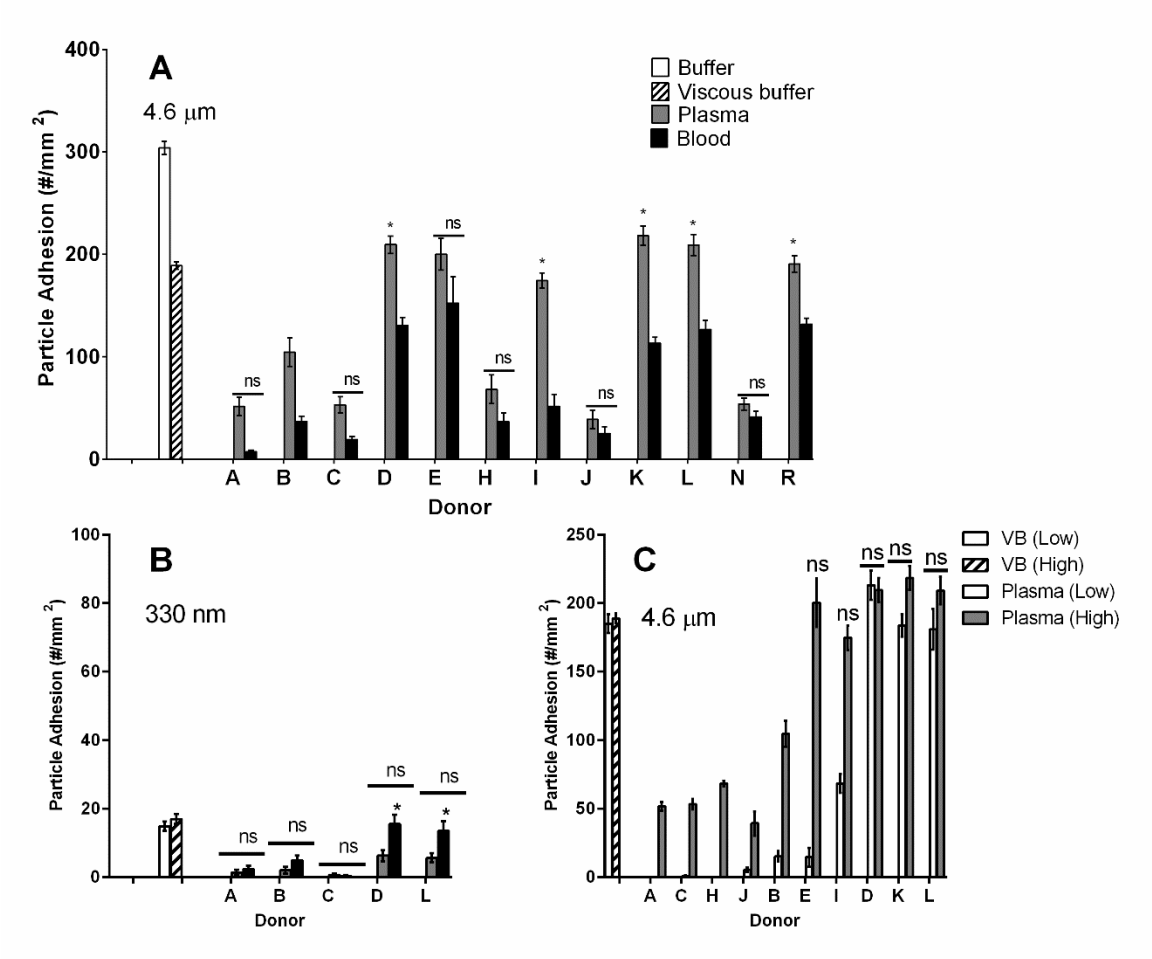


**Figure 3.4** Particle adhesion to activated HUVEC in laminar flow of individual donor plasma and blood at 200 $s^{-1}$. Adhesion of (A) 4.6 μm and (B) 330 nm PLGA spheres at high $sLe^a$ density and (C) 4.6 μm spheres at low and high $sLe^a$ density. Viscous buffer controls are shown on the left side of the graph. $sLe^a$ density = 1,800 +/- 100 sites/$\mu m^2$ (SEM) in (A), 9,000 +/- 300 sites/$\mu m^2$ (SEM) in (B) and 130+/-10 and 1800 +/- 100 sites/$\mu m^2$ (SEM) in (C). Adhesion data collected after 5 min of flow time. Particle concentration = $5 \times 10^5$ particles/mL for 4.6 μm data and $1 \times 10^6$ particles/mL for the 330 nm particles. N = 2 distinct assays for each donor. ns = Not significant at 99% confidence interval.

with a low $sLe^a$ density (130 ± 10 sites/$\mu m^2$), which is anticipated to increase the available space for protein to adsorb onto the particle. The low density $sLe^a$ particles exhibit significantly lower adhesion in plasma flow of 70% of donors relative to adhesion in viscous buffer flow (Figure 3.4C) compared to the plasma flow assays with high $sLe^a$ density particles where only 50% of donor bloods resulted in a comparable level of reduction in PLGA adhesion relative to viscous buffer.

### 3.2.3 Evaluation of the effect of flow magnitude and profile on PLGA blood flow adhesion

Adhesion of 330 nm and 1.4 μm PLGA spheres were also evaluated in assays with a high shear (500 $s^{-1}$) laminar flow and in a pulsatile flow with alternating forward/reverse flow at high shear (1000 $s^{-1}$) and a net forward flow[14]. As shown in Figure 3.5A, the levels of reduction in the adhesion of 1.4 μm spheres in high shear laminar plasma and whole blood flows relative to high shear laminar buffer flow (~80% and ~90%, respectively) are similar to the level of reduction in adhesion observed in plasma and whole blood flows versus buffer flow for the low shear laminar assays. However, when adhesion in high shear laminar whole blood flow is compared to that in high shear laminar RBC-in-buffer flow, a slightly higher reduction in adhesion is observed for the 1.4 μm spheres at high shear compared to low shear. Specifically, there is a 95% reduction in blood flow adhesion relative to adhesion in RBC-in-buffer flow at high shear compared to the aforementioned 89% reduction for the same comparison at low shear. In pulsatile flow, the overall adhesion of the 1.4 μm PLGA spheres in blood flow is minimal, with a 95% and 99% reduction in adhesion observed relative to adhesion in buffer and RBC-in-buffer flows, respectively (Figure 3.5B). For the 330 nm spheres, the reductions in particle binding in whole blood

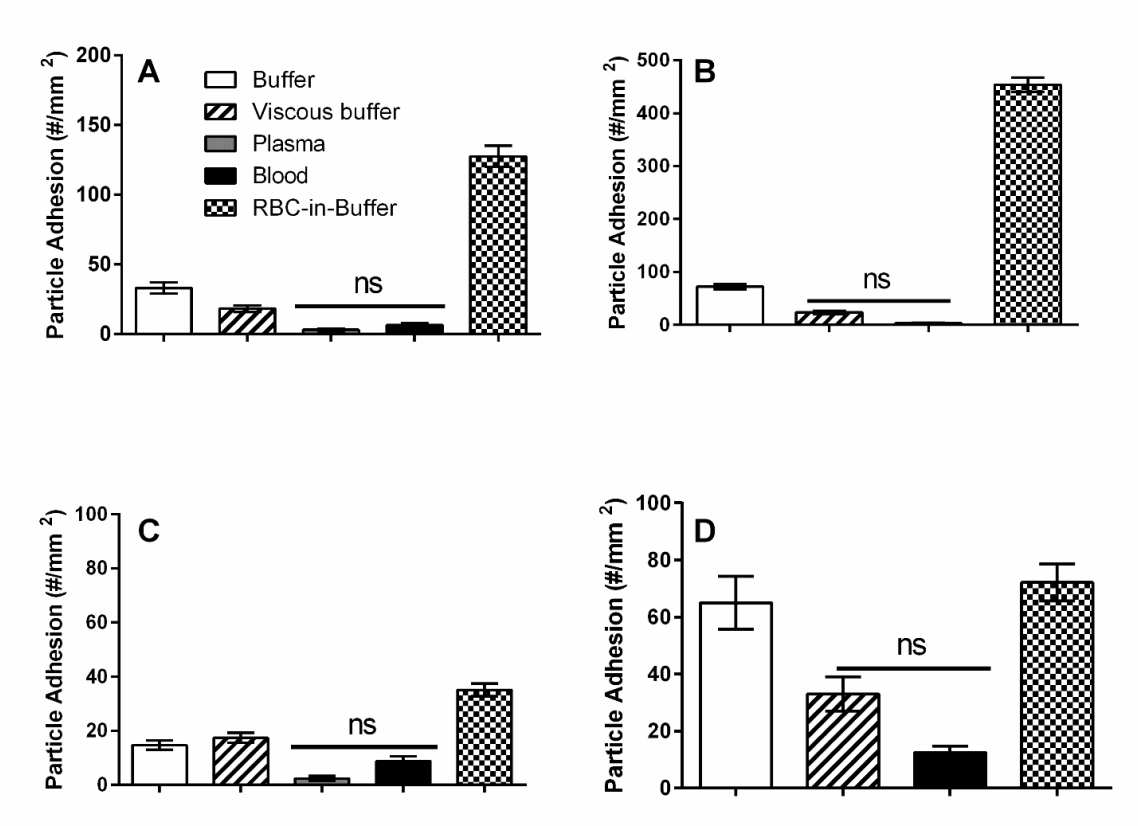


**Figure 3.5** Average adhesion of 1.4 μm and 330 nm sLe$^a$–coated PLGA spheres to activated HUVEC in buffer, viscous buffer, plasma, blood, and RBC-in-buffer flows. Panels (A) and (B) shows the adhesion of 1.4 μm spheres in laminar shear at 500 $s^{-1}$ and pulsatile flow with peak shear at 1000 $s^{-1}$, respectively. Panels (C) and (D) show the adhesion of 330 nm PLGA spheres in laminar shear at 500 $s^{-1}$ and pulsatile flow with peak shear at 1000 $s^{-1}$, respectively. sLe$^a$ density = 1700 +/- 100 sites/$\mu m^2$ (SEM) for 1.4 μm spheres and 7000 +/- 300 sites/$\mu m^2$ (SEM) for 330 nm spheres. Particle concentration = $5 \times 10^5$ particles/mL for 1.4 μm data and $1 \times 10^6$ particles/mL for the 330 nm particles. Laminar flow was run for 5 min and pulsatile flow for 15 min. N = 3 distinct trials (donors) for the plasma and blood flow assays. ns = Not significant at 99% confidence interval.

flow at higher laminar shear and in pulsatile flow relative to simple buffer flows of the same flow type are generally lower than observed for the low shear laminar flow, with 40% and 80% reduction observed, respectively (Figure 3.5C–D).

### 3.2.4 Evaluation of potential plasma protein effects on other VTC material types

To evaluate whether the observed negative plasma protein effect on particle flow adhesion is unique to PLGA or extends to particles of other material types, adhesion of $sLe^a$-coated polystyrene (PS) spheres to activated HUVECs from laminar blood flow was evaluated similar to the PLGA assays. The size and surface charge of the $sLe^a$-coated PS particles were comparable to that of PLGA spheres evaluated (Table 3.2). In contrast to PLGA particles, the adhesion of 5 μm PS particles (similar $sLe^a$ density as PLGA particles) in whole blood is higher than their adhesion in buffer flow similar to our previous reports (Figure 3.6A)[2,15].

**Table 3.2** Zeta potential measurement for 2 μm particles

| ***Material*** | ***Surface*** | ***Medium*** | ***Zeta Potential (mV)*** |
|---|---|---|---|
| PS | $sLe^a$ | 50% Plasma (in PBS) | -6.5 +/- 2.5 |
| PLGA | $sLe^a$ | 50% Plasma (in PBS) | -4.6 +/- 3.2 |

Moreover, the binding levels of PS in whole blood are comparable among all donor bloods evaluated. As such, there is no significant difference in PS adhesion between most low- and high- binding donor blood assays in contrast to that observed with PLGA (e.g., compare donor D to donors C and H in Figure 3.6A). A quick analysis of the blood flow adhesion of $sLe^a$-coated silica particles in blood flow relative to RBCs-in-VB and, similar to PS yielded a mild reduction in blood flow relative to PLGA (Figure 3.7). This observation that particles of other materials main robust blood flow adhesion suggests that the plasma

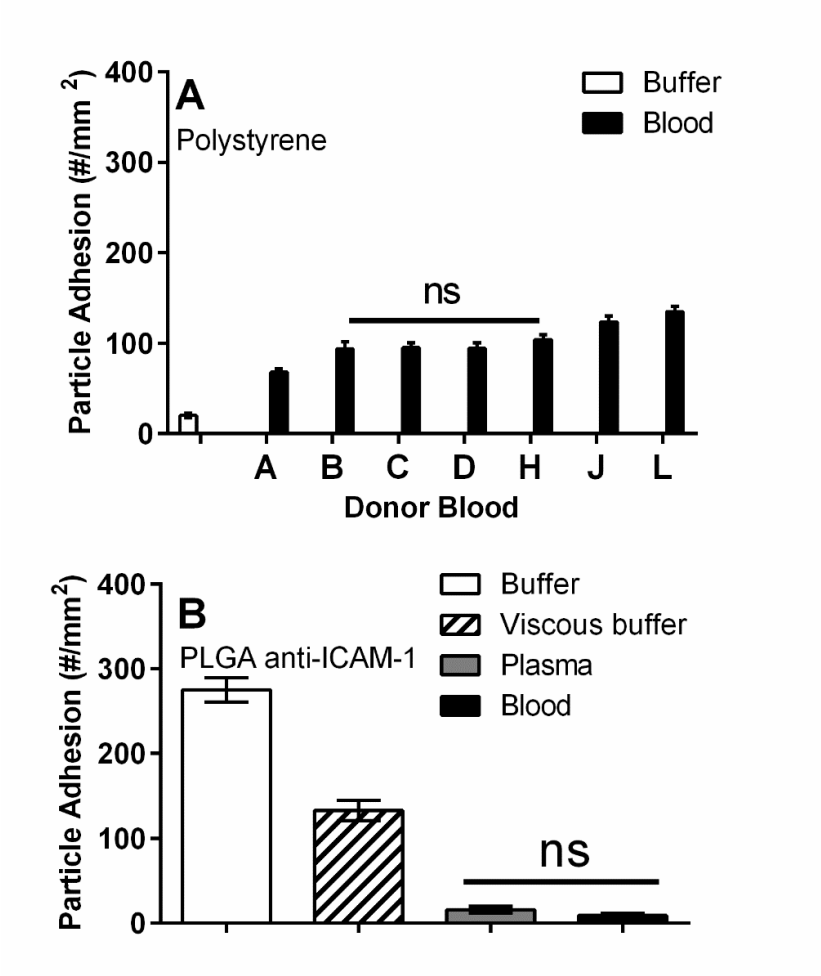


**Figure 3.6** Adhesion of sLe$^a$–coated PS spheres or anti-ICAM-coated PLGA spheres to activated HUVEC under various flow conditions. (A) Adhesion of 5 μm sLe$^a$–coated PS spheres in laminar whole blood and buffer flows to activated HUVEC at 200 $s^{-1}$ for 7 human subjects. N = 2 (distinct trials) for each blood bar. (B) Average adhesion of 4.6 μm anti-ICAM-coated PLGA spheres to activated HUVEC from laminar buffer, plasma, or whole blood flow of three low PLGA binding donors at 200 $s^{-1}$. Laminar flow was run for 5 min. Particle concentration in flow = $5 \times 10^5$ spheres/mL. sLe$^a$ density = 1,800 +/- 200 sites/$\mu m^2$ (SEM) and anti-ICAM-1 density = 3500 +/- 500 sites/$\mu m^2$ (SEM). N = 3 distinct trials (donors) for the plasma and blood flow assays. ns = Not significant at 99% confidence interval.

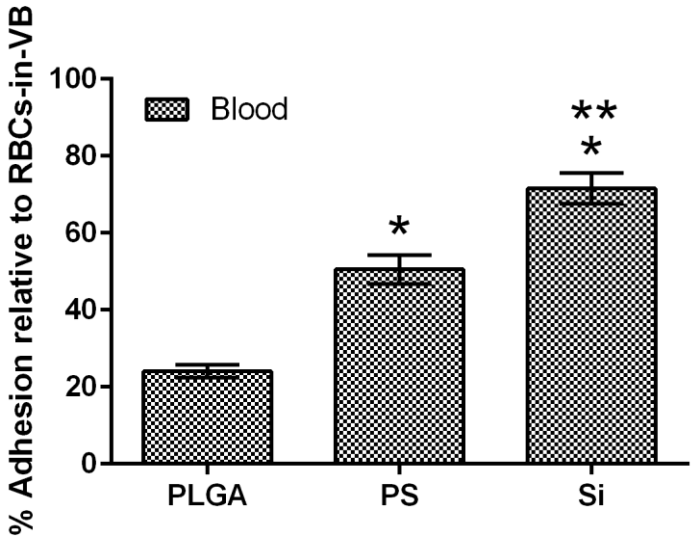


**Figure 3.7** Adhesion of 500 nm sLe$^a$-coated PLGA, polystyrene, and silica spheres to activated HUVEC in blood flow relative to RBCs-in-VB. Site densities (#/μm$^2$) were obtained as follows: PLGA 3200 +/- 900; PS 3100 +/- 20; Si 4400 +/- 200. Particle concentration in flow = 1 × 10$^6$ spheres/mL. *= significant at 99% confidence relative to PLGA trial, **= significant at 99% relative to PS trial.

protein corona effect observed for PLGA spheres is likely due to polymer material characteristic, rather than targeting ligand chemistry/interaction, inducing differential plasma protein adsorption. Indeed, when experiments were performed with anti-ICAM-1 (antibody)-coated PLGA spheres, a similar negative binding trend was observed for these particles as was seen with the $sLe^a$-coated PLGA spheres (Figure 3.6B); yet, in our previous work we show substantial binding of anti-ICAM-1 coated PS microspheres in human blood flow assays[16]. Overall, the successful binding of $sLe^a$-coated PS spheres in blood flow shown in Figure 3.6A (and anti-ICAM-1 coated PS spheres in the aforementioned previous publication) highlights that the lack of PLGA binding to HUVECs in blood flow is not due to human blood components negatively affecting the functionality of the HUVEC-expressed protein target. Finally, we evaluated whether incorporation of polyethylene glycol (PEG) chains alters the HUVEC binding of PLGA particles. PEG chains were conjugated to the surface of 1.4 μm PLGA spheres at a density of 16,000 site/$\mu m^2$ estimated to be in the brush conformation as we previously described[16]. In addition, a similar $sLe^a$ density as the non-PEGylated particles was attached to the chain ends. The PEGylated PLGA spheres demonstrate the same negative adhesion trend in whole blood flow as observed for non-PEGylated PLGA spheres (Figure 3.8). The adhesion trend for a high-HUVEC binding donor (L) versus a low-HUVEC binding donor (J) is also the same as observed for non-PEGylated PLGA spheres. In our previous publication, we show PEGylated 1.4 μm PS spheres to effectively bind to activated HUVECs from human blood flow[16].

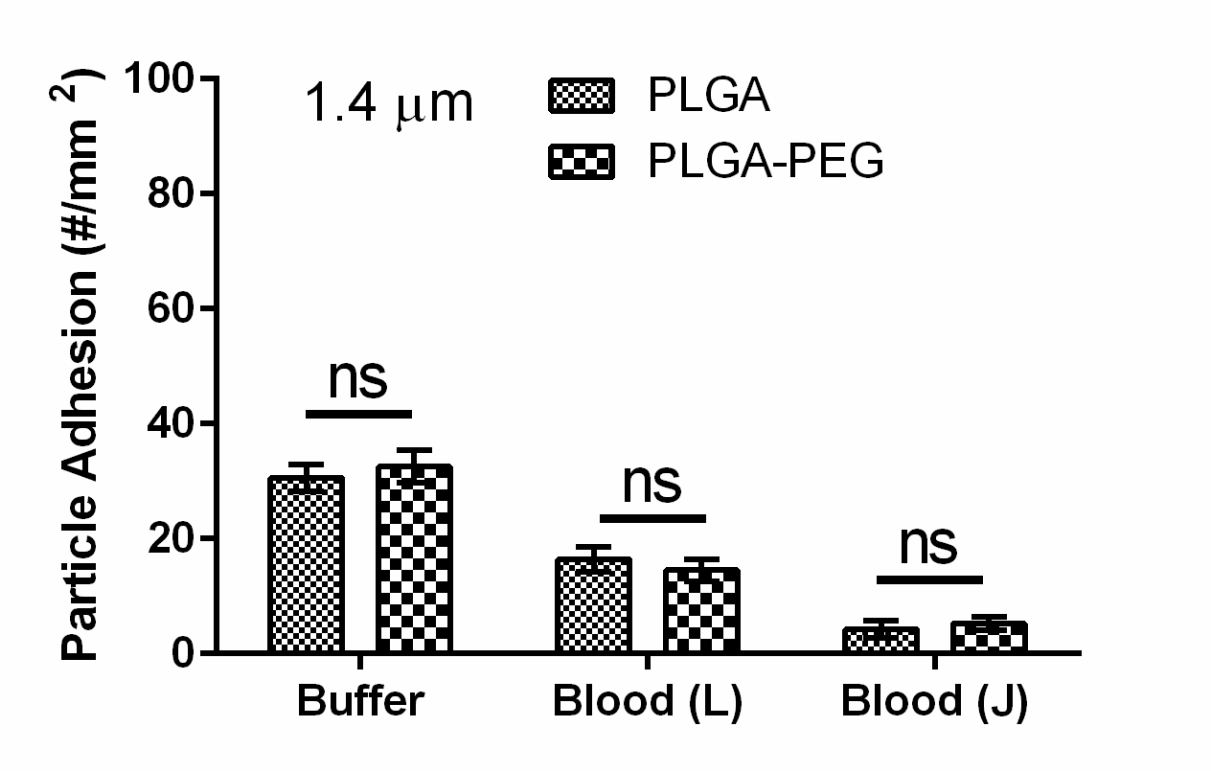


**Figure 3.8** Adhesion of PEGylated and non-PEGylated 1.4 μm $sLe^a$-targeted spheres to HUVEC in laminar buffer or whole blood flow at 200 $s^{-1}$ (5 min). A PEG density of 16,000 site/$\mu m^2$ estimated to be the brush conformation is used. $sLe^a$ density = 1,800 +/- 200 sites/$\mu m^2$ for both PEGylated and un-PEGylated particles. Particle concentration in flow = $5 \times 10^5$ particles/mL. ns = Not significant at 99% confidence interval.

### 3.2.5 Characterization of protein adsorption on PLGA versus PS spheres

To further probe whether differential protein adsorption on PLGA particles relative to PS is the cause of their differential adhesion to activated HUVECs in blood flow, the plasma protein corona was evaluated on sLe$^a$-coated particles via SDS-PAGE for PS and PLGA particles in low-HUVEC and high-HUVEC binding donors. Figure 3.8A shows a representative SDS gel for the 5 μm PLGA and PS spheres. There were visible differences in the corona acquired by PS microspheres opsonized for 1 hour in plasma (incubation followed by washing in buffer) and the corona found on PLGA spheres (Figure 3.9A: Lanes 2 and 5 versus 3 and 4). Interestingly, there were also visible differences in the corona acquired by PLGA opsonized in plasma of a low HUVEC versus a high HUVEC PLGA binding donor (Lane 3 versus 4) particularly at the 150 kDa mark where PLGA spheres appear to acquire more proteins in the plasma that supported low PLGA flow adhesion compared to plasma that supported high PLGA binding. The corona acquired by PS microspheres was similar with opsonization in a low or high-HUVEC binding donor (Lane 2 versus 5). Evaluation of the corona of PLGA particles incubated in low-HUVEC binding plasma at various time points, from 0 to 60 min, suggests there is a correlation between the presence and intensity of the 150 kDa band on the SDS gel for PLGA and the extent of reduction in particle blood flow adhesion to HUVECs as shown in Figure 3.9B. The plasma protein interference with binding was also shown to occur as early as 30 secs of particle exposure to plasma/blood and maximizes after only 5 min of exposure. Further analysis via mass spectrometry shows that the corona on sLe$^a$-PLGA particles (found in both high and low HUVEC binding donors) contains unique peptides not found in the corona of sLe$^a$-PS spheres opsonized in the low HUVEC binding donor plasma as depicted in Figure 3.9C

(Table 3.3). An additional subset of proteins found in the low-HUVEC binding PLGA corona but absent from the high-HUVEC binding sLe$^a$-PLGA corona is listed Table 3.4. Taken together, these tables list all the proteins found uniquely in the low-HUVEC binding PLGA-sLe$^a$ corona but not in the PS-sLe$^a$ corona of the same low-HUVEC binding donor. A majority of the unique peptides found on PLGA (particularly when opsonized in low PLGA binding blood) are related to different subclass/subtype of immunoglobulins that belong to a cluster associated with proteins similar in structure to chain L of the insulin growth factor (IgF-Ii) antibody complex.

To preliminarily confirm that large immunoglobulins such as ones identified above are involved in the diminished adhesion of PLGA particles in human blood, we evaluated the buffer flow adhesion of sLe$^a$-coated PLGA spheres opsonized for 1 hour in 25% plasma of a low PLGA binding donor depleted of 98% of the albumin and all immunoglobulins using a commercial depletion kit (PureProteome Depletion Kit; EMD Millipore) and compared to the adhesion of the same particles soaked in non-depleted plasma of the same donor. PLGA particles opsonized with depleted 25% plasma displayed the same high level of binding in buffer flow as non-opsonized particles whereas particle opsonized in non-depleted, 25% plasma continued to exhibit low adhesion as was the case for non-depleted, 100% plasma (Figure 3.10). Furthermore, when the PLGA particles were opsonized with 5% plasma (non-depleted) to account for the reduction in the total protein in the protein-depleted 25% plasma, particle adhesion was still significantly reduced compared to non-opsonized particles.

## 3.3 Discussion

The data presented here show that PLGA VTCs do not effectively adhere to inflamed HUVECs in laminar and pulsatile flow patterns with shear rates ranging from 200-1000 $s^{-1}$. We conclude that this phenomena is linked to the unique adsorption of specific "negative proteins" onto the surface of PLGA particles. This conclusion is supported by data from control experiments that show higher binding of PLGA particles with buffer and RBC-in-Buffer flows compared to the values observed in whole blood or plasma-only flows of the same flow type and shear magnitude. Also, a preliminary mass spectrometry analysis of the hard protein corona on particles revealed unique proteins, mostly immunoglobulin subclasses/subtypes, found in the protein corona on PLGA but not in the corona on PS particles when exposed to the same donor blood. It is likely that PS particles do not exhibit reduced adhesion in human blood (or plasma) flow due to the critical negative plasma proteins having a low affinity for these materials. This assertion that different material chemistry affects the type of adsorbed plasma proteins on particles of similar size and surface charge is in line with a previous report by others. Specifically, Deng *et al*. reported that nanospheres of different metal oxides having the same size and surface charge adsorb different plasma proteins[10]. We also find that the negative effect of plasma proteins on the adhesion of PLGA particles in blood flow was apparent for all particle sizes explored, from 4.6 μm down to 330 nm, despite the fact that particle size is known to affect the quantity and quality of proteins in the corona of nanoparticles[6,17]. This lack of a major effect of PLGA particle size on their blood flow adhesion to HUVECs in this work may be due to the affinity of the relevant plasma proteins for PLGA surfaces not being significantly affected within the range of particle size

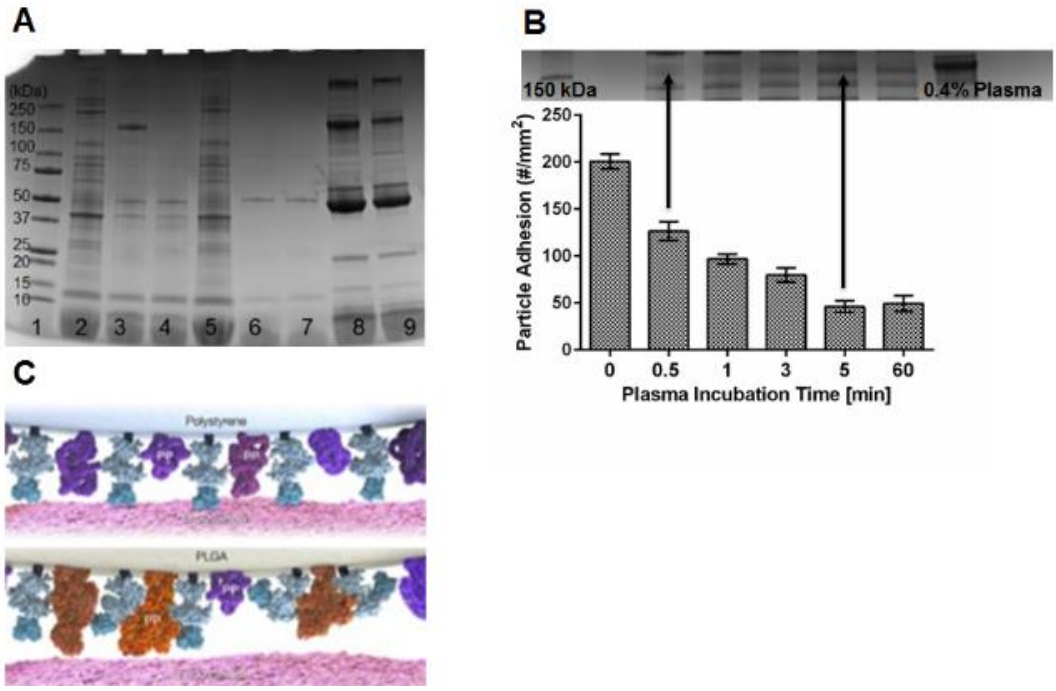


**Figure 3.9** Analysis of proteins adsorbed to particle surfaces as a function of material type and plasma incubation time. (A) SDS-gel electrophoresis analysis of proteins adsorbed on PS (5 μm) and PLGA (5 μm) spheres after 1 hr incubation in plasma. (Lane 1) Molecular weight standard. Proteins adsorbed onto particle surfaces were analyzed from the following conditions: PLGA soaked in a high (Lane 2) and low (Lane 3) HUVEC binding donor plasma; PS soaked in a low (Lane 4) and high (Lane 5) HUVEC binding donor; and PLGA (Lane 6) and PS (Lane 7) soaked in 1% BSA solution. The protein profile in a 0.4% plasma of the low (Lane 8) and high (Lane 9) HUVEC binding donor was run as well. (B) Correlation of the buffer flow (200 $s^{-1}$ laminar) adhesion of plasma opsonized PLGA (4.6 μm) spheres as a function of plasma incubation time (bottom) with the presence/development of a protein band at ~150 kDa in the protein corona of PLGA spheres as a function of time as observed with SDS-gel electrophoresis analysis (top). (C) A depiction of differential plasma protein (PP) adsorption on PLGA and PS spheres.

**Table 3.3** Unique peptides found on PLGA particles in low-HUVEC binding plasma

| | | **Molecular weight (kDa)** |
|---|---|---|
| **Cluster of Chain L, Crystal Structure Of Igf-Ii Antibody Complex** | | |
| 1 | protein Len,Bence-Jones | 24 |
| 2 | recombinant IgG4 heavy chain [Homo sapiens] | 43 |
| 3 | Chain A, Human Factor Viii C2 Domain Complexed To Human Monoclonal Bo2c11 Fab | 23 |
| 4 | immunoglobulin lambda 2 light chain [Homo sapiens] | 23 |
| 5 | Chain H, Crystal Structure Of Human Anti-Steroid Fab 5f2 In Complex With Testosterone | 24 |
| 6 | immunoglobulin variable region [Homo sapiens] | 17 |
| 7 | unnamed protein product [Homo sapiens] | 55 |
| 8 | Chain A, Crystal Structure Of An Autoimmune Complex Between A Human Igm Rheumatoid Factor And Igg1 Fc Reveals A Novel Fc Epitope And Evidence For Affinity Maturation | 26 |
| 9 | Chain L, Crystal Structure Of Human 2909 Fab, A Quaternary Structure-Specific Antibody Against Hiv-1 | 23 |
| 10 | Chain L, Crystal Structure Of Fab Del2d1, A Deletion Variant Of Anti-Influenza Antibody 2d1 | 23 |
| **Cluster of actin, cytoplasmic 2 [Homo sapiens]** | | |
| 11 | POTE ankyrin domain family member F [Homo sapiens] | 121 |
| 12 | PREDICTED: actin, aortic smooth muscle isoform 2 [Equus caballus] | 37 |
| **Cluster of v-src sarcoma (Schmidt-Ruppin A-2) viral oncogene homolog (avian) [Homo sapiens]** | | |
| 13 | Chain A, Crystal Structure Of Src Kinase Domain In Complex With Cgp77675 | 32 |
| **Complement factor H-related protein 5 precursor** | | |
| 14 | complement factor H-related protein 5 precursor [Homo sapiens] | 64 |
| **Cluster of unnamed protein product** | | |
| 15 | unnamed protein product [Homo sapiens] | 141 |
| **Cluster of growth-inhibiting protein 25 [Homo sapiens]** | | |
| 16 | Chain A, Crystal Structure Of Cleaved Human Alpha1-Antichymotrypsin At 2.7 Angstroms Resolution And Its Comparison With Other Serpins | 41 |
| 17 | Chain A, Alpha1-Antichymotrypsin Serpin In The Delta Conformation (Partial Loop Insertion) | 45 |
| **Apolipoprotein A-V precursor [Homo sapiens]** | | |
| 18 | apolipoprotein A-V precursor [Homo sapiens] | 41 |
| **Cluster of unnamed protein product [Homo sapiens]** | | |
| 19 | unnamed protein product [Homo sapiens] | 139 |

**Table 3.4** Unique peptides found on PLGA particles in low-HUVEC binding donor plasma and absent from PLGA particles exposed to high-HUVEC binding donor plasma

| | | **Molecular weight (kDa)** |
|---|---|---|
| **Cluster of Chain L, Crystal Structure Of Igf-Ii Antibody Complex** | | |
| 1 | immunoglobulin light chain [Homo sapiens] | 23 |
| 2 | Ig lambda chain – human | 25 |
| 3 | immunoglobulin lambda 2 light chain [Homo sapiens] | 23 |
| 4 | immunoglobulin lambda light chain VLJ region [Homo sapiens] | 28 |
| 5 | Ig A L | 23 |
| 6 | Ig lambda chain NIG76 precursor – human | 23 |
| 7 | immunoglobulin light chain variable region [Homo sapiens] | 23 |
| 8 | Ig nonfunctional kappa-chain (C-region), partial [Homo sapiens] | 12 |
| 9 | immunoglobulin light chain [Homo sapiens] | 24 |
| 10 | immunoglobulin lambda light chain, partial [Homo sapiens] | 23 |
| 11 | immunoglobulin lambda 2 light chain [Homo sapiens] | 23 |
| 12 | Chain L, Tr1.9 Fab Fragment Of A Human Igg1 Kappa Autoantibody | 23 |
| 13 | IgM kappa chain [Homo sapiens] | 24 |
| 14 | Chain L, Crystal Structure Of Anti-Hiv-1 Fab 537-10d In Complex With V3 Peptide Mn | 23 |
| 15 | unnamed protein product [Homo sapiens] | 57 |
| 16 | immunoglobulin lambda light chain VLJ region [Homo sapiens] | 28 |
| 17 | Chain L, Crystal Structure Of The Neutralizing Fab Fragment Abd1556 Bound To The Bmp Type I Receptor Ia | 22 |
| 18 | immunoglobulin kappa light chain variable region [Homo sapiens] | 16 |
| **Cluster of histidine-rich glycoprotein precursor [Homo sapiens]** | | |
| 19 | unnamed protein product [Homo sapiens] | 60 |
| **Cluster of beta-1-syntrophin [Homo sapiens]** | | |
| 20 | syntrophin, beta 1 (dystrophin-associated protein A1, 59kDa, basic component 1) [Homo sapiens] | 58 |

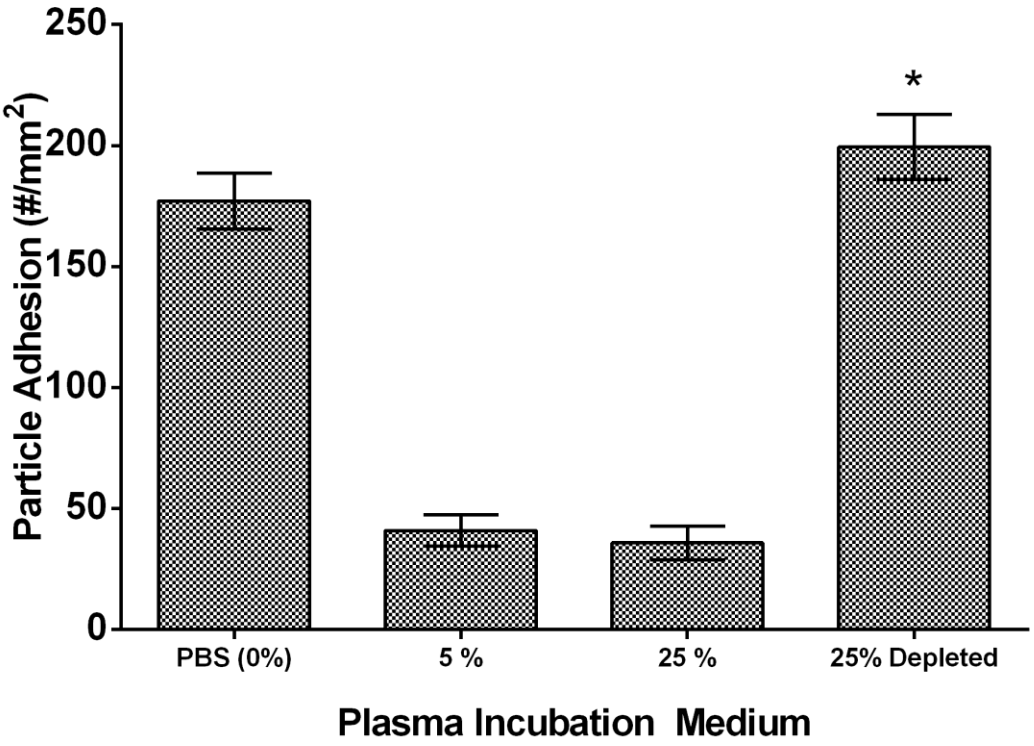


**Figure 3.10** Adhesion of 5 μm PLGA particles at a low $sLe^a$ density (200 +/- 200 sites/$\mu m^2$) to HUVEC in laminar buffer flow at 200 $s^{-1}$ (5 min). Particles were soaked for 1 hour in 1 mL in PBS (0% plasma) or in low HUVEC binding donor plasma at 5% 25%, or 25% with depletion of albumin and immunoglobulins prior to flow in buffer for 5 min. * = Not significant at 99% confidence interval relative to PBS control.

explored. Indeed, about a third or more of plasma proteins in the corona of ultra-small nanoparticles are reported to be conserved with changes in particle size[6,17]. Our results show that the extent of the negative adhesion effect of plasma proteins on PLGA particles is donor dependent, particularly for the largest spherical size evaluated. This "donor effect" is likely linked to variation in plasma protein composition, type, and amount of individual proteins, across different individuals, which results in different levels of the critical negative plasma proteins being absorbed on PLGA particles when exposed to different donor blood. Indeed, recent studies have reported the existence of significant plasma protein diversity within the general human population, irrespective of gender and ethnic background[18,19]. As such, we postulate that PLGA particles in the blood of low-HUVEC binding donors acquire a higher amount of the critical negative plasma proteins, due to higher abundance of these proteins, which leads to a greater reduction in their HUVEC adhesion in the flow of plasma from these donors than observed in the plasma of high-HUVEC binding donors. This assertion is supported by the observation of a thicker protein band at the 150 kDa protein size range on the SDS-PAGE gel for the corona stripped from ~5 μm PLGA particles soaked in plasma from a low-HUVEC binding donor compared to the corona obtained from ones soaked in plasma from a high-HUVEC binding donor. The significantly lower adhesion of the 330 nm spheres in the plasma flow of high binding donors relative to adhesion in viscous buffer versus the lack of a plasma protein impact on the adhesion of 5 μm spheres in the plasma flow of the same high binding donors relative to viscous buffer would suggest that effect of plasma proteins on particle adhesion is more pronounced for the smaller spheres. As aforementioned, protein adsorption processes are the result of thermodynamic gradients that depend on the space available, e.g., particle size,

for adsorption to take place[17,20]. As such, it is likely that the distinction between a high and a low HUVEC binding donor in terms of plasma protein concentration is less impactful when there is a small surface area for adsorption. However, it is also possible that the larger surface area for contact, and hence more copies of targeting ligand, presented to the EC monolayer by the 4.6 μm spheres facilitate a binding advantage relative to the smaller spheres for assays conducted at a fixed ligand density (e.g., 1.4 μm spheres), though the larger spheres also experience greater hydrodynamic forces (scale directly with particle diameter[21]) that disrupts their adhesion. Overall, in light of this robust negative effect of the plasma protein corona on the adhesion of the 330 nm PLGA spheres with an actual size range from ~170–500 nm, it is anticipated that PLGA nanospheres with sizes in the 50–100 nm range are likely to also exhibit negative adhesion in human blood flow. Future studies include modifying the particle fabrication techniques used here to obtain PLGA nanoparticles in this size range to confirm this assertion. Finally, though there was no significant donor effect observed with the adhesion of PS spheres in blood relative to buffer flow, the slight reduction in the adhesion of PS particles in the blood of donor A, which consistently conferred the greatest reduction in PLGA adhesion (Figure 3.4A), compared to adhesion of PS in the blood of other donors may suggest that particles of any material type can have their vascular-targeted adhesion negatively impacted at a high enough plasma concentration of the negative proteins in blood.

The lack of a significant difference in the PLGA adhesion levels between plasma and whole blood flow assays for low HUVEC binding donors suggests that the effect of the adsorbed plasma proteins is large enough in these cases, i.e., high adsorption of critical negative proteins, to make any blood cell-particle interactions that may impact adhesion

level inconsequential (Figure 3.4A, donors A, C, H, J and N). Conversely, the level of adsorption of plasma proteins on PLGA in the blood of high HUVEC binding donors is likely not as robust such that PLGA adhesion is only mildly affected in the flow of plasma from these donors. However, when particle-blood cell interactions (e.g., collisions) that have previously been reported between microspheres and RBCs and WBCs[15] are present in whole blood flow, it served to further disrupt particle adhesion. This explains the larger reduction in the adhesion of 5 μm spheres in whole blood assays relative to plasma for high-HUVEC binding donors. The distinction between plasma flow adhesion and whole blood adhesion is less pronounced for the smaller spheres evaluated likely due to a reduced (or possibly absent) effect of blood cell-particle interaction for the smaller sizes. We previously reported that the adhesion of 5 μm spheres are significantly reduced in laminar blood flow as the blood hematocrit, or RBC concentration, is increased from 30 to 45% while the adhesion of nanospheres and small microspheres remains the same or is slightly higher with the same increase in blood hematocrit[15]. Here, the presence of RBCs in flow helps concentrate the smaller particles at the wall relative to plasma flow[2] but with no negative impact from blood cell interactions; hence the higher adhesion of the 330 nm particles in whole blood relative to plasma flows for high-HUVEC binding donors. However, the impact of a higher concentration of the 4.6 μm spheres at the wall in blood flow on their adhesion would be negated by the cell-particle collisions that tend to disrupt adhesion for this particle size. This cell-particle phenomenon also in part explains why the 330 nm and 1.4 μm spheres exhibit significantly enhanced binding in RBC-in-buffer relative to buffer flow (Figure 3.1 C-D).

The fact that targeting ligand density affects the adhesion of PLGA particles in different donor blood would suggest that the critical negative proteins adsorbed on PLGA are interfering with particle-HUVEC binding by weakening the affinity of the receptor-ligand interactions as alluded to in the discussion of the observed donor effect in the previous section. Specifically, in certain donor bloods (i.e., low HUVEC binding donors) where PLGA particles can attract a high amount of the critical negative proteins, the kinetics of the attached ligand is significantly weakened and hence a large reduction in the capacity of the targeted particle to bind in flow is observed irrespective of a high or low ligand density or, as aforementioned, whether or not the vascular wall interaction is occurring in whole blood (the presence of collisions from blood cells) or plasma flow (Figure 3.4). In other donor bloods where the concentrations of the negative plasma proteins are likely appropriately lower, PLGA adhesion is minimally affected in plasma flow when the PLGA particles are at a high targeting ligand density. However, there is still some moderate weakening of ligand kinetics occurring in these cases, which is highlighted by the significantly reduced particle adhesion when a low targeting ligand density (donors B, E and I) is present on the particle surface. For these donor bloods, the exaggeration of the negative adhesion of PLGA particles at low ligand density relative to high ligand density may not necessarily be due solely to greater changes in ligand affinity associated with a larger amount of adsorbed proteins on particles but could also be due to low avidity of the moderately weakened ligands. That is, there is not enough of the moderately weakened ligand to support adhesion at a fixed wall shear stress in flow.

Finally, it is not surprising that PEGylation of PLGA particles has no apparent effect on their negative adhesion in human blood. While the use of PEG spacers located

between the material surface and the targeting ligand is a strategy that is often employed to reduce protein adsorption on VTCs, it is known that protein adsorption is always present at some basal level on PEG grafted VTCs. For example, Gref et al. showed that PEG-coated surfaces can still support protein adsorption via direct interactions with the core material even at high PEG density, poly(lactic acid) (PLA), PLGA and poly(ε-caprolactone) (PCL) nanoparticles coated with the same high density of PEG where shown to adsorb different levels and types of protein on their surfaces[22]. However, it remains possible that use of an ultra-high surface PEG density resulting in minimal protein adsorption on the carrier surface may abate the negative effect of plasma[23]. In our ongoing work, we are exploring whether variation in PEG density and chain length can alter PLGA particle adhesion to the vascular wall in blood.

## 3.4 Conclusions

In this work, the adsorption of certain plasma proteins from human blood onto PLGA carriers were found to prevent these particles from effectively adhering to activated HUVECs in *in vitro* assays, an effect that was not observed for particles of other material types. Our results also show that the extent of the negative adhesion effect of plasma proteins on PLGA particles is dependent on specific blood donors and the targeting ligand density but not the targeting ligand type. Overall, the presented data suggests that specific knowledge of the plasma protein composition across different humans may be critical to VTC design and their successful clinical use, i.e., highlighting the need for a shift toward personalized medicine in the design of targeted therapeutics. Alternatively, it is possible that with a detailed understanding of the specific proteins that affect particle vascular targeting, novel biomaterials can be designed to resist the adsorption of these proteins in

order to achieve enhanced vascular targeting irrespective of the plasma composition of different individuals. A potential limitation to this study, however, is in our evaluation of blood flow adhesion *in vitro* over culture endothelial cells. A detailed conclusion of the effect of plasma proteins on particle margination may necessitate evaluation via *in vivo* in animal models—though differences in plasma protein composition between human and common animals used in experimental research may complicate such analysis. Our future studies will aim to specifically identify which individual plasma proteins in human blood are associated with low PLGA margination as well as to further investigate the existence of this plasma protein effect for other biomaterials. Furthermore, we will conduct preliminary *in vitro* assays of particle margination in mouse blood flow to identify any potential difference in PLGA (and other biomaterials) adhesion relative to human blood as a first step toward future *in vivo* analysis of plasma protein modulation of vascular-targeted particle margination.

## References


1. Allen, T. M. & Cullis, P. R. Drug delivery systems: entering the mainstream. *Science* **303,** 1818–1822 (2004).

2. Charoenphol, P., Huang, R. B. & Eniola-Adefeso, O. Potential role of size and hemodynamics in the efficacy of vascular-targeted spherical drug carriers. *Biomaterials* **31,** 1392–1402 (2010).

3. Lee, T.-R. *et al.* On the near-wall accumulation of injectable particles in the microcirculation: smaller is not better. *Sci. Rep.* **3,** 2079 (2013).

4. Müller, K., Fedosov, D. A. & Gompper, G. Margination of micro- and nano-particles in blood flow and its effect on drug delivery. *Sci. Rep.* **4,** (2014).

5. Yan, Y. *et al.* Differential Roles of the Protein Corona in the Cellular Uptake of Nanoporous Polymer Particles by Monocyte and. *ACS Nano* **7,** 10960–10970 (2013).

6. Lundqvist, M. *et al.* Nanoparticle size and surface properties determine the protein corona with possible implications for biological impacts. *Proc. Natl. Acad. Sci.* **105,** 14265–14270 (2008).

7. Mirshafiee, V., Mahmoudi, M., Lou, K., Cheng, J. & Kraft, M. L. Protein corona significantly reduces active targeting yield. *Chem. Commun. (Camb).* **49,** 2557–2559 (2013).

8. Salvati, A. *et al.* Transferrin-functionalized nanoparticles lose their targeting capabilities when a biomolecule corona adsorbs on the surface. *Nat. Nanotechnol.* **8,** 137–143 (2013).

9. Fleischer, C. C., Kumar, U. & Payne, C. K. Cellular binding of anionic nanoparticles is inhibited by serum proteins independent of nanoparticle composition. *Biomater. Sci.* **1,** 975–982 (2013).

10. Deng, Z. J. *et al.* Differential plasma protein binding to metal oxide nanoparticles. *Nanotechnology* **20,** 455101 (2009).

11. Safi, M., Courtois, J., Seigneuret, M., Conjeaud, H. & Berret, J. F. The effects of aggregation and protein corona on the cellular internalization of iron oxide nanoparticles. *Biomaterials* **32,** 9353–9363 (2011).

12. Galimard, A. *et al.* Thirty-femtogram detection of iron in mammalian cells. *Small* **8,** 2036–2044 (2012).

13. Kittler, S. *et al.* The influence of proteins on the dispersability and cell-biological activity of silver nanoparticles. *J. Mater. Chem.* **20,** 512–518 (2010).

14. Charoenphol, P. *et al.* Targeting therapeutics to the vascular wall in atherosclerosis--carrier size matters. *Atherosclerosis* **217,** 364–370 (2011).

15. Charoenphol, P., Onyskiw, P. J., Carrasco-Teja, M. & Eniola-Adefeso, O. Particle-cell dynamics in human blood flow: implications for vascular-targeted drug delivery. *J. Biomech.* **45,** 2822–2828 (2012).

16. Onyskiw, P. J. & Eniola-Adefeso, O. Effect of PEGylation on Ligand-Based Targeting of Drug Carriers to the Vascular Wall in Blood Flow. *Langmuir* **29,** 11127–11134 (2013).

17. Tenzer, S. *et al.* Nanoparticle size is a critical physicochemical determinant of the human blood plasma corona: A comprehensive quantitative proteomic analysis. *ACS Nano* **5,** 7155–7167 (2011).

18. Yovita, H., Djumhana, A., Abdurachman, S. A. & Saketi, J. R. Correlation between anthropometrics measurements, prealbumin level and transferin serum with Child-Pugh classification in evaluating nutritional status of liver cirrhosis patient. *Acta Med Indones* **36,** 197–201 (2004).

19. Pakharukova, N. A., Pastushkova, L. K., Moshkovskii, S. A. & Larina, I. M. Variability of the healthy human proteome. *Biochem. Suppl. Ser. B Biomed. Chem.* **5,** 203–212 (2011).

20. Walkey, C. D. & Chan, W. C. W. Understanding and controlling the interaction of nanomaterials with proteins in a physiological environment. *Chem. Soc. Rev.* **41,** 2780–2799 (2012).

21. Decuzzi, P., Lee, S., Bhushan, B. & Ferrari, M. A Theoretical Model for the Margination of Particles within Blood Vessels. *Ann. Biomed. Eng.* **33,** 179–190 (2005).

22. Gref, R., Lück, M. & Quellec, P. 'Stealth'corona-core nanoparticles surface modified by polyethylene glycol (PEG): influences of the corona (PEG chain length and surface density) and of the core. *Colloids Surfaces B Biointerfaces* **18,** 301–313 (2000).

23. Medina, S. H. *et al.* Targeting hepatic cancer cells with pegylated dendrimers displaying N-Acetylgalactosamine and SP94 peptide ligands. *Adv. Healthc. Mater.* **2,** 1337–1350 (2013).

# CHAPTER 4: PLASMA IMMUNOGLOBULINS DRIVE CORONA-INDUCED NEGATIVE ADHESION EFFECTS ON PLGA DRUG CARRIERS


## ABSTRACT

The plasma protein corona has been identified to have deleterious effects on nanoparticle targeting efficiency to reactive substrates as well as human blood flow *in vitro*. Although protein size has been implicated in corona-induced negative targeting effects, the role of specific proteins in this process remains largely unknown. This work explores the adhesion of PLGA drug carriers pre-soaked in plasma which has been depleted and replaced with specific immunoglobulin proteins, in effort to pinpoint which immunoglobulin class is largely responsible in causing corona-induced negative adhesion. Here, it is observed that particles soaked in immunoglobulin depleted plasma enjoy full adhesion recovery relative to non-depleted plasma. Furthermore, particles soaked in immunoglobulin depleted plasma spiked with an antibody solution containing ~70% IgA1 causes full adhesion knockdown resulting in adhesion levels similar to that observed with particles pre-soaked in non-depleted plasma (~60% reduction relative to buffer). However, when particles were soaked in immunoglobulin depleted plasma spiked with antibody solutions with $\geq$ 95% IgG and IgM, minimal adhesion knockdown was observed (4-25% reduction relative to buffer). Overall, this study reveals that corona-induced negative adhesion of PLGA drug carriers is largely driven by the adsorption of IgA1 protein in blood plasma. Furthermore, this work could serve as an important parameter in predicting targeted drug carrier adhesion efficiency in human blood flow.

## 4.1 Introduction

The rapidly forming NP plasma protein corona has been implicated in a number of drug delivery phenomena, including clearance, biodistribution, circulation time, and recently—NP targeting[1–5]. It has been observed that the corona exerts a negative impact on deposition of nanoparticles to reactive surfaces and targeted cell uptake efficiency in the presence of fetal bovine and human serum. These studies have typically viewed the corona as a "shell" which screens the ligands from interacting with their receptors[4,5]. This corona effect has been described to jeopardize ligand function, conformation, and surface receptor recognition.

Although protein size (i.e., molecular weight) has recently been implicated as an important contributor to the observed negative corona effects on targeted NP deposition[4], the role of individual proteins in driving corona-induced effects remains largely unknown. Previously, immunoglobulins (Igs) were linked to plasma-induced negative adhesion of PLGA microparticles in blood flow. Here, the impact of Igs is further explored via probing the role of specific Ig protein types in modulating the extent of corona-induced negative adhesion of PLGA drug carriers. Specifically, PLGA nanoparticles pre-soaked in depleted plasma (IgG removed versus all Igs removed), and buffer and non-depleted plasma are tested in a parallel plate flow chamber assay. Furthermore, IgG, IgA, and IgM are re-added to Igs depleted plasma to test whether the presence of a specific protein re-establishes adhesion reduction as observed with particles soaked in non-depleted plasma. It is observed that re-addition of an immunoglobulin solution containing $\geq$20% IgA1 mass fraction in the soaking medium results in nearly full adhesion knockdown. Overall, this work suggests that corona-induced effects on PLGA adhesion in blood flow are heavily linked to plasma

IgA1 and to a lesser extent, IgG and IgM. Furthermore, this work could be used to predict PLGA drug carrier adhesion efficiency in blood flow based on an individual's Ig composition and concentration.

## 4.2 Results

### 4.2.1 Assessment of immunoglobulin depletion kit specificity and efficiency

Commercially obtained depletion kits were employed for the removal of IgG, IgA, and other immunoglobulins from human plasma. The efficiency and specificity of the Ig depletion columns employed here were assessed via ELISA and SDS-PAGE of the depleted plasma samples as well as the isolated protein solutions obtained from column elution. For the IgG depleted sample, a Protein A column was employed. Protein A is known to bind IgG with high affinity and IgM, IgA with weak affinity. IgA depletion was performed via an IgA depletion column which consisted of affinity purified anti-IgA beads designed to only bind human IgA. To obtain all Igs depleted plasma, an Immunoglobulin/Albumin depletion kit was employed which has been tested via ELISA by the manufacturer and shown to deplete >99% of all Igs in plasma or serum. In addition, IgG + IgA depleted plasma was obtained by sequential exposure of plasma to the Protein A column followed by the IgA depletion column. Table 4.1 lists the % protein retained in plasma post exposure to the different columns/beads relative to non-depleted plasma obtained via sandwich ELISA. IgG, IgM, and IgA1 together constitute ~98% of all immunoglobulin content and thus is taken as an approximation for the total plasma Ig content. Overall, the Protein A column designed to deplete IgG showed high specificity, removing ~92% of plasma IgG and retaining 80% of IgA1. Some loss in IgM was observed (~50%). On the other hand, the IgA depletion column was rather nonspecific as the IgA

depleted sample was also devoid of ~99% of IgG and IgM. Similar results were observed for the IgG + IgA depleted sample. The Igs depleted plasma showed no detectable signal for IgG, IgM, or IgA1 which is consistent with manufacturer testing.

**Table 4.1** Assessment of Ig concentration post depletion column/bead exposure

| ***Plasma sample type*** | ***% IgG retained*** | ***% IgM retained*** | ***% IgA1 retained*** |
|---|---|---|---|
| IgG depleted | 7.9±6.4 | 54.4±1.6 | 80.2±1.5 |
| IgA depleted | 1.4±0.7 | 1.0±0.7 | 0 |
| IgG + IgA depleted | 1.4±0.3 | 0 | 0 |
| Igs depleted | 0 | 0 | 0 |

To test whether specific Igs can re-establish corona-induced adhesion reduction, the isolated products obtained from the IgG and IgA depletion columns were collected via elution with glycine. Figure 4.1A shows the fractional Ig composition (measured via ELISA) collected from the Protein A column (IgG*), IgA depletion column (IgA*), and IgA* x-IgG, which was obtained by collecting the eluted product from the IgA column with IgG depleted plasma. In addition, an SDS-PAGE of the depleted plasma and eluted samples for IgG* and IgA* is shown in Figure 4.1B-C. Since IgG, IgM, and IgA1 constitute ~98% of all Ig content, the normalized Ig fraction is based on the sum of the abundance of these three proteins. Contributions from IgA2, IgD, and IgE were not tested or included in these assays as it is known these proteins have a much lower concentration in blood than IgG, IgM, and IgA1. IgG* was approximately 95% IgG, 3% IgM, and 2% IgA1. IgA* contained mostly IgG (~76%) but did contain ~14% more IgA1 by volume along with a slight increase in IgM content relative to IgG*. For IgA* x-IgG, the IgA1 fraction was ~72%, IgG ~17%, and IgM, ~11%. In addition, commercial IgM was employed which is tested by the manufacturer via HPLC to have purity of ≥ 95%.

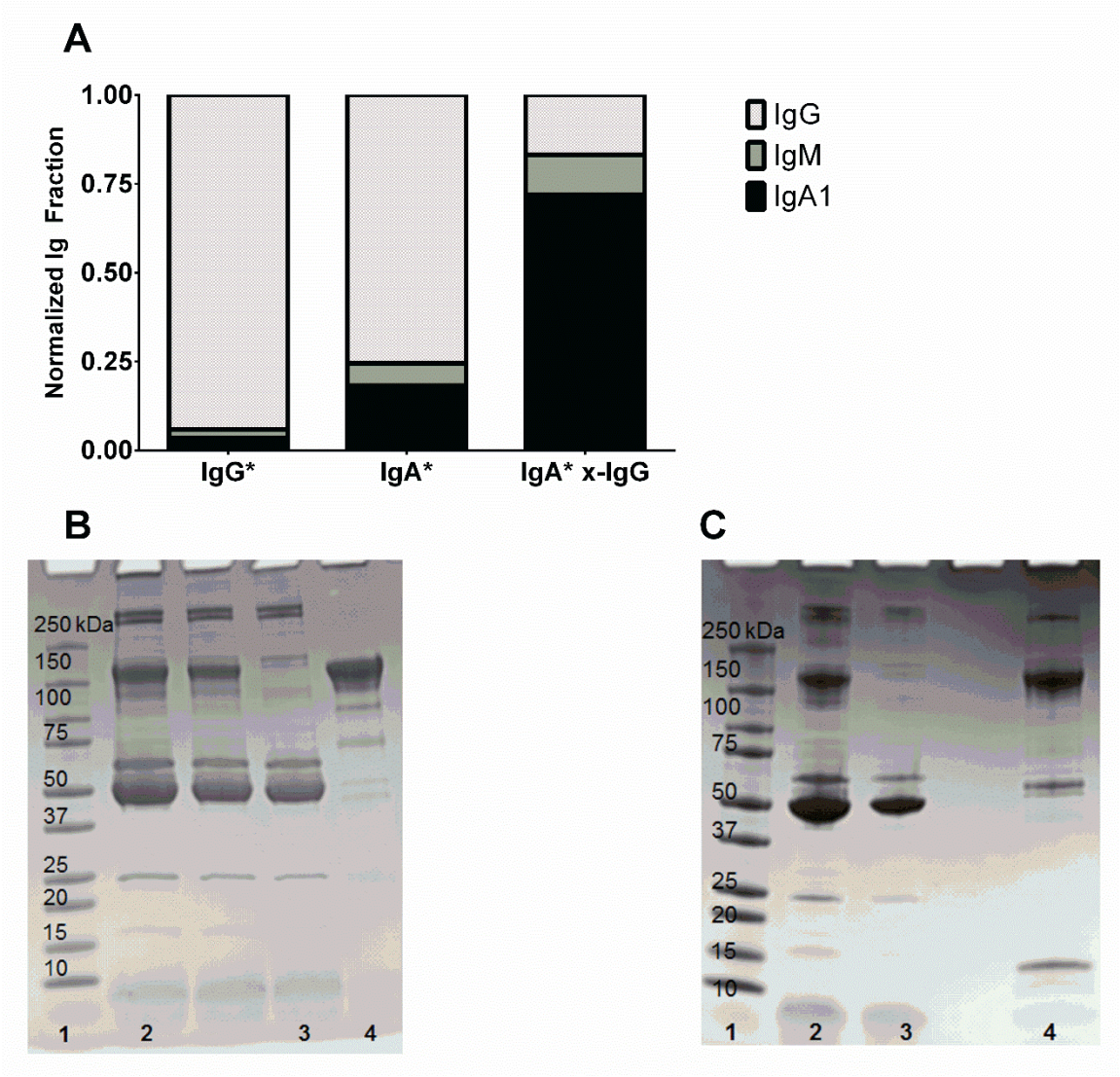


**Figure 4.1.** A) ELISA Quantification of plasma IgG, IgM, and IgA1 fractions in the eluted product from the Protein A column (IgG*), IgA depletion column (IgA*), and in the case where IgG depleted plasma was exposed to the IgA depletion column (IgA* x-IgG). B) SDS-PAGE of IgG depleted plasma and IgG*: Lane 1 – standard, Lane 2 – 2% plasma, Lane 3 – 2% plasma (IgG depleted), and Lane 4 – IgG*. C) SDS-PAGE of IgA depleted plasma and IgA*: Lane 1 – standard, Lane 2 – 2% plasma, Lane 3 – 2% plasma (IgA depleted), and Lane 4 – IgA*.

### 4.2.2 Evaluation of PLGA particle adhesion pre-soaked in depleted plasma

The goal of this work is to evaluate the role of individual Ig proteins in modulating the previously observed corona-induced negative adhesion of PLGA particles in blood flow[6]. 500 nm PLGA nanoparticles are used in this work given their relevance to drug delivery. IgG is a natural candidate to consider since this protein alone constitutes ~75% of the total Ig content in plasma. In these experiments, Sialyl-lewis$^a$ (sLe$^a$) coated PLGA particles (2300 $\pm$ 500 sites/$\mu m^2$) were pre-soaked for 1 hour in IgG depleted plasma, IgG + IgA depleted plasma, all Igs depleted plasma, non-depleted plasma, or buffer followed by the PPFC assay in plasma free blood flow (i.e., RBCs-in-VB, at 38% hematocrit) over inflamed human umbilical vein endothelial cells (HUVECs). All data was normalized to the adhesion obtained when pre-soaking in PBS buffer. 25% plasma solutions were employed for these assays since depletion kit utility requires a plasma dilution step. In addition, due to the nonspecific nature of the IgA depletion column, plasma depleted of IgA only was not possible.

Although PLGA particles soaked in only IgG removed plasma did not significantly recover adhesion, pre-soaking in plasma depleted of IgG + IgA or all Igs resulted in significant adhesion recovery when averaged across multiple donors (Figure 4.2A). PLGA particle adhesion pre-soaked in IgG-depleted plasma was also explored for individual donors and interestingly, significant adhesion recovery was observed only in the case of particles soaked in IgG-depleted plasma from donor N (Figure 4.2B) which also showed a high plasma IgG concentration (Figure 4.2C). All donors exhibited significant adhesion in Igs depleted plasma.

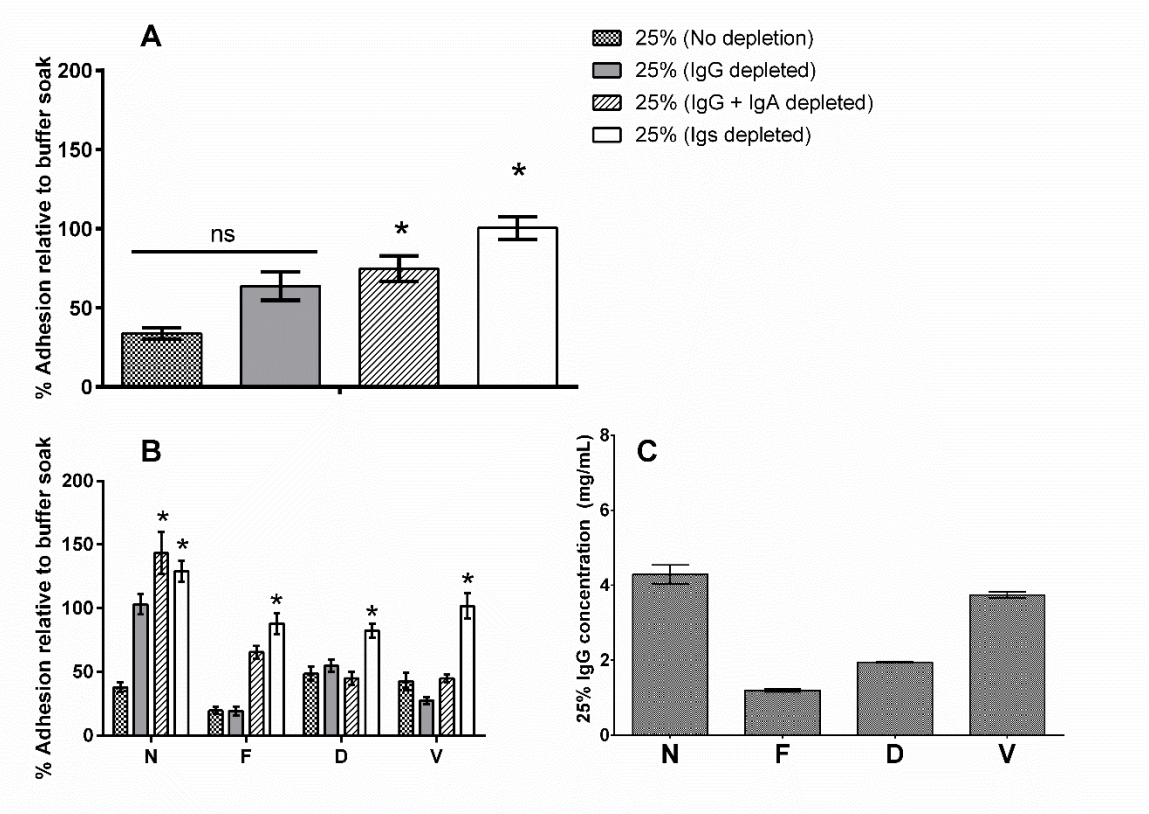


**Figure 4.2.** A) Adhesion of sle[a]-targeted PLGA particles soaked for 1 hr in 25% plasma (No depletion), 25% IgG depleted plasma, 25% IgG + IgA depleted plasma, 25% Igs depleted plasma, prior to a parallel plate flow chamber assay in RBCs-in-VB (38% hematocrit) at 200 $s^{-1}$. * = $p < 0.01$ compared to 25% (No depletion) trial, concentration $1 \times 10^6$ # particles/mL, n = 3 (averaged across donors N,F,D,V). B) PLGA particle adhesion in the same mediums as (A) but on a donor-to-donor basis. C) ELISA of IgG concentration in the various donors.

### 4.2.3 Evaluation of PLGA particle adhesion pre-soaked in Igs depleted plasma with re-addition of specific Ig proteins

In addition, particles were also pre-soaked in Igs depleted plasma which had been spiked with IgG*, IgA*, IgA* x-IgG, and commercial IgM to probe whether replacement of approximately individual Ig protein classes in the soaking medium is solely capable of re-establishing corona-induced negative adhesion (Figure 4.3). IgG* was re-added to 25% Igs depleted plasma soaking medium at ~5 mg/mL, mainly to test whether a high physiological IgG concentration could explain the lack of sensitivity to IgG depletion. In addition, a concentration of ~5 mg/mL is similar to donor N, which showed unique sensitivity to IgG depletion (Figure 4.3A). Overall, minimal adhesion knockdown of PLGA particles was observed when pre-soaked in Igs depleted plasma + 5 mg/mL IgG* (Figure 4.3A). However, soaking in Igs depleted plasma spiked with IgA* at ~1 mg/mL or IgA* x-IgG at a physiological IgA concentration resulted in significant adhesion knockdown resulting in no statistical difference relative to the non-depleted plasma control. A physiological IgA concentration chosen for the IgA* x-IgG sample since this solution was mostly IgA. In addition, commercial IgM was re-added at 0.2 mg/mL which is consistent with the physiological level for donor D and resulted in significant adhesion knockdown, but to a lesser extent than the re-addition of IgA* or IgA* x-IgG. Physiological concentrations of IgA1 and IgM were based on the ELISA measurements in Figure 4.3B. Figure 4.3C shows the SDS-PAGE of the various solutions that the particles were pre-soaked in prior to the adhesion assay.

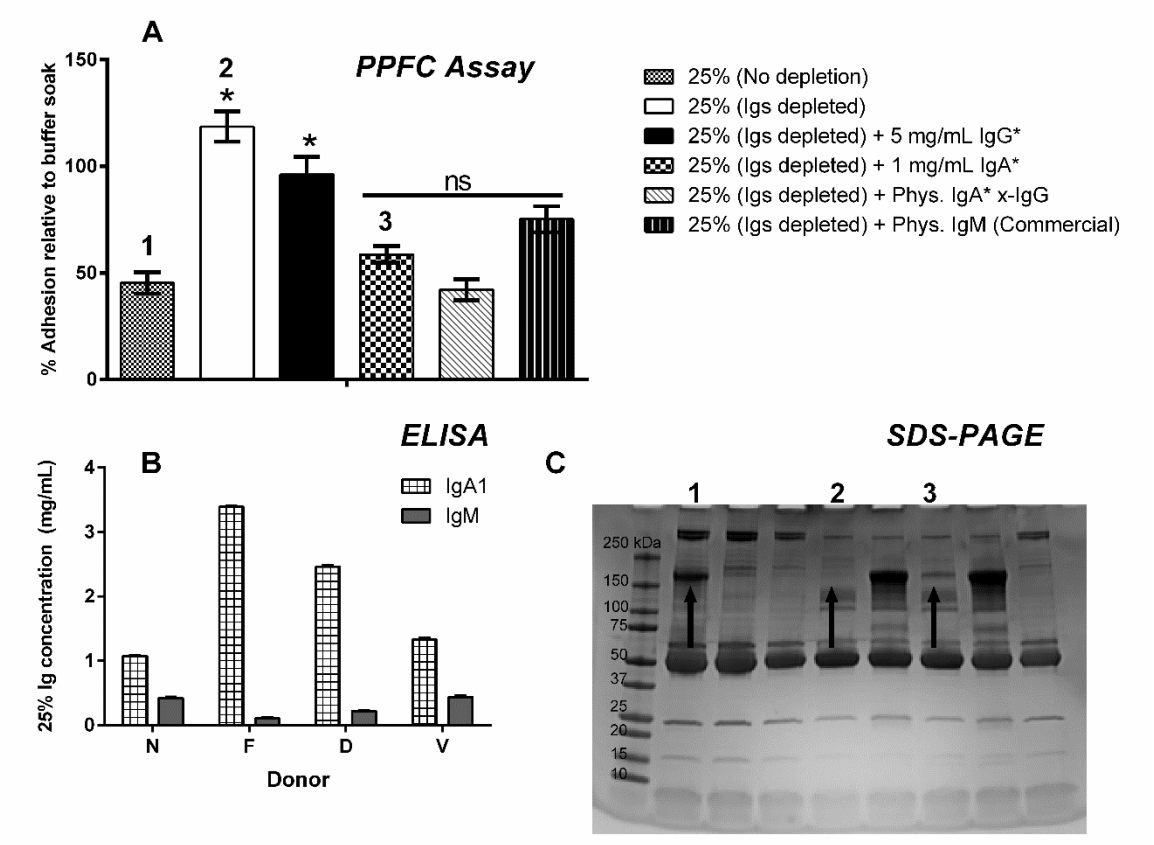


**Figure 4.3.** A) Adhesion of sle[a]-targeted PLGA particles soaked for 1 hr in 25% plasma (No depletion), 25% Igs depleted plasma and 25% Igs depleted plasma + 5 mg/mL IgG*, 1 mg/mL IgA*, IgA* x-IgG, and commercial IgM prior to a parallel plate flow chamber assay in RBCs-in-VB (38% hematocrit) at 200 $s^{-1}$. * = $p < 0.01$ compared to 25% (No depletion) trial, concentration $1 \times 10^6$ # particles/mL. B) ELISA testing of IgA1 and IgM concentrations for different donors. C) SDS-PAGE of the 25% plasma solutions PLGA particles were soaked with prior to flow assay; Lane 1: molecular weight ladder, Lane 2: no depletion, Lane 3: IgG depleted, Lane 4: IgA depleted, Lane 5: Igs depleted, Lane 6: Igs depleted + 5 mg/mL IgG*, Lane 7: Igs depleted + 1 mg/mL IgA*, Lane 8: Igs depleted + 5 mg/mL IgG* + 1 mg/mL IgA*, Lane 9: IgA + IgG depleted.

## 4.3 Discussion

The data presented in this work seeks to pinpoint the role of specific plasma Ig proteins in orchestrating corona-induced negative adhesion of PLGA particles in human blood flow. The Ig population in human plasma is dominated by IgG, which comprises ~75% of the human Ig content. Due to its high abundance, it was hypothesized that this protein is a major player in causing PLGA adhesion reduction. Surprisingly, depletion of IgG alone (Figure 4.2A) did not result in considerable recovery in adhesion for nearly all donors tested. An exception was observed in the case of particles soaked in IgG-depleted donor N plasma (Figure 4.2B). However, when particles were soaked in donor N plasma depleted of all Igs and spiked with donor N IgG*, minimal adhesion knockdown was observed, suggesting that adhesion knockdown depends on the presence of other Igs. When averaged across multiple donors, depletion of IgG + IgA as well as all Igs resulted in full adhesion recovery (i.e. no difference relative to soak in buffer) (Figure 4.2A). Although depletion of IgG alone from the soaking medium did not result in significant particle adhesion recovery, this could be linked to differences in the IgG concentration as some donors (i.e. F,D) had lower IgG concentrations than donor N where an effect was observed upon IgG removal. The potential for IgG to re-establish adhesion reduction was probed via soaking particles in 25% Igs depleted plasma + 5 mg/mL IgG* (a high physiological concentration); however, no significant effect was observed suggesting that IgG, despite being the most abundant IgG protein, is likely at most a minor contributor to the reduced PLGA adhesion observed post plasma soaking (Figure 4.3). However, when PLGA particles were soaked in Igs depleted plasma spiked with solutions of higher IgA fraction (i.e. IgA*, IgA* x-IgG), significant adhesion knockdown was observed, suggesting this

protein to be a major player in orchestrating PLGA adhesion reduction. Other Igs such as IgM likely exhibit secondary roles evidenced by adhesion knockdown observed with particles soaked in IgM spiked solutions (Figure 4.3).

## 4.4 Conclusions

Overall, this work confirms the role of Igs in driving plasma-induced PLGA adhesion reduction through Ig depletion and re-addition experiments. The most abundant Ig protein, IgG, surprisingly exhibits a minor, if any role in establishing plasma-induced PLGA adhesion reduction. Contrastingly, IgA appears to be the critical Ig class responsible for orchestrating PLGA adhesion reduction. Further work will seek to limit IgA adsorption via covalent coating with dysopsonin proteins such human serum albumin and apolipoproteins.

## References


1. Kang, B. *et al.* Carbohydrate-Based Nanocarriers Exhibiting Specific Cell Targeting with Minimum Influence from the Protein Corona. *Angew. Chemie - Int. Ed.* **54,** 7436–7440 (2015).

2. Dai, Q., Walkey, C. & Chan, W. C. W. Polyethylene glycol backfilling mitigates the negative impact of the protein corona on nanoparticle cell targeting. *Angew. Chem. Int. Ed. Engl.* **53,** 5093–5096 (2014).

3. Aggarwal, P., Hall, J. B., McLeland, C. B., Dobrovolskaia, M. a & McNeil, S. E. Nanoparticle interaction with plasma proteins as it relates to particle biodistribution, biocompatibility and therapeutic efficacy. *Adv. Drug Deliv. Rev.* **61,** 428–437 (2009).

4. Mirshafiee, V., Mahmoudi, M., Lou, K., Cheng, J. & Kraft, M. L. Protein corona significantly reduces active targeting yield. *Chem. Commun. (Camb).* **49,** 2557–2559 (2013).

5. Salvati, A. *et al.* Transferrin-functionalized nanoparticles lose their targeting capabilities when a biomolecule corona adsorbs on the surface. *Nat. Nanotechnol.* **8,** 137–143 (2013).

6. Sobczynski, D. J. *et al.* Plasma protein corona modulates the vascular wall interaction of drug carriers in a material and donor specific manner. *PLoS One* **9,** e107408 (2014).

# CHAPTER 5: IMPACT OF BIODEGRADABLE MATERIAL TYPE ON CORONA-INDUCED NEGATIVE ADHESION OF DRUG CARRIERS IN HUMAN BLOOD FLOW


## ABSTRACT

Previous work has revealed that the plasma protein corona in blood flow significantly reduces vascular-targeted drug carrier (VTC) adhesion efficiency *in vitro,* particularly for poly(lactic-co-glycolic) acid (PLGA) microspheres. However, the impact of the plasma protein corona on VTC adhesion efficiency of other common biodegradable materials (e.g., polylactic acid (PLA), polycaprolactone (PCL)) remains relatively unknown. Here, the potential role of biodegradable VTC material type on the extent of corona-induced adhesion reduction is explored via *in vitro* parallel plate flow chamber (PPFC) assays. Overall, it is observed that the extent of corona-induced VTC adhesion reduction is tempered depending on the material type employed. Specifically, PCL exhibited mild reduction in whole blood (WB) (~25% reduction) compared to PLA and PLGA (~75% reduction). In addition, PCL is observed to adsorb less immunoglobulin (Ig) protein than PLA or PLGA, a protein type previously linked as a major player in this process. In addition, increased ligand density was observed to mitigate corona-induced effects on PLA and PLGA. Overall, this work suggests that hydrophobic materials such as PCL may have better potential as a vascular-targeted carrier for intravenous therapy application due to its superior adhesion in whole blood relative to plasma-free blood compared to other commonly employed biodegradable drug carriers.

## 5.1 Introduction

Previously, rapid plasma protein adsorption onto PLGA-VTCs was shown to drastically reduce VTC adhesion efficiency to human umbilical vein endothelial cells (HUVECs) in human blood flow. In addition, the extent of plasma-associated reduced adhesion was dependent on ligand density, human donor, and flow profile and these effects were linked to the adsorption of large immunoglobulins in the PLGA corona, which were not significantly present in the polystyrene (PS) corona[1]. Although PLGA VTCs exhibited significant corona-induced adhesion reduction in blood flow, the impact of the protein corona on the adhesion efficiency of other common biodegradable VTCs such as PLA and PCL remains relatively unknown. Biodegradable polyesters, including PLGA, PLA, and PCL differ in their hydrophobicity which is a critical parameter that influences the type, amount, and conformation of surface-bound corona proteins[2,3]. This work explores the role of biodegradable polyester VTC material type on the adhesion efficiency of sialyl-Lewis$^a$ (sLe$^a$) and anti-ICAM-1 targeted NPs (~500 nm in diameter) over a range of ligand densities in human blood flow via *in vitro* PPFC assays. Non-pegylated (non-PEG) particles are employed in the experiments throughout this study to highlight the differential impact of material type in any observed effect of the plasma protein corona, which can shed light on the extent of surface modification required for VTCs of different materials to successfully reduce or alter plasma protein adsorption. Furthermore, the field has shown growing interest in exploiting the protein corona by tailoring its composition to favor adsorption of specific proteins for cell targeting[4–10].

## 5.2 Results

### 5.2.1 Evaluation of the adhesion efficiency of various VTCs in human blood flow

The focus of this work is to evaluate the performance of common biodegradable polyesters in modulating the impact of the protein corona on targeted drug carrier adhesion in human blood flow. PS particles serve as a control in these assays to compare with previous publications. VTC adhesion was evaluated in a PPFC assay in whole blood. The percent (%) control adhesion of $sLe^a$-targeted VTC material types with similar size (Table 5.1) and ligand density in WB relative to that in the plasma-free blood (RBCs-in-VB) is shown in Figure 5.1. PLGA and PLA experienced major adhesion reduction in blood flow (>60% reduction), whereas PCL and PS spheres maintain substantial resistance to the plasma protein corona effect where only ~25% reduction in control adhesion is observed.

**Table 5.1**. Particle size characterization

| *Material* | *Z-Average (nm)* | *PDI* |
|---|---|---|
| PLA | 635 | 0.25 |
| PLGA | 428 | 0.18 |
| PS | 529 | 0.12 |
| PCL | 600 | 0.27 |

### 5.2.2 Evaluation of targeting ligand density and type on blood flow adhesion of biodegradable VTCs

The extent of PLGA plasma-associated adhesion reduction depends on the targeting ligand density as previously observed with $sLe^a$-targeted microspheres[1]. In Figure 5.2A, the $sLe^a$ site density for the different biodegradable polyesters was increased to ~15,000 sites/$\mu m^2$ and is likely close to the saturation limit for these particles. Nearly full adhesion recovery in whole blood relative to RBCs-in-VB was observed for these materials evidenced by small differences between adhesion in whole blood and RBCs-in-VB.

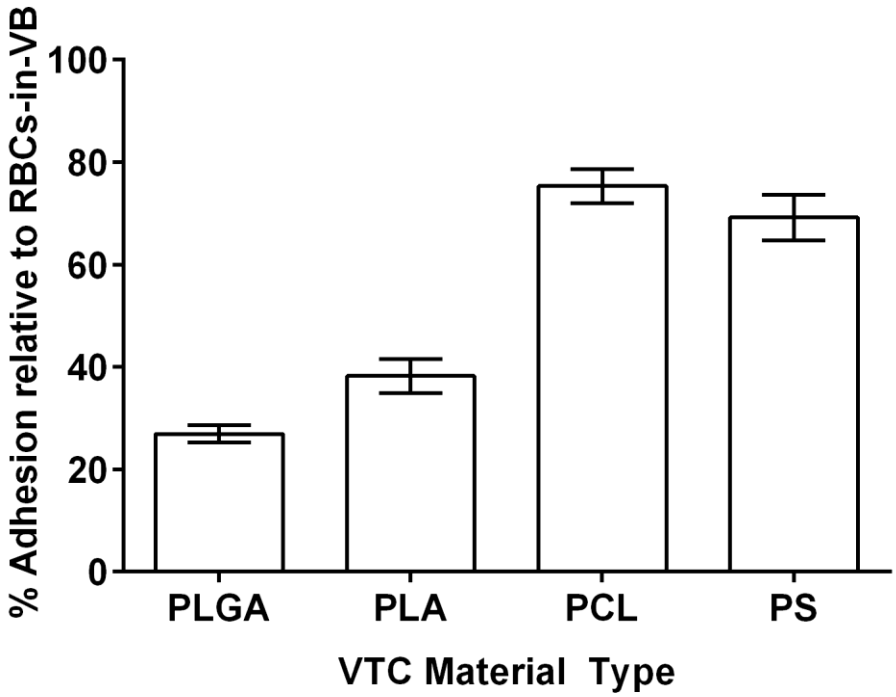


**Figure 5.1** HUVEC adhesion (% relative to RBCs-in-VB Control) for PLGA, PLA, PCL, and PS VTCs in whole blood after 5 min of flow at a shear rate of 200 $s^{-1}$. The site densities with standard error were calculated for each material: PLGA 8600 +/- 600; PLA 7500 +/- 50; PCL 7100 +/- 1200; PS 9200 +/- 300.

In addition, the ligand type ($sLe^a$ versus anti-ICAM-1) was explored for the biodegradable materials at a lower site density in Figure 5.2B. No significant difference in adhesion reduction was observed across these ligand types for the biodegradable materials. In addition, PLGA particles were coated with a high anti-ICAM density to test whether significant recovery in adhesion is possible with other ligand types. Figure 5.2C shows that even at ~19,000 anti-ICAM-1 sites/$\mu m^2$, no significant adhesion recovery is observed. This is an important observation as this site density range is near saturation and thus, for anti-ICAM-1 particles site density is unable to circumvent plasma induced adhesion reduction.

### 5.2.3 Characterization of zeta potential and protein corona profile on VTCs

As observed in Figure 5.1, the negative impact of plasma proteins is dependent on the type of biodegradable VTC. To better understand these results, the zeta potential and protein profile were evaluated for these materials. Highly similar zeta potential values were observed across all material types. Evaluation of the protein profile via SDS-PAGE revealed differences in the amount of specific protein bands, namely at the 50 and 150 kDa mark. Specifically, it was observed that PLGA and PLA coronae formed in WB exhibit increased adsorption (1.47 +/- 0.10 folds via ImageJ) of 150 kDa protein (e.g., immunoglobulins) relative to PCL (Figure 5.2B). In addition, PCL exhibited increased albumin adsorption (1.55 +/- 0.10 increase in relative intensity) compared to PLGA and PLA particles. In Figure 5.3C, it is observed that PS particles also adsorb increased albumin relative to PLGA.

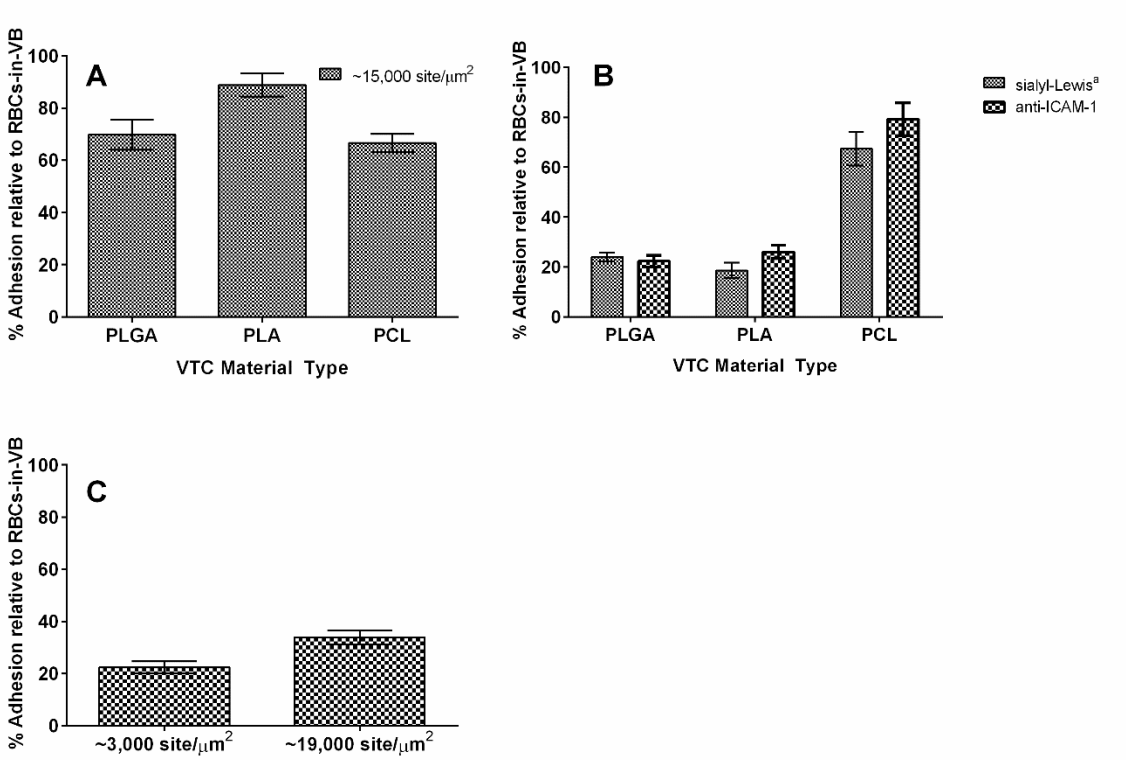


**Figure 5.2** A) HUVEC adhesion (% relative to RBCs-in-VB Control) for PLGA, PLA, PCL, and PS VTCs in whole blood after 5 min of flow at a shear rate of $200s^{-1}$. Site densities for A) were obtained as follows: PLGA 15300 +/- 900; PLA 12300 +/- 100; PCL 14500 +/- 700. B) Effect of targeting ligand type on adhesion efficiency, with the following site densities (#/$\mu m^2$): $sLe^a$, (All materials) 3000 +/- 500; anti-ICAM-1, PLGA 3700 +/- 200; PLA 4000 +/- 100; PCL 3200 +/- 20. C) HUVEC adhesion of high density anti-ICAM-1 coated PLGA particles (19300 +/- 500) versus 3700 +/- 200 sites/$\mu m^2$. Particle concentration was fixed to $1 \times 10^6$ particles/mL in all assays.

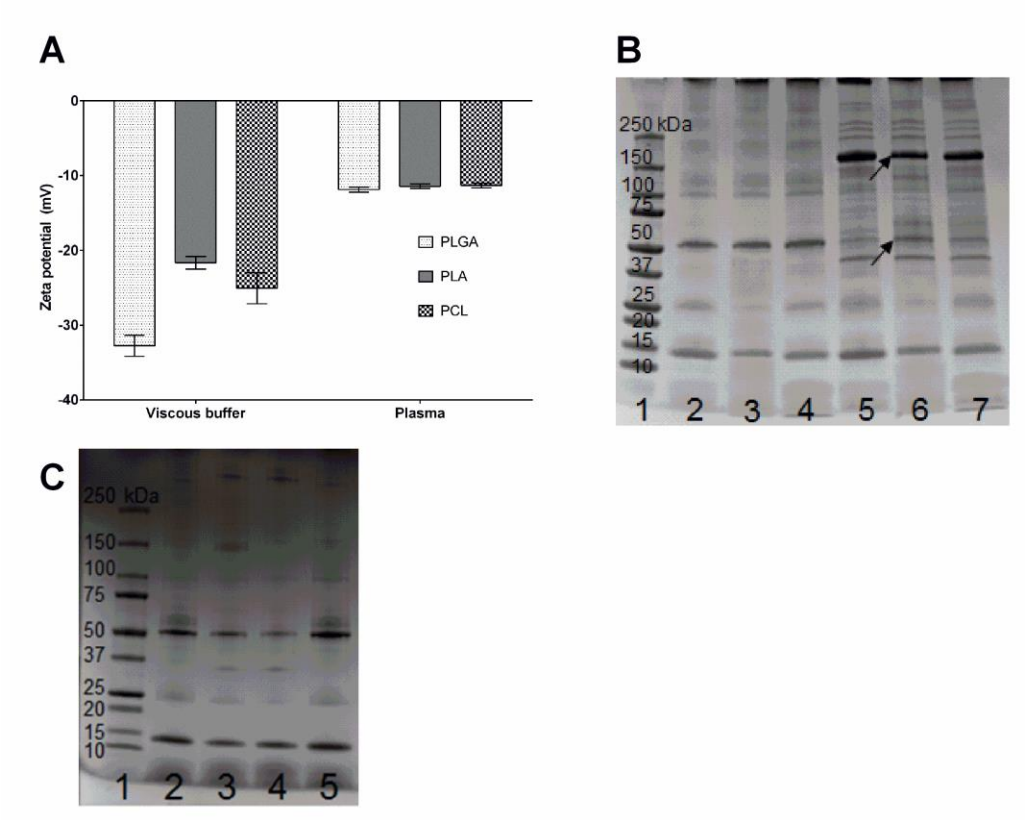


**Figure 5.3** A) Zeta potential measurements for sLe$^a$-coated VTCs of PLGA, PLA and PCL. B) SDS-PAGE of surface bound protein coronae formed on PLGA, PCL, and PLA VTCs exposed to VB and ACD plasma. Lane 1: molecular weight standard, Lane 2: PLGA corona from VB soak, Lane 3: PCL corona from VB soak, Lane 4: PLA corona from VB soak, Lane 5: PLGA corona from plasma soak, Lane 6: PCL corona from plasma soak, Lane 7: PLA corona from plasma soak. C) SDS-PAGE of surface bound protein coronae formed on ~5 μm PLGA and PS VTCs exposed to VB and ACD plasma. Lane 1: molecular weight standard, Lane 2: PS corona in low HUVEC binding donor plasma, Lane 3: PLGA corona from high HUVEC binding donor plasma, Lane 4: PLGA corona in high HUVEC binding donor plasma, Lane 5: PS corona from high HUVEC binding donor plasma

### 5.2.4 Evaluation of covalent attachment of albumin to improve PLGA adhesion efficiency in human blood flow

Although higher site densities resulted in significant adhesion recovery of $sLe^a$-coated spheres, anti-ICAM-1 coated particles did not benefit from an increased targeting ligand density. Thus, tailoring the PLGA plasma protein corona is explored in an attempt to mitigate the negative adhesion impact of the protein corona on PLGA particles. Specifically, covalent attachment of human serum albumin (HSA) to the PLGA surface is performed. Recent literature has exploited HSA attachment to nanoparticles to increase circulation time and limit non-specific adsorption of opsonin proteins (e.g., immunoglobulins)[11,12]. Figure 5.4 shows that covalent attachment of HSA to PLGA-anti-ICAM-1 particles does not improve the adhesion efficiency in whole blood relative to RBCs-in-VB.

## 5.3 Discussion

The experimental data presented in this work shows that the choice of biodegradable VTC material type has a substantial impact on the adhesion efficiency in human blood flow and targeting ligand density was shown to play an important role in the extent of the adhesion differences between material types. Overall, PLGA and PLA particles exhibited major reduction in blood flow whereas PCL particles were largely resistant to corona-induced. However, the negative effect of the plasma protein corona on PLGA and PLA $sLe^a$ particle adhesion for all materials was shown to be largely mitigated when high ligand density (near saturation) was used (Figure 5.2A). In addition, the role of ligand type was briefly explored and found to play a minimal role with the exception that high density anti-ICAM-1 coated PLGA

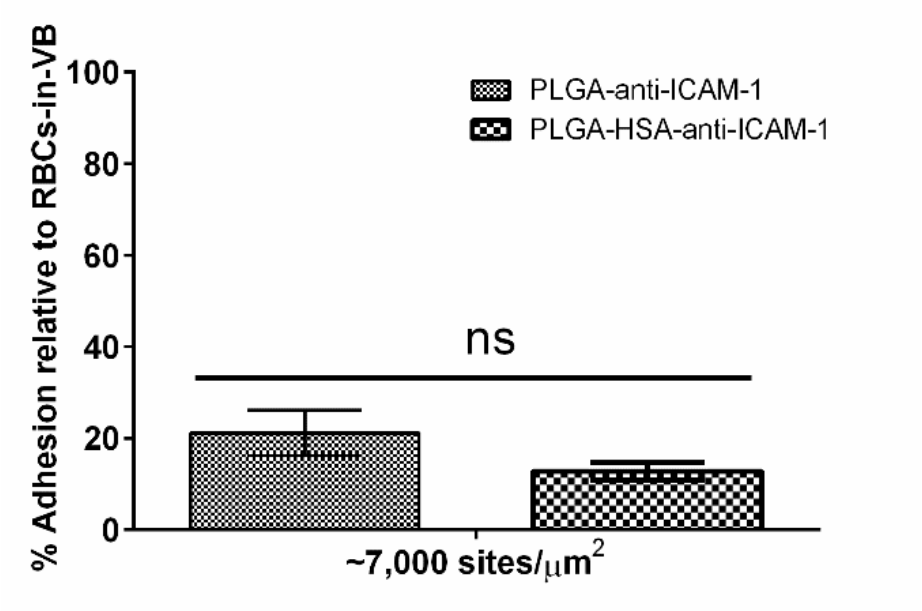


**Figure 5.4** HUVEC adhesion (% relative to RBCs-in-VB Control) for PLGA anti-ICAM-1 particles (6600 +/- 50 sites/$\mu m^2$) along with PLGA anti-ICAM-1 particles covalently linked with human serum albumin (HSA) with 8000 +/- 140 anti-ICAM-1 sites/$\mu m^2$. ~3600 sites of human serum albumin were covalently coupled to the PLGA-HSA-anti-ICAM-1 particles confirmed via an anti-human Albumin-FITC antibody.

particles did not exhibit adhesion recovery in blood flow. This could be due to the slow kinetics of antibody interactions relative to selectin/sLe$^a$, thus preventing adhesion recovery with higher ligand surface coverage.

Although ligand density was observed to abate the impact of the plasma protein corona at high ligand density, significant differences were observed at the lower site density ranges where PCL and PS experienced mild reduction in blood flow compared to PLGA and PLA. It is important to note that the optimal targeting density does not necessarily translate to the highest density possible. Indeed, a recent study has shown that the optimal ligand density for superparamagnetic iron oxide (SPIO) NPs for different NP size and ligand type was at an intermediate density of ~10,000 ligands/μm$^2$, potentially a result of receptor clustering effects[13]. Although this study employed a different particle ligand/receptor system, it suggests here that the high density data may not be optimal *in vivo*, due to increased non-specificity[14]. Now, in theory, it can be expected that upon plasma exposure for plasma-sensitive PLGA and PLA particles with a high targeting ligand density, the effective density would be lower and therefore the variability between particle material types would result in differences in targeting specifity. Thus, it is worthwhile to understand the differences in adhesion efficiency observed across material types at lower targeting ligand density.

Given that the zeta potential of the materials studied here were largely similar in buffer and plasma, electrostatic interactions likely does not explain the large differences in adhesion induced by the plasma protein corona. Hydrophobicity, on the other hand, is known to vary significantly between these materials[15]. Furthermore, hydrophobicity is known to play a critical role in the magnitude, composition, and confirmation of the plasma

protein corona[2]. Specifically, increased hydrophobicity is associated with increased protein adsorption and acceleration of opsonization, leading to faster clearance from the bloodstream[16]. Since the amount of protein adsorption in the different coronae depends on hydrophobicity, this is a potential cause for differential adhesion due to plasma protein interaction. However, given the highly similar zeta potential readings across these materials, it is not expected that the amount of total protein adsorbed in the corona significantly varies between these materials. Thus, it is hypothesized that differences in the composition of the corona (i.e., abundance of particular proteins) caused by hydrophobicity is the driver of the observed differential adhesion interactions of the polyester particles. SDS-PAGE was performed in this work for PLGA, PLA, and PCL particles with the goal to understand the adhesion assay via correlation of the corona profile across different materials. It is observed in Figure 5.2B and 5.3 that the VTC materials largely resistant to corona-induced adhesion reduction (PCL and PS) adsorbed less Igs and more albumin relative to poorly performing PLGA and PLA. The reduced Igs adsorption may explain the differential adhesion efficiency of PCL and PS particles relative to PLGA and PL since high molecular weight immunoglobulins (Igs) were previously implicated in orchestrating corona-induced adhesion reduction of PLGA microparticles in human blood flow[1,17]. Furthermore, albumin is known to have higher affinity for hydrophobic particles and has been reported to increase circulation time of NPs by limiting opsonization (e.g., adsorption of IgG)[11,18] given the dysopsonic nature of this protein. Thus, the hypothesis to favorably tune the corona was tested via covalent attachment of HSA on anti-ICAM-1 coated PLGA particles to improve their blood flow adhesion efficiency. Anti-ICAM-1-coated particles were chosen for the HSA attachment experiment since no significant benefit was observed

for this ligand type at a high ligand density and thus, this corona-tailoring approach could offer an alternative avenue to improve adhesion of these particles. However, no significant improvement in adhesion of PLGA-HSA-anti-ICAM-1 coated particles was observed over the non-HSA conjugated particle control. This could be due to the fact that additional surface albumin molecules are needed to generate an effect, given that the surface is still largely dominated by NeutrAvidin. In a recent study, immunoglobulin proteins were covalently attached to silica nanoparticles in an effort to increase targeted uptake to macrophages, but this strategy was impeded by other corona proteins and no increase in uptake was observed for Ig-coated spheres, suggesting than a corona layer deposits on top of the protein ligand causing interference in binding efficiency[19]. Thus, it may be the case here that the altered corona which forms on the surface of HSA-coated particles still adsorbs a sufficient amount of critical "negative" proteins (e.g., immunoglobulins) in the corona, resulting in an unfavorable immunoglobulin-rich corona and no benefit in PLGA particle adhesion between blood and RBCs-in-VB.

As observed in Fig. 5.1 and 5.2B, the trend in % control adhesion at lower to moderate site densities suggests PCL may be a better candidate as a VTC for vascular diseases. However, it is important to note that PLGA has been observed to maintain a higher bioavailability than PCL *in vivo*[20], and PLGA has more favorable degradation profiles for drug delivery applications.

## 5.4 Conclusions

This work explored the role of material type—particularly, biodegradable polymers—on the previously observed plasma-induced negative adhesion effect observed primarily with PLGA microspheres. Here, it is observed that biodegradable polyesters do

behave differently; namely, that PCL enjoys minimal reduction in blood flow relative to PLGA and PLA, potentially a result of differences in hydrophobicity causing the observed reduced Ig adsorption on PCL spheres. Although the adhesion efficiency for $sLe^a$ particles of all materials was largely abated at high ligand density, lower densities may translate better for *in vivo* targeting. Overall, PCL was more robust than the other polyesters studied here in terms of blood flow adhesion efficiency but there are other differences between these polymers such as degradation rate and bioavailability which need to be considered. Lastly, covalent attachment of dysopsonins (i.e., HSA) onto PLGA did not repel the impact of the corona; however, further tuning of surface protein density and testing of other protein candidates may prove beneficial in this approach.

## References


1. Sobczynski, D. J. *et al.* Plasma protein corona modulates the vascular wall interaction of drug carriers in a material and donor specific manner. *PLoS One* **9,** e107408 (2014).

2. Rahman, M., Laurent, S., Tawil, N., Yahia, L. H. & Mahmoudi, M. *Protein-Nanoparticle Interactions*. (Springer, 2013).

3. Gessner, A., Waicz, R., Lieske, A., Paulke, B. & Ma, K. Nanoparticles with decreasing surface hydrophobicities : influence on plasma protein adsorption. *Int. J. Pharm.* **196,** 245–249 (2000).

4. Salvati, A. *et al.* Transferrin-functionalized nanoparticles lose their targeting capabilities when a biomolecule corona adsorbs on the surface. *Nat. Nanotechnol.* **8,** 137–143 (2013).

5. Kang, B. *et al.* Carbohydrate-Based Nanocarriers Exhibiting Specific Cell Targeting with Minimum Influence from the Protein Corona. *Angew. Chemie - Int. Ed.* **54,** 7436–7440 (2015).

6. Kreuter, J. *et al.* Covalent attachment of apolipoprotein A-I and apolipoprotein B-100 to albumin nanoparticles enables drug transport into the brain. *J. Control. Release* **118,** 54–8 (2007).

7. Kreuter, J. Nanoparticulate systems for brain delivery of drugs. *Adv. Drug Deliv. Rev.* **47,** 65–81 (2001).

8. Kreuter, J. *et al.* Apolipoprotein-mediated transport of nanoparticle-bound drugs across the blood-brain barrier. *J. Drug Target.* **10,** 317–325 (2002).

9. Dobrovolskaia, M. A., Aggarwal, P., Hall, J. B. & Mcneil, S. E. Preclinical Studies to Understand Nanoparticle Interaction with the Immune System and Its Potential Effects on Nanoparticle Biodistribution. *Mol. Pharm.* **5,** 487–495 (2008).

10. Caracciolo, G. *et al.* Cancer cell targeting of lipid gene vectors by protein corona. *Nanotechnology* 354–357 (2012).

11. Ogawara, K. I. *et al.* Pre-coating with serum albumin reduces receptor-mediated hepatic disposition of polystyrene nanosphere: Implications for rational design of nanoparticles. *J. Control. Release* **100,** 451–455 (2004).

12. Roser, M., Fischer, D. & Kissel, T. Surface-modified biodegradable albumin nano- and microspheres. II : effect of surface charges on in vitro phagocytosis and biodistribution in rats. *Eur. J. Pharm. Biopharm.* **46,** 255–263 (1998).

13. Elias, D. R., Poloukhtine, A., Popik, V. & Tsourkas, A. Effect of ligand density, receptor density, and nanoparticle size on cell targeting. *Nanomedicine Nanotechnology, Biol. Med.* **9,** 194–201 (2013).

14. Howard, M. *et al.* Vascular Targeting of Nanocarriers : Perplexing Aspects of the Seemingly Straightforward Paradigm. *ACS Nano* 4100–4132 (2015).

15. D'Addio, S. M. *et al.* Effects of block copolymer properties on nanocarrier protection from in vivo clearance. *J. Control. Release* **162,** 208–217 (2012).

16. Aggarwal, P., Hall, J. B., McLeland, C. B., Dobrovolskaia, M. a & McNeil, S. E. Nanoparticle interaction with plasma proteins as it relates to particle biodistribution, biocompatibility and therapeutic efficacy. *Adv. Drug Deliv. Rev.* **61,** 428–437 (2009).

17. Namdee, K., Sobczynski, D. J., Onyskiw, P. J. & Eniola-Adefeso, O. Differential Impact of Plasma Proteins on the Adhesion Efficiency of Vascular-Targeted Carriers (VTCs) in Blood of Common Laboratory Animals. *Bioconjug. Chem.* (2015).

18. Mahon, E., Salvati, A., Bombelli, F. B., Lynch, I. & Dawson, K. A. Designing the nanoparticle – biomolecule interface for ' targeting and therapeutic delivery'. *J. Control. Release* **161,** 164–174 (2012).

19. Mirshafiee, V., Kim, R., Park, S., Mahmoudi, M. & Kraft, M. L. Impact of protein pre-coating on the protein corona composition and nanoparticle cellular uptake. *Biomaterials* **75,** 295–304 (2016).

20. Snehalatha, M., Venugopal, K., Saha, R. N., Babbar, A. K. & Sharma, R. K. Etoposide loaded PLGA and PCL nanoparticles II: biodistribution and pharmacokinetics after radiolabeling with Tc-99m. *Drug Deliv.* **15,** 277–287 (2008).

# CHAPTER 6: THE IMPACT OF ANTICOAGULANT ON CORONA-INDUCED NEGATIVE ADHESION ON DRUG CARRIERS IN BLOOD FLOW

## ABSTRACT

Upon injection of vascular-targeted drug carriers (VTCs) into blood, plasma proteins rapidly coat the surface forming the protein corona. Previous work has observed that the protein corona can impact a variety of drug delivery phenomena, including targeted drug carrier adhesion to the vascular wall. To date, the bulk of the work evaluating the impact of the protein corona on drug carrier functionality has employed various mediums, including bovine serum, cell media, human serum, and anticoagulated plasma. Anticoagulants are known to influence the proteomic profile of plasma and as such may mediate the previously observed plasma-related carrier effects. In this work, we explore the role of plasma anticoagulant on altering the protein corona impact on the specific adhesion of targeted drug carriers to the vascular wall via an *in vitro* parallel plate flow chamber assay. Specifically, we characterized the binding efficiency of model carriers of various material types to activated HUVECs in heparinized, citrated, and non-anticoagulated blood flows. Particle adhesion to activated HUVECs is substantially reduced in blood flow, particularly in heparinized and serum blood flow, depending on the targeting ligand density and material type.

## 6.1 Introduction

Previously, rapid plasma protein adsorption onto poly(lactic-co-glycolic) acid (PLGA)-based VTCs was shown to drastically reduce their adhesion efficiency to inflamed endothelium in human blood flow; however, these effects were mainly non-existent for polystyrene (PS), silica (Si), and titanium dioxide ($TiO_2$) particles[1–3]. This plasma protein adhesion effect was due to unique protein corona formed on PLGA; namely, PLGA VTCs acquired specific immunoglobulin (Ig) sized (~150 kDa) antibody proteins[1], which were not significantly present on PS particles. However, this previous work may be limited since all assays were performed with anticoagulated (citrated) plasma. Although serum (no anticoagulant) and anticoagulated plasma are both routinely used to assess NP-protein interactions, these mediums have their own unique protein composition and this is known to influence the impact of the protein corona on cellular uptake[4–6]. Indeed, a recent study comparing the protein corona formation on silica NPs exposed to human plasma and serum observed that plasma-exposed silica NPs experienced increased cellular uptake relative to serum exposed silica NPs[6], which was linked to specific adsorption of opsonic coagulation proteins such as fibrinogen onto plasma-exposed but not serum-exposed NPs (fibrinogen is depleted in serum). However, the role of anticoagulant on protein corona formation and its potential role in prescribing VTC adhesion efficiency to the vascular wall in human blood flow remains relatively unknown. This work seeks to elucidate how different anticoagulants or their absence modulates VTC adhesion efficiency in human blood flow via differences in the particle protein corona.

## 6.2 Results

### 6.2.1 Impact of anticoagulant on the adhesion efficiency of various VTC materials

The main objective here is to evaluate how different anticoagulants and their absence potentially alter the impact of the plasma protein corona on VTC adhesion to the vascular wall in human blood flow. Specifically, PLGA, PLA, PCL, PS, and Si particle adhesion was evaluated in a PPFC assay with heparinized or ACD anticoagulated whole blood (WB) or RBCs-in-Serum (no anticoagulant) and compared to adhesion of particles in RBCs-in-VB. Biodegradable PLGA, PLA, and PCL are primarily explored here while PS and Si serve as controls in our assays to allow comparison to existing literature. ACD and heparin are chosen as they both are commonly used anticoagulants. ACD chelates calcium ions, thus preventing the clotting process, whereas heparin acts by binding to antithrombin III, causing inactivation of thrombin. VTC diameters ranged from ~400-700 nm as previously listed in Table 5.1. Table 6.1 lists the average $sLe^a$ ligand site density for the various VTC materials.

Figure 6.1 shows the adhesion levels of all $sLe^a$-targeted particles to an activated HUVEC monolayer in flow of anticoagulated WB (heparin or ACD) or with RBCs-in-Serum (no anticoagulant) relative to the adhesion of the same particles in RBCs-in-VB (control). For PLGA particles, vascular wall adhesion observed in ACD WB was 75% lower than the adhesion level of the same particles observed in RBCs-in-VB. A similar reduction in adhesion was obtained for PLGA in heparinized WB and RBCs-in-Serum, where the levels of adhesion observed were 74% and 89% lower than the control (Figure 6.1), respectively. In contrast, the adhesion levels for PS, Si, and PCL particles in ACD WB were only moderately lower relative to the control (< 40% reduction). However,

similar to PLGA and PLA, significantly lower adhesion occurred for these materials in RBCs-in-Serum, where ~80% reduction was observed relative to the control. Heparinized WB resulted in low adhesion compared to the control for PLA and PS (>80% reduction), but Si and PCL showed moderate effects with less than 60% adhesion reduction observed.

**Table 6.1** VTC ligand density quantification

| ***Material*** | ***sLe$^a$ density (sites μm$^{-2}$)*** | ***S.E.*** |
|---|---|---|
| PLA, PLGA | 3500 | 700 |
| PLGA ("high") | 15300 | 900 |
| Si | 4400 | 200 |
| PS | 6000 | 300 |
| PCL | 2200 | 500 |
| PCL ("moderate") | 7100 | 1200 |

### 6.2.2 Evaluation of HUVEC adhesion of various VTCs in anticoagulant-free WB flow

Although serum is anticoagulant free, the clotting process depletes coagulation factors, fibrinogen, fibronectin, and may artificially raise the level of other proteins relative to that in anticoagulated plasma. One medium that may provide a better model of human blood *in vivo* is anticoagulant-free (ACF) whole blood. For these assays, blood without anticoagulant was drawn from healthy donors and used immediately in flow assays. As shown in Figure 6.2, PS, Si, PLGA, and PCL VTCs experienced ~80% reduction and PLA, 95% reduction relative to their respective control assay. Overall, the low adhesion relative to RBCs-in-VB observed in ACF WB is in line with the low adhesion observed in RBCs-in-Serum (no anticoagulant added) for all VTC material types. Interestingly, PLGA performs significantly better in ACF blood (~80% reduction) compared to RBCs-in-Serum (~90% reduction).

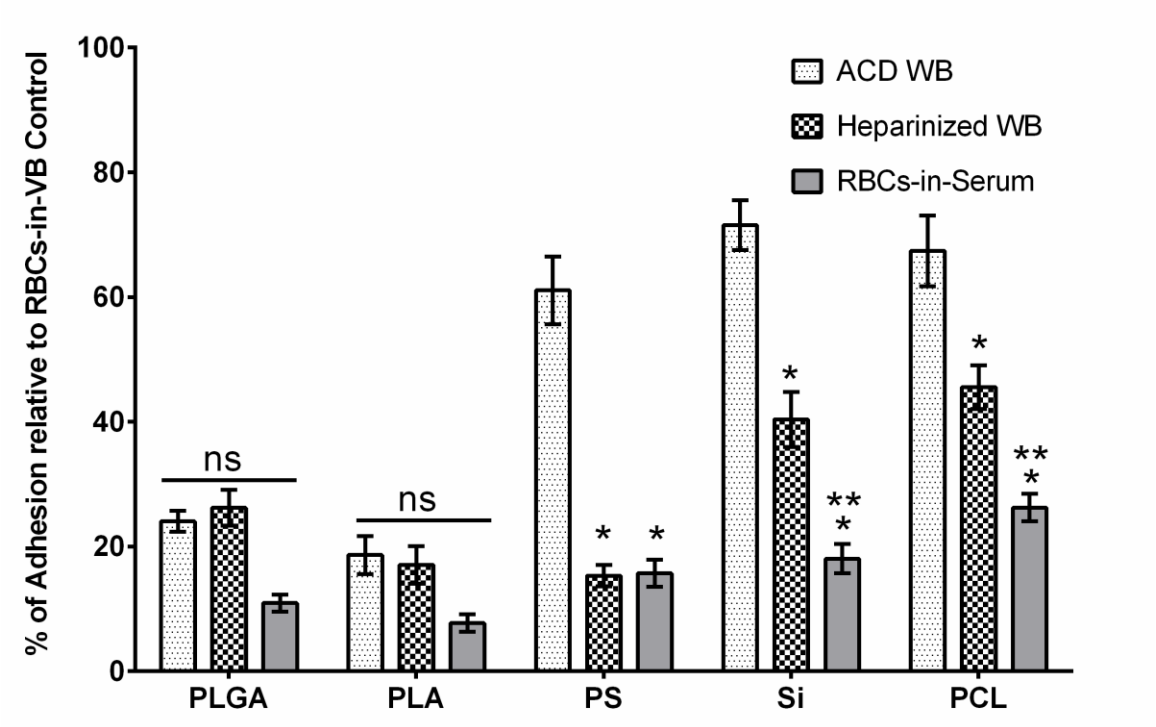


**Figure 6.1.** PPFC assay with VTCs in various anticoagulants: HUVEC adhesion (% relative to RBCs-in-VB Control) for PLGA, PLA, PS, Si, and PCL VTCs in ACD WB, heparinized WB, and RBCs-in-Serum relative to RBCs-in-VB after 5 min of flow at a shear rate of $200s^{-1}$. Particle concentration was fixed to $1 \times 10^6$ particles $mL^{-1}$. * = $p<0.01$ relative to ACD-WB trial for given material via one-way ANOVA with Tukey post-test. $n \geq 4$. ** = $p<0.01$ relative to heparinized WB trial for given material via one-way ANOVA with Tukey post-test.

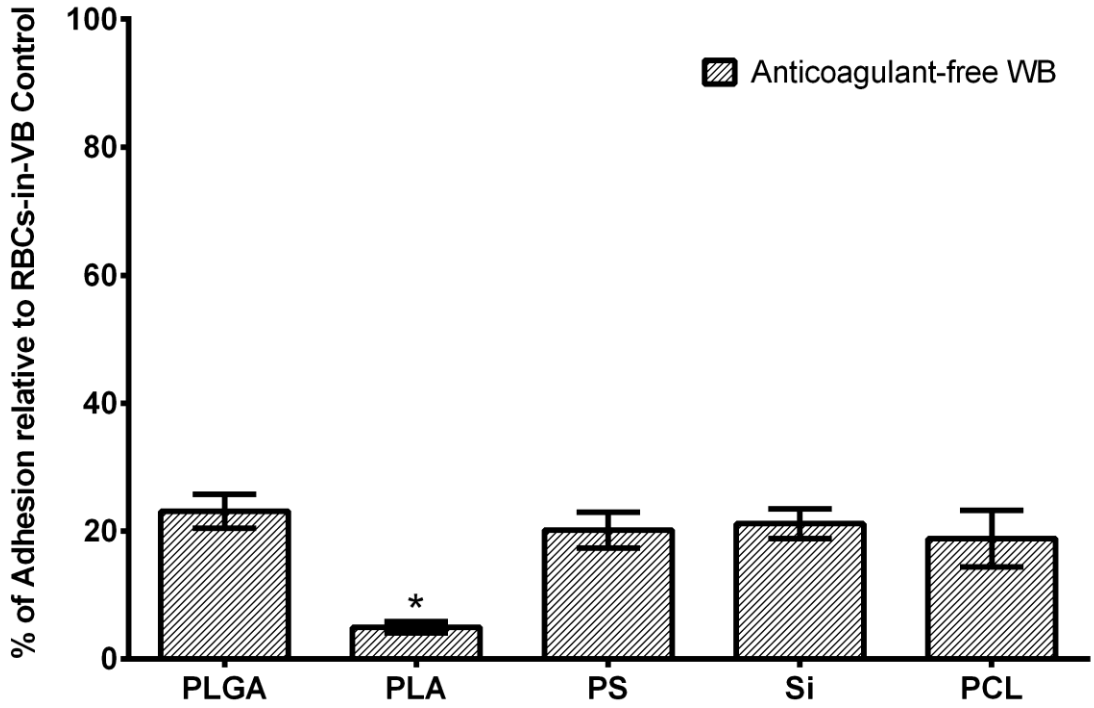


**Figure 6.2** PPFC assay with VTCs in ACF WB: HUVEC adhesion (% relative to RBCs-in-VB Control) for PLGA, PLA, PS, Si, and PCL VTCs in Anticoagulant-free WB relative to RBCs-in-VB after 5 min of flow at a shear rate of $200s^{-1}$. Particle concentration was fixed to 1 x $10^6$ particles $mL^{-1}$. * = $p<0.01$ relative to Anticoagulant-free WB trials relative to all other VTC materials.

### 6.2.3 Impact of ligand density in mitigating plasma-associated VTC adhesion reduction

Previous work observed that the targeting ligand density can play a role in mitigating the extent of the negative impact of the plasma protein corona on the adhesion of PLGA VTCs in ACD treated blood[1]. We explore this possibility here for particle adhesion in all the different blood conditions. As shown in Figure 6.3, PLGA particles with high ligand density (~15,000 $sLe^a$ sites $\mu m^{-2}$) displayed improved adhesion in ACD WB, exhibiting only 30% reduction compared to the control. In addition, ~20% improvement in adhesion relative to the control was achieved in heparinized WB with the high ligand density. Increasing the site density of PLGA VTCs exposed to serum or ACF WB did not improve their adhesion levels relative to the control. Interestingly, having a moderately higher ligand density (~7000 $sLe^a$ sites $\mu m^{-2}$) on PCL did not significantly impact their relative adhesion in ACD WB, heparinized WB, or serum (Figure 6.4). Further increases in the $sLe^a$ site density of PCL particles to ~15,000 $sLe^a$ sites $\mu m^{-2}$ offered no additional adhesion recovery when tested in ACD WB (see Chapter 5).

### 6.2.4 Evaluation of differences in VTC protein corona relative to blood characteristic

The presented results thus far showed high reduction of VTC adhesion in RBCs-in-Serum relative to ACD or heparinized WB. Although serum and plasma are both routinely used to characterize NP uptake and other relevant drug delivery processes, the protein composition of each is different, and in particular, serum does not contain fibrinogen and has lower concentration of other clotting factors and cell adhesion proteins (e.g., fibronectin), which could significantly change the protein corona formed on VTCs[7,8].

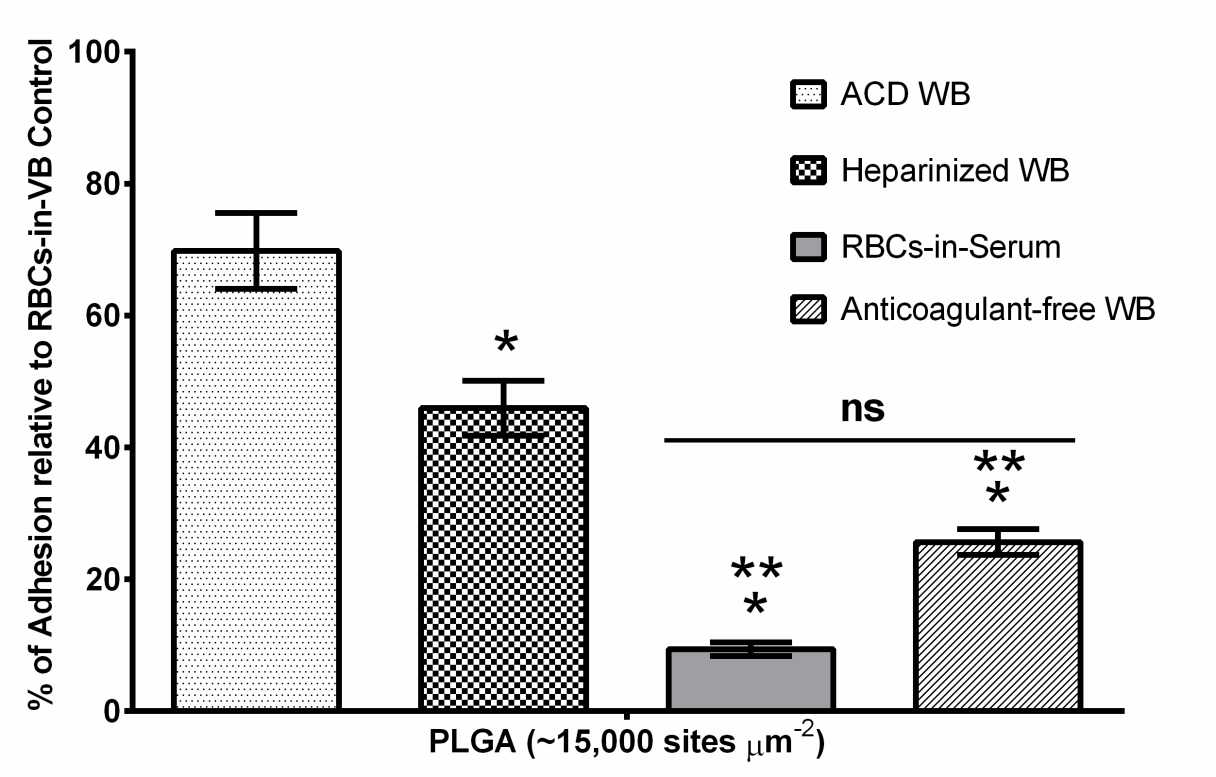


**Figure 6.3.** PPFC assay with high ligand density PLGA VTCs: HUVEC adhesion (% relative to RBCs-in-VB Control) for high ligand density PLGA VTCs (~15,000 sites/$\mu m^2$) in ACD WB, heparinized WB, RBCs-in-Serum, and Anticoagulant-free WB after 5 min of flow at a shear rate of $200s^{-1}$. Particle concentration was fixed to $1 \times 10^6$ particles $mL^{-1}$. * = $p<0.01$ relative to ACD-WB trial via one-way ANOVA with Tukey post-test. $n \geq 4$. ** = $p<0.01$ relative to heparinized WB trial via one-way ANOVA with Tukey post-test.

Interestingly, all VTCs exhibit similar zeta potential upon soaking with plasma and serum (Figure 6.5), which suggests that differential adhesion of VTCs exposed to plasma and serum flow stems from the formation of unique protein coronae in these mediums rather than electrostatic interactions. To test this hypothesis, the protein corona on PLGA VTCs is profiled using SDS-PAGE for particles exposed to serum, heparinized plasma, and ACD plasma for ~10 minutes at 37°C. Figure 6.6 shows an image of the SDS-PAGE gel for which there is a notable increase (2.0 +/- 0.4 folds via ImageJ) in the intensity of the band at the 150 kDa mark for the corona acquired from serum versus ACD plasma. We previously reported that the intensity of the 150 kDa protein band, which mainly contains Igs, directly correlated with the extent of the negative impact of plasma proteins on VTC adhesion efficiency. The heparinized plasma corona also shows some unique differences compared to ACD plasma and serum, particularly in the ~100-150 kDa range but overall appears to exhibit the least amount of protein adsorption.

## 6.3 Discussion

The data presented in this work shows that anticoagulant plays a significant role in modulating the impact of the protein corona on the adhesion efficiency of VTCs to HUVECs in human blood flow, and the extent of these corona-induced effects depend on the VTC material type and ligand density. In particular, all VTC types exhibited low levels of adhesion in RBC-containing serum flow relative to anticoagulated blood flow. We conclude that this observation is due to increased large protein adsorption (i.e., Igs) on serum relative to plasma exposed VTCs based on our previous work linking Igs as major players in driving corona-induced adhesion reduction[1,3]. Enhanced Ig adsorption in the serum versus plasma corona observed here with PLGA has also been observed on solid

lipid nanoparticles in a different study, potentially a consequence of the differential proteomic profile of these two mediums favoring Ig adsorption in serum relative to plasma[9].

Similar to the RBCs-in-Serum trials, low particle adhesion was observed in ACF WB relative to anticoagulant-containing WB trials. The main difference between RBCs-in-Serum and ACF WB is that for serum, the clotting process artificially elevates levels of various proteins as well as attenuates the concentration of others[7,10]. However, with the exception of complement factor H precursor (~150 kDa), proteins with elevated levels in serum typically fall within a lower molecular weight range, typically between 10-40 kDa. Thus, it is likely that the critical "negative" proteins including Igs in the ~150 kDa size range are conserved through the clotting process, and likely not altered in concentration between ACF and RBCs-in-Serum. Moreover, Igs such as IgG have been quantified in human serum and plasma via IgG ELISA kits (Abcam, ab100547) and in general are observed to be highly similar in concentration, typically between a range of 6-15 mg $mL^{-1}$ [11]. Thus, the negative impact of the corona on adhesion between ACF WB and RBCs-in-Serum is likely not due to artifacts of the clotting process affecting the Ig concentration. While the negative impact of plasma proteins on VTC adhesion was tempered in anticoagulated blood, VTCs adhesion was significantly lower with heparinized WB as the flow medium compared to ACD WB. This observation is not surprising since heparin and ACD anticoagulants act by different mechanisms and can have profound impacts on the overall plasma composition[7,12,13]. Heparin (which acts to prevent coagulation by catalyzing inactivation of thrombin by antithrombin III) binds to a significant number of other plasma proteins[14], and the binding of heparin/heparin sulfate to these "heparin-binding" proteins

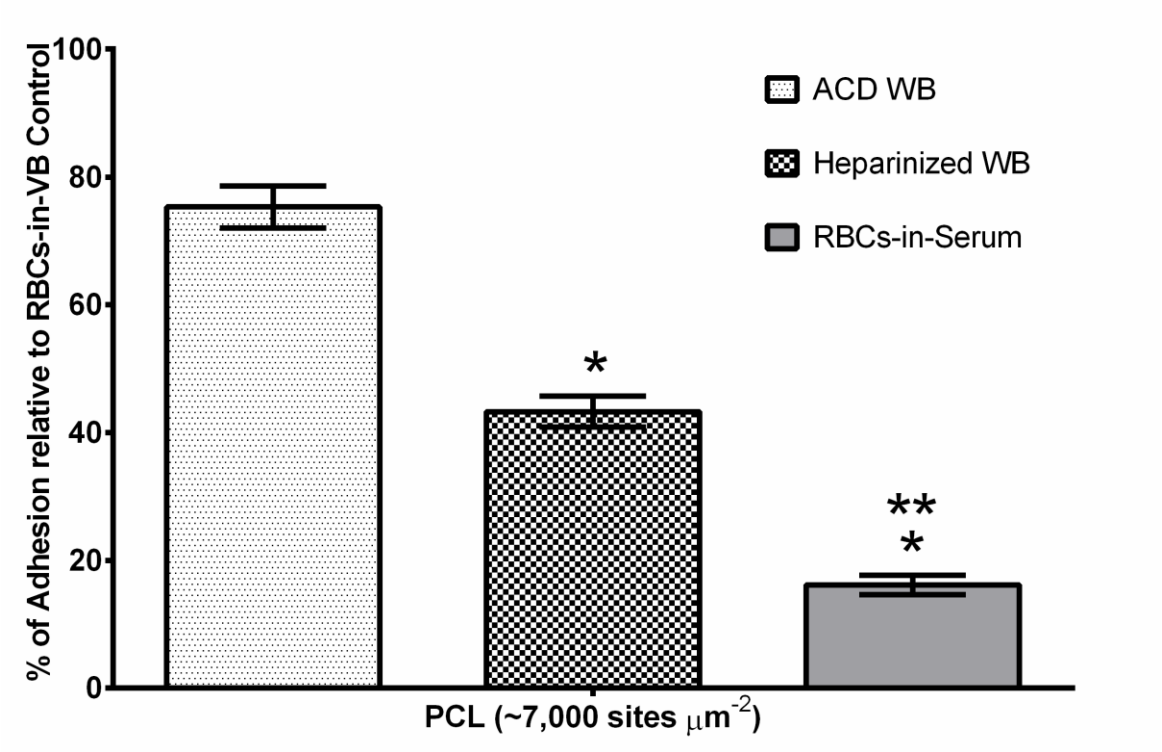


**Figure 6.4.** PPFC assay with high ligand density PCL VTCs: HUVEC adhesion (% relative to RBCs-in-VB Control) for high ligand density PCL VTCs (~7,000 sites/$\mu m^2$) in ACD WB, heparinized WB, and RBCs-in-Serum after 5 min of flow at a shear rate of $200 s^{-1}$. Particle concentration was fixed to $1 \times 10^6$ particles $mL^{-1}$. * = $p<0.01$ relative to ACD-WB trial via one-way ANOVA with Tukey post-test. $n \geq 4$. ** = $p<0.01$ relative to heparinized WB trial via one-way ANOVA with Tukey post-test.

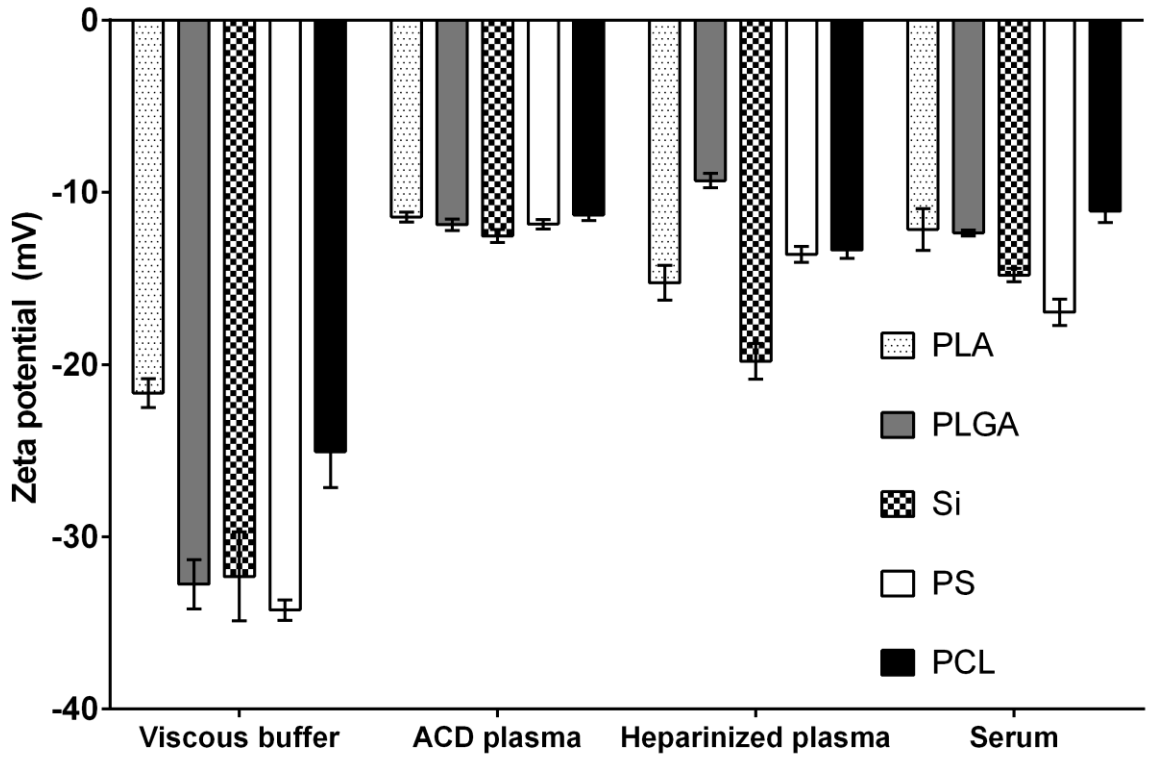


**Figure 6.5.** Zeta potential measurements for sLe$^a$-coated VTCs of various materials. VTCs were soaked in the various medium (viscous buffer, ACD plasma, heparinized plasma, serum) and washed with D.I. water. Measurements were then performed in D.I. water using a Malvern Zetasizer instrument. Concentration ranged from 0.65 – 2.5 × $10^7$ particles $mL^{-1}$.

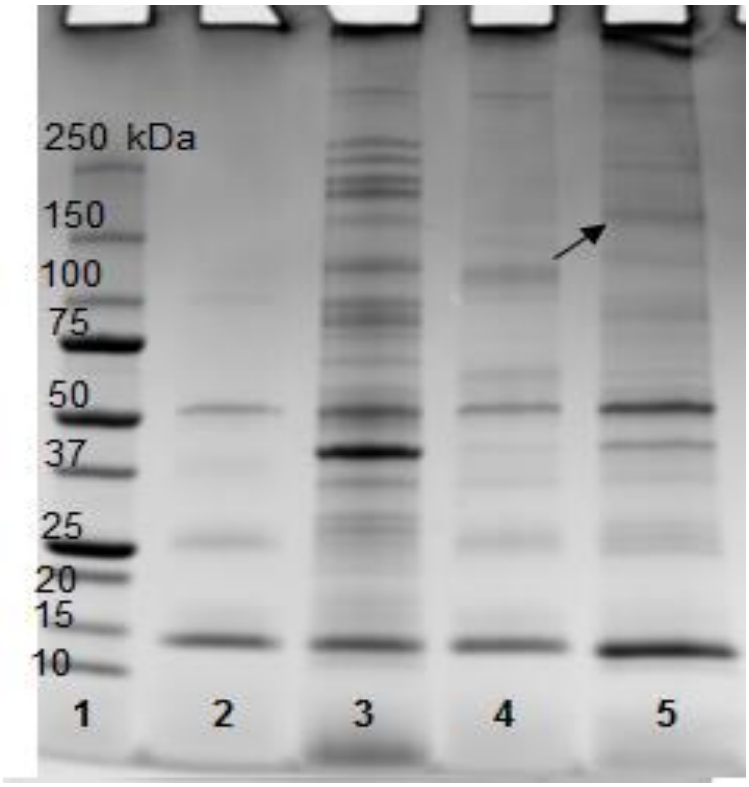


**Figure 6.6.** SDS-PAGE: Characterization of surface bound protein coronae formed on PLGA VTCs exposed to VB, plasma (ACD, heparin), and serum. Lane 1: molecular weight standard, Lane 2: corona from VB soak, Lane 3: corona from ACD plasma soak, Lane 4: corona from heparinized plasma soak, and Lane 5: corona from serum soak.

can modify their activity, metabolism, and concentration[15,16]. Anticoagulants such as ACD, chelate calcium and unlike heparin, are not expected to induce protein-protein binding to the same extent. In addition, a study by Kim et al. identified a variety of proteins with increased concentration in heparin versus citrated plasma, including α2-macroglobulin, haptoglobulin precursor, Apo-AI, Apo J precursor, and complement factor H precursor[10]. Indeed, recent work by Schöttler et al. has observed slight differences in the protein corona between polystyrene NPs exposed to heparin and citrated blood, where compositional increases in fibrinogen and decreases in vitronectin were observed in citrate relative to heparin corona, and these particles exhibited differential uptake in HeLa cells and macrophages[5]. The corona profile observed on PLGA particles here shows differences in heparin versus ACD exposed particles, which could explain the differential adhesion efficiency of VTCs in heparinized versus ACD WB flow. Specifically, the adsorption of Igs (150 kDa mark) and other large proteins which have been linked to reduced adhesion in blood flow are less prominent in the heparin versus citrate blood derived corona, despite the fact that the adhesion reduction was higher in heparin compared to ACD WB[1,3]. Thus, it may be the case that other proteins are involved in causing enhanced adhesion reduction of VTCs in heparin versus citrate blood flow. The main unique band in the heparin lane is between 100 and 150 kDa, possibly a form of haptoglobulin (~100 kDa) or complement factor H (~140 kDa), given the fact these proteins have been identified to be in higher concentration in heparin versus citrated plasma, potentially leading to increased adsorption in the corona for PLGA particles[10].

The impact of anticoagulant on protein corona-induced VTC adhesion reduction also depended on material type. Specifically, PCL and Si outperformed all other materials

in both ACD and heparinized WB, suggesting these materials are generally more resistant to the negative impacts of the plasma protein corona on VTC adhesion efficiency in blood flow. Overall, PLGA and PLA adhesion profiles closely resembled each other, where large reductions (>75%) were observed in all mediums tested. However, the material dependence of the impact of corona-induced effects observed in ACD and heparinized WB were eliminated in RBCs-in-Serum and ACD WB trials, where high percent reductions (>75%) in adhesion were observed regardless of the material type.

## 6.4 Conclusion

This study has revealed that the absence of anticoagulant magnifies the negative adhesion impact of the protein corona via enhanced Ig adsorption on drug carriers relative to that observed in anticoagulated blood flow. This work suggests that anticoagulated whole blood may result in an overestimation of drug carrier adhesion efficiency with human blood *in vivo*, given the similar low adhesion observed in both RBC-containing serum and ACF WB flow for all particle types tested. Furthermore, the magnified effects of the protein corona in the absence of anticoagulant will likely persist despite an increased ligand density, suggesting that the corona in serum or ACF WB may need to be altered via use of hydrophilic coatings or possibly proteins absent in serum (i.e., fibrinogen) as a possible avenue to counteract the negative effect of enhanced serum Ig adsorption and improve adhesion efficiency. Further studies seek to explore a combination of approaches including covalent protein attachment, particle density, and shape to improve the adhesion efficiency of PLGA and other biodegradable drug carriers in human blood flow assays.

Lastly, an inherent limitation of this work stems from the use of *in vitro* assays with blood outside the body. This system, although a predictive indicator of human blood *in*

*vivo*, likely does not fully capture the landscape for protein adsorption and expected binding efficiency in a clinical setting. Next steps to better predict adhesion efficiency in human would likely involve *in vivo* evaluation of drug carriers in a porcine model, as we have previously identified this species to be highly comparable to human with regard to corona-associated adhesion effects on drug carriers.

## References


1. Sobczynski, D. J. *et al.* Plasma protein corona modulates the vascular wall interaction of drug carriers in a material and donor specific manner. *PLoS One* **9,** e107408 (2014).

2. Thompson, A. J. & Eniola-Adefeso, O. Dense nanoparticles exhibit enhanced vascular wall targeting over neutrally buoyant nanoparticles in human blood flow. *Acta Biomater.* **21,** 99–108 (2015).

3. Namdee, K., Sobczynski, D. J., Onyskiw, P. J. & Eniola-Adefeso, O. Differential Impact of Plasma Proteins on the Adhesion Efficiency of Vascular-Targeted Carriers (VTCs) in Blood of Common Laboratory Animals. *Bioconjug. Chem.* (2015).

4. Mirshafiee, V., Kim, R., Park, S., Mahmoudi, M. & Kraft, M. L. Impact of protein pre-coating on the protein corona composition and nanoparticle cellular uptake. *Biomaterials* **75,** 295–304 (2016).

5. Schöttler, S., Klein, K., Landfester, K. & Mailänder, V. Protein source and choice of anticoagulant decisively affect nanoparticle protein corona and cellular uptake. *Nanoscale* **00,** 1–3 (2015).

6. Mirshafiee, V., Kim, R., Mahmoudi, M. & Kraft, M. L. The importance of selecting a proper biological milieu for protein corona analysis in vitro : human plasma vs. human serum. *Int. J. Biochem. Cell Biol.* (2015).

7. Ayache, S. *et al.* Comparison of proteomic profiles of serum, plasma, and modified media supplements used for cell culture and expansion. *J. Transl. Med.* **4,** 40 (2006).

8. McCafferty, M. H. *et al.* Normal fibronectin levels as a function of age in the pediatric population. *Pediatr. Res.* **17,** 482–485 (1983).

9. Müller, R. H. & Göppert, T. M. *Role of Lipid Excipients in Modifying Oral and Parenteral Drug Delivery: Basic Principles and Biological Examples*. (John Wiley & Sons, 2007).

10. Kim, H. J., Kim, M. R., So, E. J. & Kim, C. W. Comparison of proteomes in various human plasma preparations by two-dimensional gel electrophoresis. *J. Biochem. Biophys. Methods* **70,** 619–625 (2007).

11. Gonzalez-Quintela, A. *et al.* Serum levels of immunoglobulins (IgG, IgA, IgM) in a general adult population and their relationship with alcohol consumption, smoking and common metabolic abnormalities. *Clin. Exp. Immunol.* **151,** 42–50 (2008).

12. Capila, I. & Linhardt, R. J. Heparin-protein interactions. *Angew. Chem. Int. Ed. Engl.* **41,** 391–412 (2002).

13. Banfi, G., Salvagno, G. L. & Lippi, G. The role of ethylenediamine tetraacetic acid (EDTA) as in vitro anticoagulant for diagnostic purposes. *Clin. Chem. Lab. Med.* **45,** 565–576 (2007).

14. Banks, R. E. *et al.* Influences of blood sample processing on low-molecular-weight proteome identified by surface-enhanced laser desorption/ionization mass spectrometry. *Clin. Chem.* **51,** 1637–1649 (2005).

15. Conrad, E. *Heparin-binding proteins*. (Academic Press, 1997).

16. Thacker, B. E., Xu, D., Lawrence, R. & Esko, J. D. Heparan sulfate 3-O-sulfation: A rare modification in search of a function. *Matrix Biol.* **35,** 60–72 (2014).

# CHAPTER 7: CONCLUSIONS, FUTURE STUDIES, AND COMMENTS

A bulk of the work in the final section of this chapter is published as Sobczynski, D. J. *et al.* Drug carrier interaction with blood: a critical aspect for high-efficient vascular-targeted drug delivery systems. *Therapeutic Delivery* **6,** 915-934 (2015).

## 7.1 Conclusions and Major Contributions

Vascular targeting remains an important and highly beneficial alternative treatment strategy over systemic drug administration. Vascular targeting of particulate drug carriers offers vast potential for reduced side effects, improved drug bioavailability, and increased local drug concentration, resulting in a lower dose required to achieve efficacy. In addition, several diseases such as atherosclerosis, cancer, and arthritis involve vascular endothelial cell dysregulation, allowing for unique targeting opportunities for VTCs. Although vascular targeting of drug carriers is an attractive approach, current targeting formulations for vascular diseases still cause a host of deleterious side effects and only a small fraction of the dose reaches the targeted cells of interest. Understanding the complexity of drug carrier transport and adhesion in blood flow may provide critical insight into improving the specificity and efficiency of vascular-targeted carriers.

Blood vessel wall inflammation is common in the early stage of many vascular diseases and is chosen as the disease model for the *in vitro* flow chamber assays. It was observed that the adhesion of targeted PLGA carriers to E-selectin on endothelial cells in human blood flow is significantly reduced due to the presence of plasma proteins which are thought to obstruct and/or weak ligand-receptor interactions at the wall. This result was rather surprising as other materials did not demonstrate these issues when exposed to

plasma. Furthermore, the low adhesion of PLGA in blood flow suggests that it is largely sub-optimal with regard to adhesion efficiency. These extent of PLGA adhesion fouling in blood flow depended on the surface ligand density, human blood donor, and flow magnitude and profile. Plasma immunoglobulins (Igs) were identified as critical negative proteins limiting PLGA adhesion efficiency. This may be due to the size and affinity of these proteins for PLGA.

In Chapter 4, the role of Igs is explored in more detail via use of IgG and IgA depletion columns designed to tease out the contributions of these specific Ig proteins on corona-induced negative adhesion of PLGA in blood flow. Overall, depletion of IgG alone did not result in adhesion recovery, but the removal of all Ig's (e.g., IgM, IgA, IgD, IgE) consistently showed nearly full recovery in adhesion compared to particles soaked in PBS buffer. Re-addition of enriched IgA fraction (also containing IgG and IgM) to depleted Ig's plasma resulted in knockdown of the adhesion, confirming the importance of this protein in orchestrating corona-induced adhesion reduction of PLGA particles since addition of IgG alone did not cause adhesion knockdown. However, IgA is not exclusively responsible for the effect since depletion of this protein from plasma did not result in full adhesion recovery. These results are critical as they demonstrate corona-induced effects to be prescribed by individual proteins, rather than the "shell effect" which has been previously discussed in the literature. In addition, this work could be implemented to help improve prediction of therapeutic potential across different individuals. Specifically, Ig's concentration or composition could serve to indicate the degree of targeting specificity expected for a VTC.

Although PLGA is well-studied and convenient for utility in drug delivery for several reasons, it is among a class of biodegradable polyesters which also includes the homopolymer PLA and PCL. These polymers are also used for drug delivery and tissue engineering applications, and thus it is important to explore how these other biodegradable materials (i.e., PLA, PCL) behave in blood flow relative to PLGA. In Chapter 5, it is observed that PCL particles outperform PLGA and PLA in terms of blood flow adhesion efficiency, defined as the ratio of particle adhesion in blood divided by plasma-free blood (RBCs-in-VB). Employment of high ligand density on particles for these materials significantly recovered the adhesion in blood flow; however, PCL is still attractive as this material exhibits mild adhesion reduction even at lower site densities, which may be optimal for targeting *in vivo*. Dependence of VTC adhesion on material type observed here is likely linked to hydrophobicity, as this parameter is critical to corona formation. In addition, reduced Ig adsorption is observed on PCL relative to PLGA and PLA, which supports the hypothesis that plasma Ig adsorption drives low adhesion efficiency of drug carriers. This work also points out the importance of material type (linked to hydrophobicity) and suggests that the optimal polymer for vascular wall adhesion be hydrophobic despite widespread evidence that increasing hydrophobicity leads to lower circulation time and enhanced protein adsorption.

Up to this point, all assays have employed acid-citrate dextrose (ACD) as the plasma anticoagulant. The selection or absence of anticoagulant in blood causes drastic changes to the plasma proteome, which can thus influence cellular processes such as uptake via differences in the corona formed in plasma versus serum (no anticoagulant) or ACD plasma versus heparin, another common anticoagulant. Overall, it is observed that the

absence of anticoagulant enhances the extent of corona-induced adhesion reduction on PLGA as well as other materials. Furthermore, in the absence of anticoagulant (i.e., serum, non-anticoagulated blood flow) all materials exhibit high levels of reduction relative to plasma free blood (RBCs-in-VB). This work suggests that particle adhesion with human blood *in vivo* will be significantly hindered compared to that observed with anticoagulated blood *in vitro*. Furthermore, no significant benefits in adhesion were observed in non-anticoagulated blood flow even with high targeting ligand density.

## 7.2 Future studies

This dissertation has elucidated the role of the protein corona on drug carrier adhesion in human blood flow to inflamed human endothelial cells via *in vitro* flow chamber assays. In addition, the impact of specific proteins in orchestrating negative adhesion on PLGA drug carriers was explored via a combined effort through SDS-PAGE, mass spectrometry, ELISA, and plasma protein depletion studies. However, there are several directions in which the role of the protein corona could be expanded and further developed to better understand its impact in vascular targeted drug carrier adhesion:

1. **Test the adhesion of targeted fluorescent PLGA and PCL drug carriers *in vivo* using a porcine model as this animal has been identified to closely match the human system in regard to protein corona adhesion effects.**
2. **Test PLGA particle adhesion with pre-formed porcine coronae *in vivo* compared to *in vitro* in RBCs-in-VB flow medium.**

   2.1. Evaluate porcine corona formed *in vivo* and *in vitro* on PLGA via SDS-PAGE.

   2.2. Identify key differences in corona profile via mass spectrometry.

2.3. Perform similar experiment with human blood, obtaining anticoagulant-free WB to pre-form *in vivo* corona and facilitate particle collection via addition of anticoagulant.

3. **Optimize a "forced corona" approach via covalently attaching proteins and coatings to particle drug carrier surfaces in effort to improve adhesion in serum flow.**

3.1. Fibrinogen and fibronectin are known to be at least partially depleted in serum and have been identified to have adhesive properties making these proteins attractive candidates.

3.2. Explore carbohydrate coatings such as hydroxyethyl starch or zwitterions which have been identified to severely mitigate any protein adsorption and its associated effects.

3.3. Use mass spectrometry to obtain a library of potential "adhesion-positive" proteins found on PS and PCL but absent from PLGA and PLA surface coronae.

3.4. Compare serum and non-anticoagulated blood flow adhesion *in vitro* between unmodified PLGA and PLGA coated with adhesive proteins or carbohydrate coatings.

3.5. Explore the plasma protein profile via SDS-PAGE and identify key sources of differential protein binding via mass spectrometry.

4. **Develop assays to better understand how the protein corona impacts drug carrier adhesion across different human donors.**

4.1. Explore depletion assays for other blood in other anticoagulants as well as serum (no anticoagulant).

4.2. Expand the number of human subjects tested to obtain a better understanding of how specific Ig protein concentration, composition, or affinity impacts adhesion of drug carriers

4.2.1. Ig protein concentration and composition can be compared across donors via a standard sandwich ELISA.

4.2.2. Differential affinity of specific donor Ig proteins for polymer particles could be explored via a modified ELISA assay with nanoparticle-coated wells.

4.2.3. Flow cytometry or western blotting of plasma or serum-soaked particles exposed to different donors could also be implemented to gauge the relative affinity of donor specific IgG or other Igs for the nanoparticle surface.

5. Explore the adhesion of particles in serum from patients on anticoagulant therapy with the goal to understand how these therapies may impact targeted drug carrier adhesion in blood flow.

## 7.3 Concluding thoughts, comments, and potential directions for the field

This dissertation has revealed key insight into intelligent design of vascular-targeted drug carriers. Specifically, it has been observed that the plasma protein corona is critical in prescribing the adhesion efficiency of drug carriers to the vascular wall in blood flow. This initially may come as a surprising result, given that plasma protein adsorption has typically been identified to play key roles in biodistribution, cell uptake, and other drug delivery processes which are largely biomolecular phenomena. Here, the plasma protein corona is observed to affect the biophysical phenomenon of drug carrier adhesion in blood flow which is typically controlled by forces, collisions, and receptor/ligand densities. In addition, this study has taken the idea of "corona-induced" particle adhesion reduction to

a new level by identifying specific types of proteins which alone seem to dominate the effect. Specifically, the work suggests that the impact of the protein corona on biodegradable drug carriers is driven by a single protein class; namely, immunoglobulins. This observation could prove to be of great value in that it offers a specific avenue to modulate drug carrier adhesion to the endothelium; specifically by preventing IgA and IgM adsorption. Furthermore, by identifying which proteins control this unwanted adhesion reduction of polymeric drug carriers, the affinity of a particle for IgA, IgM, and potentially other Igs determined via ELISA, western blotting, or SDS-PAGE opens the possibility of using the corona to "diagnose" and predict drug carrier adhesion efficiency in blood flow. The affinity of a particular particle may depend on human donor and thus may pave the way for a personalized medicine approach. The corona may prove useful to predict drug carrier adhesion efficiency based on its propensity to adsorb certain types of proteins known to negatively affect drug delivery processes such as vascular wall adhesion.

This dissertation has shown that specific proteins control the targeting efficiency of drug carriers; specifically, large molecular weight immunoglobulins weaken the adhesion kinetics of drug carriers in blood flow. Although the natural instinct to combat this issue would involving elimination of the corona, it may also be interpreted in a different light; namely, tailoring the corona to potentially assist and improve VTC targeting efficiency. Indeed, the literature view of the impact of the protein corona on drug delivery processes, which has classically been viewed as an unwanted, negative phenomenon, has observed a shift in the last four to five years to a more positive outlook as it may hold an incredible potential to be exploited to direct particles to specific cells or regions of interest in the body[1]. For example, NPs that preferentially adsorb apolipoproteins, such as apoE, resulted

in enhanced cellular uptake by brain capillary endothelial cells. This was achieved by coating polybutyl cyanoacrylate NPs with a surfactant coating, polysorbate 80[2–5]. In addition, uptake of titanium dioxide NPs by A549 human lung epithelial cells was enhanced in the presence of FBS, due to surface adsorbed vitronectin protein[6]. Other studies have also revealed that particles of the same material but different surface properties can adsorb similar coronas but interact with cells by completely different internalization pathways. Specifically, anionic PS and cationic PS NPs incubated with FBS showed nearly identical protein coronas (mainly adsorbed BSA), yet the anionic NPs interacted with monkey kidney epithelial cells via the natural albumin receptor, whereas cationic NPs interacted with scavenger receptors, attributed to a denaturing of BSA by cationic NPs[7]. The redirection of NP-cell interaction as a result of the protein corona has also been observed in comparing uptake of serum-coated vs uncoated PS NPs, where the presence of serum resulted in NP uptake via phagocytosis, rather than clatherin-mediated endocytosis/micropinocytosis for the bare NPs[8]. In general, NPs that adsorb immunoglobulin and complement result in internalization by phagocytes, thus promoting macrophage uptake. The protein corona protects the cell from damage compared to bare NPs, as the corona-adsorbed particle minimally affects cell membrane integrity. However, these effects show protein-specific dependence, as carbon nanotubes (CNTs) coated with γ-globulins resulted in damaged cell membranes whereas fibrinogen-coated CNTs do not [9]. Thus, the adsorbed NP-protein corona has abilities to modulate cell uptake, adhesion, and cell membrane integrity. Of course, other particle parameters such as zeta potential and surface morphology can further confound these results.

Harnessing the enhanced uptake features of protein-coated NPs could be used to direct the VTC to the cell of interest. This method of thinking considers the protein corona as a natural targeting mechanism, which can be tailored to enhance association with certain cells depending on the physicochemical properties of the NP. In general, hydrophobic NPs adsorb more proteins to mask their surface from water and to absorb proteins that induce uptake by macrophages [10]. However, as an example of more directed corona-targeting, the specific corona surrounding N-isopropylacrylamide-co-N-tert-butylacrylamide (NIPAM/BAM) copolymer NPs shows enhanced vitronectin adsorption, which leads to enhanced cellular uptake via the αVβ3 integrin, an overexpressed receptor in inflamed endothelium and cancer cells [11]**.** If one aims to use the corona as a targeting mechanism, then there must be control over the composition *in vivo.* In this light, the plasma protein corona is a worthy candidate to enhance targeting efficiency of drug carriers and some current studies have begun developing models for predicting cell association based on NP-corona features[12]**.** It may also prove advantageous to develop high-throughput screening assays of various drug carrier material types to obtain a more global understanding of corona variations and use this information to design "smart" VTCs capable of adsorbing a specific protein corona for a particular drug delivery application.

The protein corona may also play a fundamental role in development of personalized medicines. Recently, a study revealed that NPs coated with plasma proteins of patients with various diseases resulted in unique corona compositions[13]. The individualized corona may prove to be a useful avenue to pursue for personalized medicine as biological interactions are heavily dependent on the corona formation. Specific NP features may be employed in blood of a certain disease in order to attract specific proteins

for enhanced cellular-targeting/uptake. Further research will likely assess different materials and properties of NPs with the goal of predicting the corona profile based on the chosen NP properties and plasma source features. Furthermore, optimal VTC targeting and uptake properties can be clarified by investigating these properties for NPs exposed to plasma from a cancer patient.

In this dissertation, the impact of the protein corona on VTC adhesion in blood flow was observed to negatively impact the targeting efficiency and it is certainly a worthwhile endeavor to seek the use of zwitterionic or carbohydrate-based coatings as avenues to substantially eliminate the formation of the corona and ideally restore the adhesion efficiency. However, it remains to be seen whether the protein corona can actually be eliminated completely *in vivo* and thus a drug delivery vehicle may always form a corona regardless of novel attempts to prevent its formation. With this in mind, the idea of tuning the corona to prevent adsorption of immunoglobulins or combat its presence via adsorption of small molecular weight dysopsonins may be a useful alternative. As discussed in this chapter, the idea of exploiting the corona by tuning its properties has shown a significant growth and interest in the literature. The use of the protein corona as a "built-in" targeting mechanism is a fascinating and exciting new direction for development of drug delivery systems. Furthermore, this field is in its infant stages and will only grow further as new studies develop. The potential of the protein corona is vast as it holds utility in drug carrier targeting efficiency, personalized medicine, and diagnostics of drug carrier formulations.

## References


1. Hamad-schifferli, K. How can we exploit the protein corona? *Nanomedicine (Lond).* **8,** 1 (2013).

2. Gao, K. & Jiang, X. Influence of particle size on transport of methotrexate across blood brain barrier by polysorbate 80-coated polybutylcyanoacrylate nanoparticles. *Int. J. Pharm.* **310,** 213–219 (2006).

3. Kreuter, J. *et al.* Covalent attachment of apolipoprotein A-I and apolipoprotein B-100 to albumin nanoparticles enables drug transport into the brain. *J. Control. Release* **118,** 54–58 (2007).

4. Kreuter, J., Alyautdin, R. N., Kharkevich, D. a. & Ivanov, A. a. Passage of peptides through the blood-brain barrier with colloidal polymer particles (nanoparticles). *Brain Res.* **674,** 171–174 (1995).

5. Wagner, S. *et al.* Uptake mechanism of ApoE-modified nanoparticles on brain capillary endothelial cells as a blood-brain barrier model. *PLoS One* **7,** e32568 (2012).

6. Tedja, R., Lim, M., Amal, R. & Marquis, C. Effects of Serum Adsorption on Cellular Uptake Profile and Consequent Impact of Titanium Dioxide Nanoparticles on Human Lung Cell Lines. *ACS Nano* **6,** 4083–4093 (2012).

7. Fleischer, C. C. & Payne, C. K. Nanoparticle − Cell Interactions: Molecular Structure of the Protein Corona and Cellular Outcomes. *ACS Accounts Chemcial Res.* **47,** 2651–2659 (2014).

8. Lunov, O. *et al.* Differential Uptake of Functionalized Polystyrene Nanoparticles by Human Macrophages and a Monocytic Cell Line. *ACS Nano* **5,** 1657–1669 (2011).

9. De Paoli, S. H. *et al.* The effect of protein corona composition on the interaction of carbon nanotubes with human blood platelets. *Biomaterials* **35,** 6182–6194 (2014).

10. Aggarwal, P., Hall, J. B., McLeland, C. B., Dobrovolskaia, M. a & McNeil, S. E. Nanoparticle interaction with plasma proteins as it relates to particle biodistribution, biocompatibility and therapeutic efficacy. *Adv. Drug Deliv. Rev.* **61,** 428–437 (2009).

11. Caracciolo, G. *et al.* Cancer cell targeting of lipid gene vectors by protein corona. *Nanotechnology* 354–357 (2012).

12. Walkey, C. D. *et al.* Protein Corona Fingerprinting Predicts the Cellular Interaction of Gold and Silver Nanoparticles. *ACS Nano* **8,** 2439–2455 (2014).

13. Hajipour, M. J., Laurent, S., Aghaie, A., Rezaee, F. & Mahmoudi, M. Personalized protein coronas: a ‘key’ factor at the nanobiointerface. *Biomater. Sci.* **2,** 1210 (2014).